Life without Replication in *Bacillus subtilis*

Von der Naturwissenschaftlichen Fakultät der
Gottfried Wilhelm Leibniz Universität Hannover

zur Erlangung des Grades
Doktorin der Naturwissenschaften (Dr. rer. nat.)

genehmigte Dissertation

von

Vivian Vanessa Muñoz Gutiérrez, MSc. (Niederlande)

2022

Referent: Prof. Dr. rer. nat. Kürşad Turgay
Korreferentin: Prof. Dr. rer. nat. Natalia Tschowri
Andere Korreferent: Prof. Dr. Heath Murray
Tag der Promotion: 26.10.2021

Schlagworte: *Bacillus subtilis*, Replication, *oriC*, CRISPR, CRISPRi

Keywords: *Bacillus subtilis*, Replication, *oriC*, CRISPR, CRISPRi

A mi familia:
Mamá, Papá y Juanjo

Zusammenfassung

Am Startpunkt des Zellzyklus wird das bakterielle Genom durch die Replikation verdoppelt. Dadurch wird sicher gestellt, dass jede Tochterzelle eine Kopie des elterlichen Genoms erhält. Die Replikation startet am Replikationsursprung (*oriC*), das sogenannte DnaA-Boxen enthält, an die das Schlüßel-Initiator-Protein DnaA spezifisch binden kann.

Eine fehlerhafte DNA-Replikation kann zu einem bakteriellen Wachstumsstillstand oder Zelltod führen. Unser Wissen über die zellulären Auswirkungen eines Replikationsstopps stammen in erster Linie aus Studien mit thermosensitiven Mutanten, der Zugabe von Antibiotika oder der Induktion durch Nährstoffentzug. Obwohl diese Studien nützlich sind, liefern sie kein vollständiges Bild über die die Auswirkung der bloßen Abwesenheit der Replikationsinitiation in der Zelle, sondern sind durch die zusätzlich erzeugten Stressbedingungen verzerrt. In dieser Studie versuchten wir, die globalen Auswirkungen des Lebens ohne Replikation im Bakterium *Bacillus subtilis* zu entschlüsseln.

Dafür haben wir zwei Strategien entwickelt. Zunächst haben wir ein Bakterienstamm hergestellt, in dem der *oriC* durch ein induzierbares und maßgeschneidertes CRISPR-Cas9-System entfernt werden kann. Nach erfolgreicher Entfernung des *oriC* konnten die Zellen keinen neuen Vorgang der DNA-Replikation starten und exprimierten ein fluoreszierendes Reporterprotein, das es uns ermöglicht hat, die Zellen mittels Durchflusszytometrie und Zeitraffermikroskopie zu selektieren und charakterisieren. Damit konnten wir die Deletion von essentiellen Sequenzen für die Replikation herstellen. Leider mussten wir jedoch feststellen, dass die Wiederherstellung und Anreicherung von nicht-replizierenden Zellen zu unzureichend und schwierig war, um mit einer globalen Charakterisierung des Proteoms dieser Zellen fortzufahren. Dennoch haben wir damit ein mögliches Werkzeug zur Charakterisierung von essentiellen Genen und genetischen Elementen in Bakterien charakterisiert.

Im zweiten Teil dieser Arbeit haben wir die Replikation mit Hilfe des CRISPRi-Ansatzes blockiert, indem wir die für die Replikation essentiellen DnaA-Boxen 6 und 7 durch spezifische sgRNA und dCas9 Expression inhibieren konnten. Wir haben den Phänotyp dieser Zellen charakterisiert und die globalen Proteomveränderungen mittels quantitativer Massenspektrometrie analysiert. Dabei konnten wir beobachten, dass Zellen ohne Replikation länger sind und weder die SOS noch die Stringent Response aktivieren. Außerdem konnten wir mittels globaler Proteinsynthese-Quantifizierung bestätigten, dass die Translationsaktivität dieser Zellen erhöht ist. Diese Ergebnisse erweitern unser Verständnis möglicher direkter oder indirekter Zusammenhänge zwischen Replikation und Translation. Gleichzeitig bieten diese Experimente einen guten Ausgangspunkt für die bessere Erforschung dieser nicht replizierenden und gleichzeitig Translations-aktiver *B. subtilis* Stämme, die auch zu einer interessanten biotechnologischen Anwendung, z.B. bei der Konstruktion verbesserter Produzentenstämme, führen könnte.

Abstract

Bacterial replication, as the starting point of the cell cycle, enables the duplication of genomic information and ensures that each daughter cell receives one copy of the parental genetic code. Replication is initiated at the origin of replication (*oriC*), which contains several sequences called DnaA boxes that serve as binding sites for the master initiator protein DnaA.

Absence or failure of DNA replication can lead to bacterial growth arrest or cell death. Our knowledge of the cellular effects of replication arrest comes primarily from studies using thermosensitive mutants, the addition of antibiotics, or the induction via nutrient depletion. Although these studies are useful, they do not provide a global picture of the mere absence of replication initiation in the cell, but are biased by the additional stress conditions. In this study, we aimed to uncover the global effect of life without replication in the model bacterium *Bacillus subtilis*.

For this purpose, we developed two strategies. First, we generated a bacterial strain in which the *oriC* can be removed by an inducible and customized CRISPR-Cas9 system. After successful deletion of *oriC,* the cells were no longer able to initiate new rounds of DNA replication and they expressed a fluorescent reporter protein that enabled us to select and characterize the cells by flow cytometry and time-lapse microscopy. Thereby, we were able to produce the deletion of essential sequences for replication. Unfortunately, we found that the recovery and enrichment of non-replicating cells was insufficient and challenging to proceed with a proteomic characterization of these cells. Nevertheless, we characterized a potential tool for the characterization of essential genes and genetic elements in bacteria.

In the second part of this work, we blocked replication using a CRISPRi approach by targeting DnaA boxes 6 and 7 with a specific sgRNA and dCas9 expression, which are essential for replication. We characterized the phenotype of these cells and analyzed global changes in the proteome by quantitative Mass Spectrometry. Threby, we could observe the replication arrested cells were elongated and did not activate neither SOS nor stringent response. Additionally, we confirmed that translation activity of these cells is upregulated. These results expand our understanding of potential direct or indirect connections between replication and translation. At the same time, these experiments provide and a good starting point for better research of non-replicating but translationally active *B. subtilis* strains. These could also lead to interesting biotechnological applications, such as construction of improved producer strains.

Table of Contents

List of Figures

List of Tables

1. Introduction

The dream of every bacterial cell is to become two cells
Francois Jacob

The definition of life has historically been controversial. Theologists, biologists, physicists, and thinkers from other areas of knowledge lack a consensus description of life. Moreover, some authors are unconvinced about finding a scientifically relevant definition that encompasses all the features of this complex phenomenon[1]. In fact, the difference between a living and non-living entity is challenging to pinpoint, but some general characteristics are frequently mentioned in the biological sciences. First, living entities can use energy to produce their own building blocks, resulting in growth and self-replication (autopoiesis). Second, living things can respond to their environment and maintain their homeostasis. Finally, all living organisms contain informational molecules (DNA and RNA). However, some organism-like entities are in a grey zone because of the lack of a self-replicating machinery or any of the other properties mentioned above; still, they might be considered 'alive'. One example of this are viruses, which depend on a host for replication and metabolism[2].

1.1 Bacterial DNA Replication

Bacteria are unicellular organisms and are considered one of the simplest forms of life that follow the generally accepted characteristics of life mentioned above. In bacteria, the cell cycle is not that clearly defined as in eukaryotes. However, there are three stages of the cell cycle: the B, C, and D periods. The B period starts from birth to the initiation of chromosome replication. The C period continues from initiation of chromosomal DNA replication to its completion. Finally, the D period goes from the completion of replication until cell division (reviewed in [3]).

During the process of replication, the genomic information is faithfully duplicated, ensuring that each daughter cell receives one copy (Figure 1A). Therefore, DNA replication can be considered the starting point of the cell cycle and a bacterium's life.

As Francois Jacob mentioned, every bacteria cell aims to replicate its DNA to form progeny. Therefore, replication is a process that must be coordinated with cell division, elongation, and chromosome segregation. The process of DNA replication consists of three phases: initiation, elongation, and termination. Here, we will describe the mechanics of these three phases, with an emphasis on replication initiation.

1.1.1 Initiation

The first studies on the role of replication initiation date back to 1968[4,5]. By the early 1990s, most of the proteins and sequences involved in this process were identified in the bacterial model organism *Escherichia coli*[6]. In the three domains of life, a replication initiator protein binds to specific DNA sequences, also known as the origin of replication (*oriC*). Bacterial DNA replication initiates at a single origin and proceeds bi-directionally to the terminus, situated roughly opposite the origin (Figure 1A).

The bacterial genome usually consists of a single circular chromosome with one *oriC*, although certain species can have multiple or linear chromosomes[7,8]. The bacterial initiator protein is DnaA, an AAA+ (ATPases associated with diverse cellular activities) ATPase, which binds to clusters of DnaA boxes in the origin of replication[9,10]. The cooperative binding of ATP-bound DnaA at the *oriC* results in the formation of a nucleoprotein helical filament that unwinds the adjacent AT-rich DNA unwinding element (DUE; reviewed in[11]). The resulting single-stranded DNA (ssDNA) serves as a loading point for replication machinery assembling (Figure 1B). In *E. coli*, DnaA recruits the AAA+ ATPase, DnaC, which loads the hexameric helicase, DnaB on the DNA. DnaC subsequently hydrolyses ATP, and finally dissociates (Reviewed in [10,12]).

B. subtilis and other Gram-positive bacteria require the additional proteins, DnaD and DnaB, to load the replicative helicase[13–19]. DnaA first recruits DnaD, followed by DnaB, and at last the helicase loader DnaI (DnaC in *E. coli*), and the helicase DnaC (DnaB in *E. coli*) [20]. After loading the helicase, the primase DnaG synthesize an RNA primer on the template DNA, leading to the helicase loader's dissociation and activation of the helicase (Figure 1C). The sliding clamp (DnaN), and the DNA polymerase are subsequently loaded, completing the replication machinery[11].

1.1.2 Elongation

DNA elongation proceeds bi-directionally through the chromosome and uses a conserved machinery, although the components vary between organisms. Replication proceeds differently between the leading and lagging strands of DNA (Figure 1C). For leading strand synthesis, DNA polymerase extends from the RNA primer made by primase (DnaG) along the leading strand, from 5′ to 3'. The sliding clamp (DnaN) interacts with the DNA polymerase and increase its processivity, allowing a synthesis speed of up to 1000 bases/second. At the lagging strand DNA is produced in short fragments from RNA primers, which are synthesized by DnaG, producing the Okazaki fragments. The RNA primers are then removed, and the fragments are connected by DNA ligase[21] (Figure 1C).

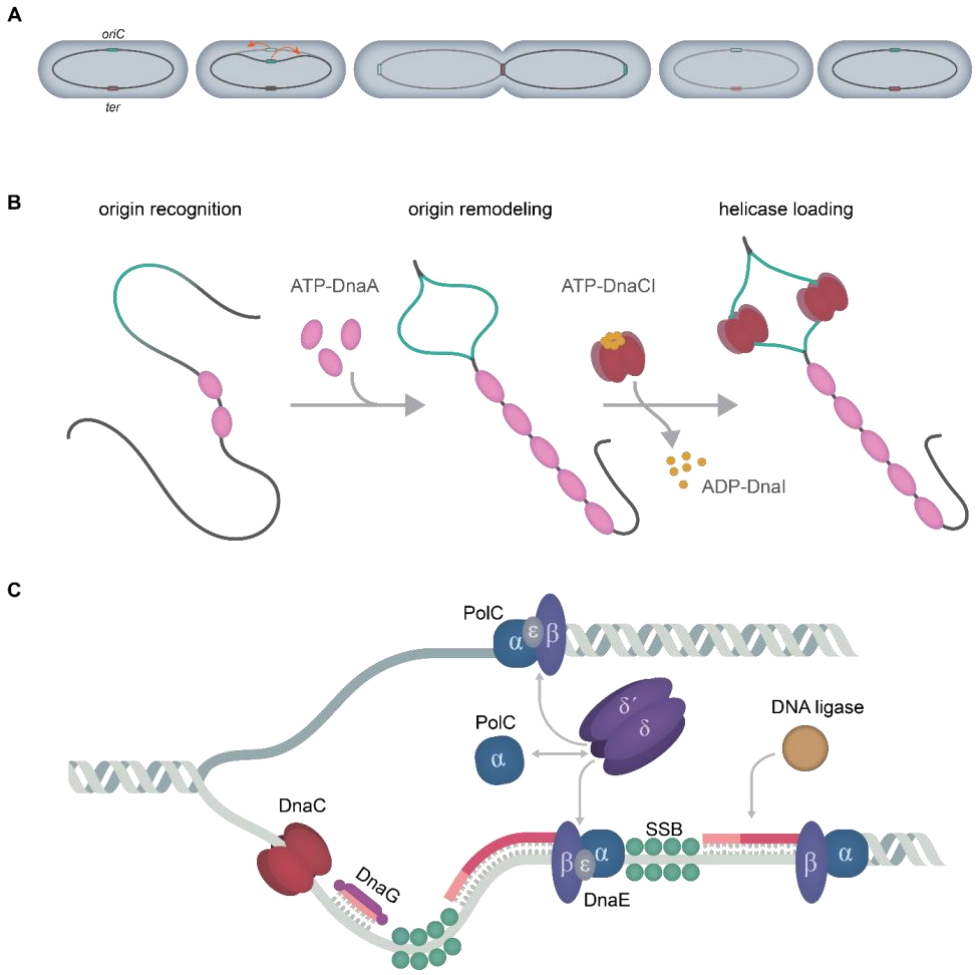

Figure 1. Schematic representation of *B. subtilis* DNA replication
(**A**) Schematic representation of the general process of DNA replication in circular chromosomes in bacteria. The origin of replication (blue) is the starting point of replication, which proceeds bidirectionally and ends in the terminator sequences (red) located opposite the *oriC*. (**B**) DnaA-mediated origin remodelling of *B. subtilis oriC*. DnaA (pink) associates as ATP–DnaA to the origin, where they oligomerize into a large nucleoprotein complex and melts the adjacent DNA-unwinding element (DUE, green). DnaI (yellow) load the helicase DnaC (red) in the unwound DUE by expending ATP. Figure adapted from Mott and Berger[22].(**C**) Illustration showing the locations of the helicase, primase, DNA polymerase, the β-clamp and the clamp loader (τ3δδ') at the replication fork in *B. subtilis*. Figure adapted from Jameson & Wilkinson[23].

B. subtilis uses two DNA polymerases, PolC and DnaE. DnaE is specific for the lagging strand synthesis, while PolC participates in both leading and lagging strand synthesis[24,25]. Evidence suggests that DnaE extends the RNA primer, and then PolC takes over and elongates the strand[25,26]. On the other hand, *E. coli* uses a single DNA polymerase enzyme, Pol III, which is composed of three subunits: the catalytic subunit, a proofreading subunit, and a non-essential subunit that may stimulate the activity of the proofreading subunit (for review [27]).

During replication, two replication fork proceed in opposite direction and are susceptible to inactivation when encountering roadblocks such as strand breaks or unrepaired DNA lesions[28]. Inactivation can provoke disassembly of the replisome and a collapse of the replication fork. Both DNA damage and collapsed forks stimulate the bacterial SOS response, a transcriptional response that controls genes involved in DNA replication, DNA repair, and cell division to maintain genome integrity and cell viability[29].

Once DNA damage occurs, the roadblocks at the forks form ssDNA, upon which RecA is loaded[29]. RecA is a highly conserved protein that composes a nucleoprotein filament with the ssDNA; this stimulates the self-cleavage of the SOS response master regulator LexA[29]. Thus, alleviating the transcriptional repression over SOS response genes[29].

1.1.3 Termination

In bacteria, replication elongation advances until the site of termination, situated roughly opposite to the initiation site (Reviewed in [30]). Replication elongation is blocked by *ter* sites that allow fork progression from only a single direction. This guarantees the complete replication of the chromosome after the forks arrive at a specific chromosomal region (terminus)[30]. In the case of *B. subtilis,* a replication termination protein Rtp (Tus in *E. coli*) binds to *ter* sites, blocking helicase progression and terminating DNA replication (reviewed in [11]). In organisms that initiate replication from multiple origins, replication typically ends in a sequence independant manner[30]. Replication forks move until they encounter another replication fork, where termination occurs.

DNA replication is mainly controlled at the step of initiation. Bacteria, such as *E. coli* and *B. subtilis*, can initiate new replication rounds before the previous one has finished, resulting in multifork replication[31]. Increased replication initiation enables faster duplication of the genome even though the elongation rate remains constant. Multifork replication occurs when bacteria are growing in nutrient rich conditions and results in each daughter cell receiving a chromosome with

multiple replication origins and replication forks[31]. In this case, cells divide faster while maintaining proper duplication of each daughter cell's genetic material. Under nutrient limitation or other stress conditions, bacteria reduce the initiation to match the growth rate, ensuring that resources are conserved[32].

1.2 Replication origins

Bacterial *oriC* regions vary remarkably in sequence, size (ranging from 250 bp to 2 kbp), and organization[33,34]. To prompt DNA replication initiation, DnaA, binds to consensus DNA elements at the *oriC*[35–38]. This binding starts DNA unwinding and, therefore, the beginning of replication[39–41]. The primary instruction to promote replication initiation is encoded in a region of the *oriC* filled with unique 9 nucleotide sequences called DnaA boxes, which form a framework for DnaA binding and assembly[42].

Origins of replication are classified as continuous or bipartite[41,43]. A continuous origin contains all its functional elements in one single intergenic region. On the contrary, bipartite origins contain those elements in two intergenic regions. For example, the *oriC* in *B. subtilis* is bipartite, containing two DnaA-box clusters separated by the *dnaA* gene[44,45] (Figure 2). In *E. coli*, the origin of replication is a continuous element.

During replication initiation, *B. subtilis oriC* forms looped structures, which are thought to be a consequence of its bipartite nature[46]. These looped structures can also develop in *E. coli oriC,* but expressing *E. coli* DnaA in *B. subtilis* does not promote unwinding[47]. This observation strengthens the notion that a mechanism of DnaA binding at the *oriC* leading to DnaA oligomerization is applicable across bacterial species. However, specific assembly and regulation of initiation encoded by each origin are likely to be species-specific.

The DnaA-boxes at the origin can be either 'strong' or 'weak' depending on their sequence conservation. The former bind both DnaA–ATP and DnaA–ADP with equal affinity, and the latter have a much greater relative affinity for DnaA–ATP[48]. DnaA can bind to both kinds of DnaA-boxes to oligomerize and induce DNA unwinding[49,50]. The DnaA–ATP recruitment is cooperative in *E. coli*. DnaA binding to strong boxes cooperatively improves DnaA binding to weak boxes, resulting in oligomer formation[49,51]. A recent publication revealed the contribution of the different DnaA-boxes in *B. subtilis* replication[52]. The authors found that the DnaA-boxes

6 and 7, adjacent to the DnaA-trios, are required for DnaA-dependent strand separation[52] (Figure 2).

The other elements that compose the origin are the DUE and the DnaA-trio. The DUE are cis-acting components that facilitate the replication origin melting[53]. The DnaA-trio is a conserved structural motif composed of a repeating trinucleotide motif. Its function is to stabilize DnaA filaments on a single DNA strand, which provides precision to this binding mechanism[54] (Figure 2), and additional binding sites for other proteins that can positively or negatively regulate the initiation process[41,43,55].

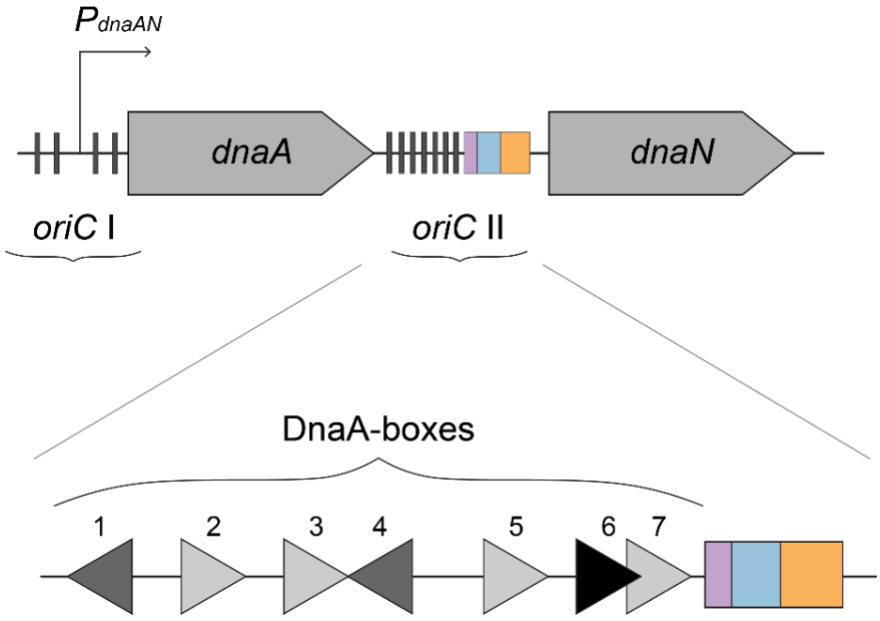

Figure 2 **Organization of the *oriC* region in *Bacillus subtilis*.**
Purple represents the GC-rich region, blue represents the open complex where the DnaA-trios are located and orange the DNA Unwinding Element (DUE). DnaA-box shade intensity correlates with its similarity to the consensus sequence. Modified from Richardson et al., 2016[56].

The origins of replication among bacterial species are well conserved, and most of them are located adjacent to the *dnaA* gene[57,58]. The genes flanking *oriC* and *dnaA* are conserved, consisting of the gene cluster *rnpA-rpmH-dnaA-dnaN-recF-gyrB-gyrA*. Unusually, the *oriC* of *E. coli* has undergone a significant rearrangement, resulting in the translocation of the origin 44 kb distant from the *dnaA* gene[58] so that it is instead flanked by the genes *gidA* and *mioC*[41]. Therefore, the origin of replication in *B. subtilis* may be more ancestral than that of *E. coli*. Hence, *B. subtilis* has a more representative organization that may provide a better model for bacterial replication origins[57] (Figure 3).

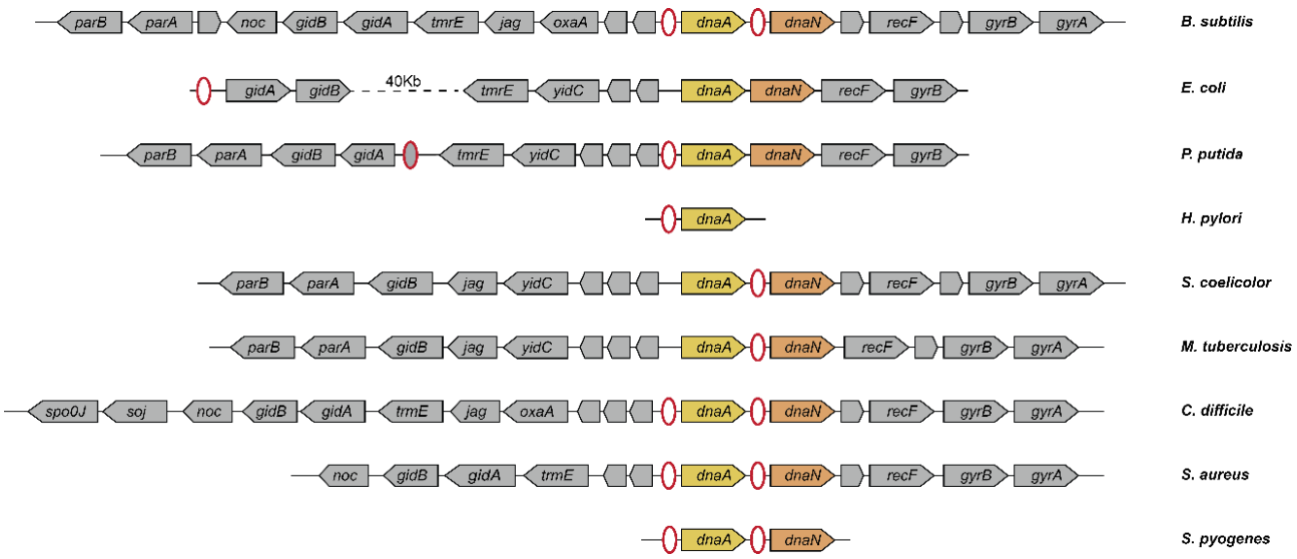

Figure 3. Origin of replication architecture across bacterial species.
Origins of replication are depicted as red circles, and replication initiation genes *dnaA* and *dnaN* are highlighted in yellow and orange, respectively, highlighting the shared structure among most bacteria. Modified from Briggs et al., 2012[57].

1.3 *Bacillus subtilis*

Bacillus subtilis is an aerobic, Gram-positive bacterium found in the soil with a diverse genetic manipulation toolbox that makes it a model organism for cell physiology and metabolism. Additionally, due to its highly efficient protein secretion system and adaptable metabolism, it has been broadly used as a cell factory for production of enzymes, chemicals, and antimicrobial materials for industry, agriculture, and medicine[59]. *B. subtilis* is also generally recognized as safe (GRAS)[60,61], which makes it desirable in industrial contexts. *B. subtilis* possesses physiological characteristics and an adaptable metabolism that facilitates its cultivation on inexpensive substrates. Additionally, *B. subtilis* single cell membrane facilitates protein secretion, simplifying downstream processing, and reducing the production costs[62].

During nutrient starvation, additional layers of DNA replication control are exerted in *B. subtilis* when it enters the pathway of sporulation, slow-growth phenotypes, or non-growing phenotypes (Further explained in: 1.5.2 Non-growing phenotypes). Much of our knowledge about the initiation of DNA replication comes from studies in the Gram-negative model organism *E. coli*. However, the location and structure of the *E. coli* origin of replication and the identification and study of the proteins which constitute the *E. coli* initiation complex suggest that it is not as universal as once thought[57]. An analysis of *oriC* in the Firmicutes species *B. subtilis* indicates that it may represent a better model for the ancestral bacterial origin of replication[57] (Figure 3). Finally, *B.*

subtilis has no known DNA replication regulators in common with *E. coli*[57]. Hence, in the next section, we will explain the replication initiation control of this bacterium.

1.4 Regulation of replication initiation in *B. subtilis*

Cells need to tightly regulate DNA replication initiation with the cell cycle to guarantee successful propagation. Deficiencies in regulating replication initiation are often detrimental to cell growth; therefore, this process is highly controlled (reviewed in [22]). Although *oriC*-dependent replication is the default mechanism in bacteria, some studies have described that in cells lacking RNase HI, replication initiates independently of DnaA and *oriC*, presumably at persisting RNA:DNA hybrids called R-loops[63,64]. However, under normal conditions, DNA replication regulation occurs primarily at the initiation stage, during or before recruiting the replication machinery[65].

The main mechanism for regulating DNA replication initiation in *B. subtilis* requires limiting cooperative binding of DnaA to the *oriC*[22]. There are four known proteins that regulate DnaA using this mechanism: YabA, DnaD, Soj, and SirA. Moreover, DnaA also autoregulates its own transcription[66]. Below the best characterized mechanisms of replication initiation are described.

1.4.1 DnaA

The initiator DnaA is a member of the AAA+ ATPase family and contains four distinct structural and functional domains[67,68]: (I) a helicase loading domain, (II) a linker domain, (III) an AAA+ (ATPase Associated with diverse cellular Activities) domain, and (IV) a DNA-binding domain[69]. In the cell, DnaA exists in both ATP- and ADP-bound forms[70]. DnaA–ATP is considered the 'active' form of the protein as this is required for oligomerization at the origin[71,72], an event that triggers DNA unwinding and ultimately assembly of the replisome. ATP hydrolysis following replication initiation subsequently inactivates DnaA[73,74].

B. subtilis possesses eight DnaA boxes (Figure 2). One of those boxes is in the promoter of *dnaA* and differs from the consensus sequence by one base. Two consensus DnaA boxes facing each other and placed 40 to 50 bp downstream of the *dnaAN* transcription start site showed the highest binding affinity in a footprinting analysis[70]. Deleting these two boxes also abolished the strong phenotype that this promoter region exerts when cloned on multicopy plasmids, likely

caused by the titration of DnaA away from the chromosomal origin[75]. These results suggest that these two consensus DnaA boxes significantly impact the autorepression of *dnaA* in *B. subtilis*. Autoregulation of *dnaA* has also been detected in other bacteria, like *E. coli*[76–78] and depends on the binding of the ATP-bound form of DnaA to DnaA boxes in its promoter region[79].

1.4.2 YabA

YabA is a small protein with two predicted domains: an N-terminal leucine zipper motif that probably facilitates protein-protein interactions and a potential C-terminal zinc cluster motif[16,80]. YabA is not homologous to other regulators of DnaA, but is conserved among low G+C Gram-positive bacteria[80,81]. YabA is a negative regulator of DnaA, and a mutation in *yabA* results in asynchronous initiation, whereas overexpression of *yabA* decreases replication initiation[80–82]. In vitro, YabA hinders cooperative binding of DnaA at the origin and prevents DnaA-DNA helix formation necessary for origin melting, independent of the ATPase activity of DnaA[83,84]. In vivo, YabA also prevents DnaA binding to the origin and other DnaA binding sites throughout the cell[83]. Besides interacting with DnaA, YabA was also found to interact with the DnaN. YabA can interact with DnaA and DnaN simultaneously, thereby forming a ternary DnaA-YabA-DnaN complex[80,85]. Fluorescently-tagged YabA colocalizes with the replisome during DNA replication through its interaction with DnaN, and recruits DnaA to the replisome[81,82,85]. In summary, YabA interacts with DnaA and DnaN titrating DnaA to avoid over-initiation of replication.

1.4.3 DnaD

DnaA recruits DnaD to the origin and, along with DnaB, is required to recruit the helicase loader DnaI[20]. In addition to its role in starting the replication initiation, DnaD also negatively regulates DnaA binding at the origin. In vitro, DnaD inhibits cooperative binding of DnaA at the origin[86] and inhibits DnaA-DNA helix formation[84]. Like YabA, DnaD does not affect the ATPase activity of DnaA[86]. The effects of DnaD on replication initiation have not been studied in vivo, as it is an essential protein. DnaD also associates with DnaA at other DnaA binding sites throughout the chromosome. It is also proposed that DnaA and DnaD cooperate at *oriC* to melt the DNA duplex during replication initiation[87].

1.4.4 Soj

Soj is a negative regulator of DnaA that inhibits DnaA-DNA helix formation at the origin[88]. Soj is a homolog of the chromosome partitioning protein (ParA) and was isolated as a suppressor of Spo0J (ParB) [89]. The conserved Par system functions by partitioning chromosomes and low-copy plasmids in bacteria and is composed of two trans-acting factors, ParA, which interacts with ParB[90,91]. Spo0J (ParB) binds to *parS* sites in the chromosome near *oriC*[92,93]. The *parS* sites facilitate the spreading of Spo0J to nearby DNA regions, creating large nucleoprotein complexes around the *parS* sites[94,95]. The Spo0J-*parS* partitioning complex is required to recruit the structural maintenance of chromosomes (SMC) protein complex to the *oriC* region and ensure proper DNA segregation.

Soj (ParA) is a Walker-type ATPase that binds cooperatively to non-specific DNA when in an ATP-bound dimer form and helps segregate chromosomes through its interaction with Spo0J[96,97]. Spo0J stimulates the ATP hydrolysis activity of Soj, causing Soj to dissociate from DNA[96,98]. When unbound to ATP, Soj exists in a monomeric state capable of binding DnaA and inhibiting DnaA-DNA helix formation at the origin[1,2]. Dimeric Soj bound to DNA near the origin relieves this inhibition and stimulates replication initiation[98].

1.4.5 SirA

SirA is the sporulation inhibitor of replication and inhibits DNA replication initiation during the transition from vegetative growth to sporulation[99]. Under starvation conditions, cells activate a phosphorelay pathway that results in phosphorylation (activation) of the transcriptional regulator, SpoOA, which is the main determinant for entering sporulation[100]. Cells entering sporulation undergo asymmetrical division, producing a larger mother cell and a smaller forespore[101,102]. A final round of DNA replication results in one chromosome remaining in the mother cell, while the other is transported to the forespore[101,103]. DNA replication must be regulated to ensure the chromosome copy number is at two upon entering sporulation. SirA expression is activated by the master sporulation regulator SpoOA[104,105]. SirA directly binds to the N-terminus of DnaA and co-localizes with DnaA at the origin[106,107]. SirA negatively inhibits replication initiation in cells entering sporulation by preventing DnaA binding at the origin[105,106]. Artificial expression of *sirA* during vegetative growth is conditionally lethal and leads to anucleate cells and guillotined chromosomes [105,106].

1.5 Life without Replication

1.5.1 Processes that influence replication in bacteria

Some bacteria, such as *B. subtilis,* can adopt different non-growing or slow-growing phenotypes depending on their exposed stress (Figure 4). In conditions of nutrient starvation, and other conditions like UV radiation or temperature changes, a subpopulation of *B. subtilis* cells can sporulate[100,108]. Endospores contain the full copy of the cells genetic material and can resume growth when the conditions become favourable again. On the other hand, non-sporulating *B. subtilis* cells can also survive different stresses by acquiring a vegetative but slow-growing phenotype[109]. The transcriptome analysis of these cells revealed that they are distinct from exponential and stationary phase cells, adopting a "oligotrophic growth state"[109]. The main environmental processes that influence replication in bacteria are discussed in detail below.

1.5.1.1 Nutrient limitation

Starvation is one of the main reasons for growth arrest in the biosphere. Most bacteria in natural environments do not grow because they lack essential nutrients like carbon, nitrogen, phosphate, oxygen, or other relevant trace elements[110] (Figure 4A). Under laboratory conditions, when microbes lack the nutrients necessary for growth, they enter stationary phase. When energy sources are no longer present in the environment, they must decide whether to continue to use their metabolic program to harvest the available energy.

Carbon starvation: *E. coli* exhibits a wide range of phenotypes under nutrient limitation[111]. In contrast, the phenotype of *B. subtilis* is dominated by the possibility to form endospores under these conditions[112]. Switching bacteria from a medium rich in carbon sources like glucose to one without it causes adaptation at the transcriptional and metabolic level[111]. In *E. coli*, this switch remodels the bacterial response after 5 minutes of carbon exhaustion with a remarkably high CO_2 and energy production rate that lasts for several hours despite a non-growing phenotype[111]. Multi-omic data revealed that this phenomenon is caused by *E. coli* feeding on internal sources such as glycogen, proteins, and RNA during this phase. Consequently, non-growing bacteria continue to be metabolically active even in the absence of external carbon sources. In *B. subtilis*, analysis of protein reallocation during glucose starvation showed that biomass appeared to be reallocated from proteins involved in amino acid biosynthesis to enzymes of the central carbon metabolism[113–

[115]. Additionally, *B. subtilis* can also acquire a persister phenotype propelled by exposure to antibiotics or increased ppGpp levels[116].

Nitrogen starvation: Nitrogen is an essential nutrient that constitutes approximately 12% of the biomass in bacteria, and its external supply is necessary for growth[110]. Because nitrogen limitation is often used to control bacteria growth in industrial bioprocesses, many researchers aim to characterize nitrogen starved cells. *E. coli* cells cease growth in the absence of nitrogen but continue consuming glucose at an around 20-fold lower rate than during exponential growth[110,117], showing accumulation of alpha-ketoglutarate, a metabolite from the tricarboxylic acid cycle (TCA) that inhibits glucose uptake by the phosphotransferase system[118]. Apart from lower overall fluxes in central carbon metabolism, flux distributions in the tricarboxylic acid (TCA) cycle during nitrogen starvation are comparable to non-starved growth conditions[117]. Similarly, the glucose uptake rate in *B. subtilis* cells that cannot undergo sporulation under nitrogen starvation was similar to that of *E. coli*[112]. This suggests that cells have a substantial energy demand met by the TCA cycle even in absence of growth.

Phosphate starvation: Phosphate starvation is a less explored nutrient than carbon and nitrogen. In *E. coli*, the most significant changes in phosphate starving cells' metabolic levels are phosphorylated metabolites, such as sugar-phosphates and ATP[112]. Glucose uptake rate during phosphate starvation is 10% lower than in exponentially growing cells but is still higher than in nitrogen starved cells. A possible reason for the elevated glucose uptake could be a compensation for the high decrease in the energy charge. In *B. subtilis*, phosphate starvation is regulated by the phosphate stimulon, which consists of two main regulators: the phosphate starvation-specific Pho regulon and the σ^B general stress regulon[119]. There is also a small group of phosphate starvation-induced proteins (e.g., YjbC, YfhM, and YxiE) with unknown control mechanism[119].

1.5.1.2 Environmental factors

Several environmental factors such as oxygen, temperature, and pH can affect bacterial growth and survival (Figure 4B). However, bacteria have adapted to survive different stress conditions due to their ubiquitous nature (Figure 3B). Below a brief description of these factors.

Oxygen: Many bacteria switch to fermentative metabolism in the absence of oxygen. Nevertheless, obligate aerobes stop growth without oxygen. One of the best-studied obligate aerobes is *Mycobacterium tuberculosis*, which enters a non-growing state upon oxygen depletion[120]. This bacterium encounters oxygen scarcity under infection conditions in its host due

to the host immune response. During a hypoxic growth arrest, *M. tuberculosis* maintains its NAD+/NADH ratio. In bacteria, the NADH/NAD+ ratio is a key indicator of adaptability to an environment and community structure. *M. tuberculosis* achieves this by inhibiting fatty acid catabolism and switching the carbon flux towards the reductive TCA cycle[120].

pH: The pH of the environment can also arrest growth by altering the proton gradient around the cell membrane, thus disrupting the proton motif force resulting in less ATP. Bacteria possess several metabolic responses that allow them to survive and grow at critical pH values, mainly increasing proton motif force. *B. subtilis* responds to high pH levels by upregulating various cytochrome oxidase complexes and low pH levels by upregulating ATPases to compensate for a less efficient energy generation under those conditions[121]. Similarly, deletion of the F(1)Fo-ATPase in *E. coli* decreased survival at low pH values[122].

Salt stress: Other environmental factors such as high salt concentrations and hyperosmotic stress can also result in growth arrest. These conditions trigger water release from the cell to the environment or medium. The proteome and transcriptome profiles of stationary *B. subtilis* under 6% NaCl conditions indicate a general stress response[123,124]. Many proteins and transcripts that were upregulated were associated with the σ^B regulon[125]. Additionally, salt stress activates the import of potassium (K+) ions, which trigger the synthesis[123] and import[126] of the osmoprotectant proline. Under salt stress conditions, proline is no longer synthesized by ProB and ProI, whose activity is decreased by high proline levels[125]. Instead, the isoenzymes ProJ and ProH are upregulated, whose activity is not inhibited by proline levels, allowing the production of high cellular levels of proline[125].

1.5.1.3 Stress-modulating factors

Reactive oxygen species (ROS): ROS can also induce growth arrest (Figure 4C). The challenge with ROS is that they can rapidly damage different cell components. Thus, bacteria need a fast response against them. *E. coli*, for instance, respond within less than 5 s to the addition of H_2O_2 by increasing the flux through the pentose phosphate pathway (PPP), which leads to overproduction of NADPH that is necessary for ROS scavenging[127]. A multi-omics characterization of *Salmonella enterica* response to ROS showed that the most downregulated proteins under this stress are the ones in the citric acid cycle (TCA cycle)[128]. In *B. subtilis*, the superoxide specific marker proteins MetE and YitJ are involved in methionine biosynthesis and regulated by the S-box transcription anti-termination system[129]. Further superoxide-specific marker proteins are YbaL and YpsC[129].

Antibiotic exposure: Antibiotics to treat bacterial infections can lead to different outcomes; one is cell death, and the other is a non-growing state (Figure 4C). The small subpopulation of bacteria that are growth-arrested upon antibiotic exposure is called persisters[130]. Several studies showed that metabolism impacts the efficacy of antibiotics and that antibiotics impact bacterial metabolism[131,132].

Although antibiotics perturb the metabolome and prevent growth, it appears that cells can retain a high metabolic activity. In one study, *E. coli* and *S. aureus* treated with the Chloramphenicol and Linezolid (translational inhibitors) continued to use oxygen at a rate two-fold lower than normal growth conditions although their growth was halted[133]. Moreover, metabolome data shows an excess of amino acids, nucleotides, and TCA cycle intermediates, displaying an imbalance of these molecules in the cell due to the arrested translation, cell growth and respiration. When *Vibrio cholerae* cells were treated with tetracycline, their induced non-growing cells showed an constant glycolysis flux compared to growing cells[134]. Likewise, metabolomics data demonstrated the accumulation of specific metabolites. Thus, bacteria do not coordinate protein synthesis with metabolism when translation is arrested by blockage of the ribosome.

Antibiotic-induced persisters in *B. subtilis* stem from a metabolic switch, GTP depletion by ppGpp induction. Brief exposure to a sublethal dosage of bactericidal cell wall antibiotic can increase the surviving portion of the cells, allowing antibiotic resistance in the population[116]. In summary, under antibiotic exposure, some bacteria are non-growing but retain their metabolic activity, which can result is an increase of biomass-associated precursors and energy.

1.5.1.4 Biotechnology approaches

Cell cycle control can explain many processes involved in replication and metabolism[135–138]. Therefore, synthetic biology and metabolic engineering aim to provide novel methods to control the rate of bacterial replication or growth rate and integrate them into genetic circuits for productive phenotypes[139].

In industrially relevant contexts, as cells enter a non-growing but metabolically active state, the synthesis of desirable proteins and metabolites becomes limited. For instance, *Lactobacillus lactis* gradually loses its ability to grow on solid media within weeks under carbon starvation, but maintained intact cell membrane and metabolic activity for months[140]. Under such conditions, cell

response might vary between species, but induction of the stringent response is generally observed. Moreover, transcription and translational machinery, DNA replication, and cell division are strongly repressed under these conditions[141].

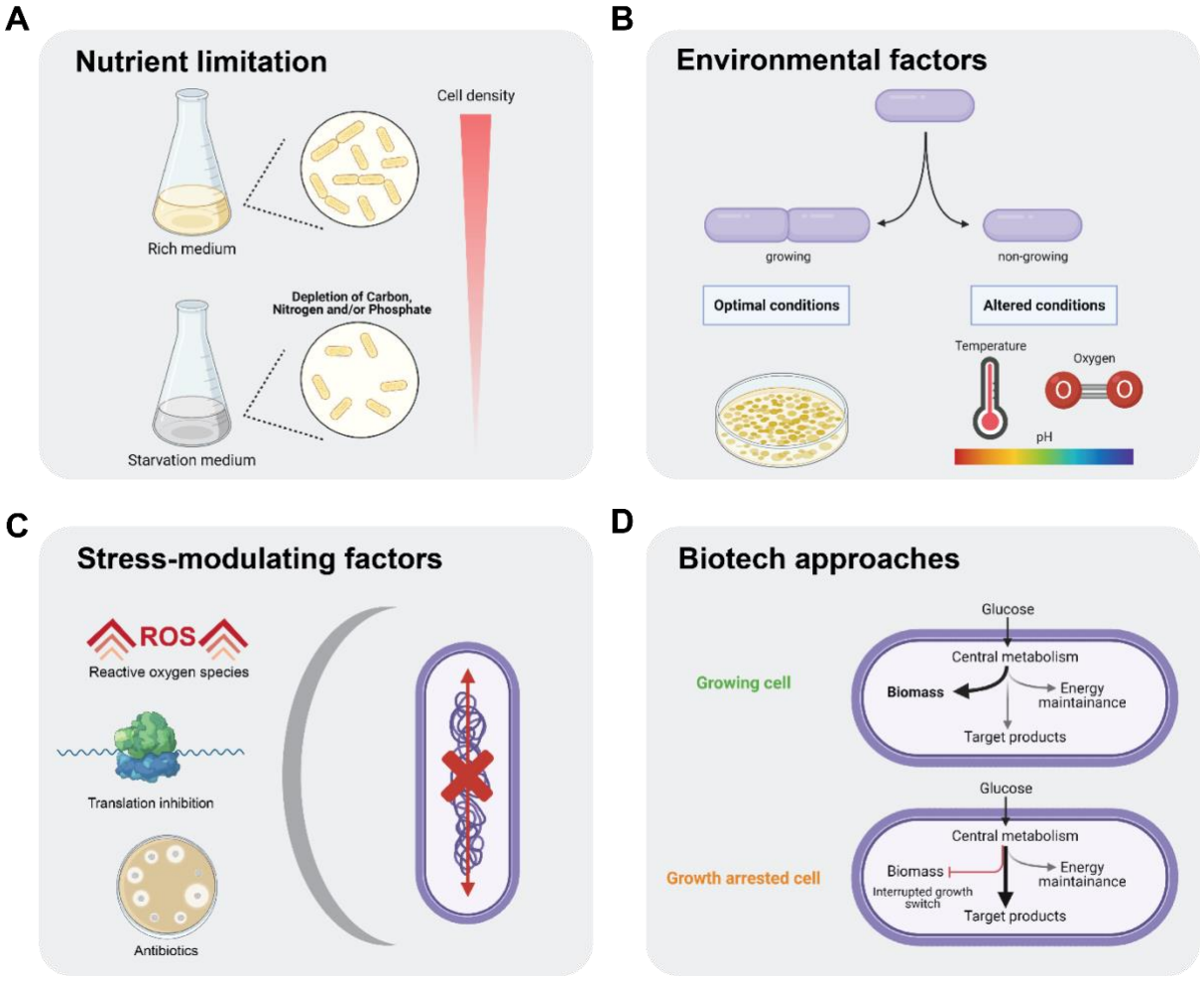

Figure 4. Factors leading to non-growing phenotypes.
(A) Nutrient starvation consists of depleting of carbon, nitrogen, and/or phosphate, limiting bacterial growth. Normally, chemically defined media and minimal media are used for these purposes. (B) Altering environmental conditions such as oxygen, temperature and pH can lead to non-growing phenotypes. (C) Several stress modulating factors can inhibit cell growth and cell replication. The most common ones are reactive oxygen species, translation inhibition with different chemical components and antibiotic exposure. (D) Carbon flux can be redirected from biomass to production of proteins, chemicals, or metabolites of interest upon activation of genetic switches that controls growth. Figure modified from Li and others, 2016[142]. Some parts of this figure were created with BioRender.com

To avoid the drawbacks during industrial processes, metabolic engineering aims to create producer cells that repurpose biomass formation resources to proteins and metabolite synthesis[143]

(Figure 4D). For this reason, the metabolism of non-growing cells could be adavatageous for metabolite production and safety. Non-growing cells can be generated, for example, through the conversion of biogenic amines[144] or the depletion of nutrients, as mentioned above.

Different approaches can be used to identify suitable targets for growth inhibition. A common approach is based on gene knockouts, where essential genes for cell growth can be identified by the failure of constructing knockout mutants or by conditional lethality. On the other hand, the controlled silencing of genes is an attractive alternative to gene deletions.

CRISPR interference (CRISPRi) (explained in the next section) has been used to unravel growth switches suitable for decoupling growth and enhancing protein production[142,145]. Using a sgRNA library of 12238 loci in the *E. coli* genome, the authors identified targets that inhibited growth and continued GFP production[145]. Overall, the study provided key targets to understand and produce non-growing phenotypes of industrial relevance.

Other non-growing phenotypes that are at the interface between living and non-living are SimCells (Simple Cells[146,147]. SimCells are genome-free bacterial cells that provide a chassis to insert cellular functions to produce desirable metabolites[146]. So far, they have been generated in *E. coli*, *Pseudomonas putida*, and *Ralstonia eutropha* by removing the native chromosome through inducible degradation and replacing it with synthetic genetic circuits targeted to produce potential anticancer drugs like catechol[147]. One of the most significant advantages of this approach is that cell chassis are maintained over long periods of time and the absence of chromosome makes them safe and easy to use in industry[146–148].

1.5.2 Methods used to study replication arrest

RepN/oriN: Several approaches have been used to study the consequences of the lack of replication or cell division in bacteria. The first studies unraveling the role of the *oriC* involved generating *oriC*-deleted mutants by integrating a plasmid replicon into the chromosome[149]. The activity of the plasmid origin (*oriN*) required its cognate initiator protein (RepN), and both of them act independently of native *oriC*/DnaA[149]. This allowed the deletion of the native *oriC* facilitating the detection of essential sequences without selecting suppressor mutants.

Conditional mutants: Other ways to study replication and division arrest consist of genetic and chemical methods to conditionally block proteins associated with cell growth, division, or replication. For example, Arjes *et al.* in 2014 showed that conditionally blocking the cell division

initiator protein, FtsZ, inhibits cell division in *B. subtilis* and *Staphylococcus aureus*. Interestingly, inhibited cell division led to DNA replication arrest, which resulted in reduced cell growth. Arrested cells were metabolically active but could not initiate new rounds of either DNA replication or division, even when supplied with enough nutrients or when returned to permissive conditions[150].

Fluorescence-activated cell sorting (FACS) and microfluidics: Significant constraints in the complete characterization of non-growing phenotypes are the cell overgrowth of remaining growing phenotypes and isolation of enough cell material to conduct multi-omics approaches. However, the recent advances in bacterial flow cytometry and microfluidics have facilitated the description of non-growing phenotypes at the single-cell level. For example, a proportion of *Salmonella* cells can enter a reversible state of growth arrest, which allows them to tolerate environmental stress such as antibiotics. By performing fluorescence-activated cell sorting (FACS) in enriched non-growing cells and dual-RNAseq, they found these cells are not dormant but are actively modulating their environment[151]. Moreover, persister *S. aureus* has been recovered, isolated and enriched directly from persistent infections and show by multi-omics approaches that host-mediated stress and antibiotic exposure were the factors that persister formation[152].

Synthetic biology approaches: This alternative approach that combines engineering and molecular biology tools has been used to produce non-growing phenotypes at a larger scale. These genetic circuits[139,153] and CRISPRi growth switches[142,145,154] have led to the creation of non-replicating and non-growing phenotypes allowing new methods for cell synchronization[155], different cell size variants and understanding the underlying physical principles of cell size and replication control, or to repurpose biomass formation to metabolite or protein production in industrially relevant contexts[142,145].

The generation of non-growing phenotypes teaches us more about bacterial cell physiology under conditions where bacteria are not actively replicating. In fact, in natural environments like the soil or infection contexts, bacteria do not face optimal conditions[109,156].

Temperature-sensitive mutants: Temperature-sensitive (Ts) mutants affecting replication have been described in several bacterial species. Ts mutants possess a single mutation in a gene, whose gene products are active under permissive temperatures but display a marked drop in the activity under non-permissive temperatures. On many occasions, the effect is reversible; therefore, returning to optimal temperatures reinstates the activity of the gene product to levels similar to the wild type. In *E. coli*, large-scale screening of about 1.4 million colonies was evaluated for

thermosensitive DNA replication. Among the 2266 Ts mutants discovered, 110 could not undergo DNA synthesis but retained protein synthesis at 41 degrees[158].

In *Bacillus subtilis*, one of the most common temperature-sensitive mutants is located in the *dnaA* gene. In this strain, bacteria could not grow at non-permissive conditions (49°C)[159]. A single amino acid mutation in DnaA can obstruct replication initiation in this strain, and the cell can resume growth once returned to a permissive temperature[159]. The initial observation proposed that the amount of DnaA determines the potential of the cell to initiate replication[159]. However, more recent studies have challenged this premise, indicating that the amount of DnaA may not determine the level of DNA replication initiation. To test this hypothesis, cell division was challenged by lowering the amount of DnaA in the cell, but this did not affect DNA replication initiation[160]. The use of Ts mutants also allowed the observation that *oriC* remains associated with the membrane throughout the DNA replication cycle, in a DnaA-dependent manner[161]. New studies have indicated that *B. subtilis* regulates initiation, in part, by controlling the interaction between DnaB and DnaD at the membrane, thereby regulating the activity of the helicase loader DnaC[17].

Other connections that link replication with DNA synthesis have been studied in *B. subtilis* by isolating Ts mutants[162–164]. In *Staphylococcus aureus*, similar replication Ts mutants were derived by point mutations in DnaB and DnaI, and confirmed the involvement of these two proteins in the synchronous regulation of chromosome replication[19].

1.6 Using CRISPR and CRISPRi

Bacteria are the most abundant life form on earth but are outnumbered by bacteriophages, viruses that specifically infect bacteria[165]. Bacteria have evolved various mechanisms to protect themselves from phages. Bacterial defense mechanisms include: (i) preventing phage adsorption, (ii) inhibiting injection of the phage genome into the cell, (iii) cutting the phage genome, or (iv) aborting a later step of the lytic cycle (Reviewed in [165–168]).

Innate bacterial defense mechanisms include restriction-modification and abortive infection systems. More specific immunity against bacteriophages and other mobile genetic elements is provided by adaptive defense mechanisms, such as CRISPR (Clustered Regularly Interspaced Short Palindromic Repeat)-Cas (CRISPR-associated)[169,170]. In this process, a short DNA sequence of the phage is integrated into the CRISPR loci, an operon of genes that code for the CRISPR-associated (Cas) proteins and a CRISPR array consisting of a library of captured foreign DNA sequences from former infections, interspaced by short identical

repeats, producing sequence-specific immunity against the invading bacteriophage. CRISPR-Cas systems have been classified into two classes, six types and additional subtypes. Here, we focus on the bacterial type II CRISPR-Cas system, which contains the dual-RNA-guided endonuclease Cas9 and has been extensively studied and increasingly used as a genome-editing tool[171–176], and its modified version called CRISPRi, which has been widely used to control gene expression in bacteria (Reviewed in [177]).

1.6.1 CRISPR-Cas9

Class 2 CRISPR systems have been harnessed into a versatile and powerful programmable genome editing and engineering technology. To reprogram a CRISPR system, one can simply replace the native sequences in the CRISPR array with the desired target sequences and rely on the natural processing and assembly of the ribonucleoprotein complex. Type II systems depend on a ternary complex comprising the effector (Cas9), the processed crRNA, and a trans-activating CRISPR RNA (tracrRNA), which both form an RNA duplex through the complementarity of the tracrRNA to the repeat regions of the crRNA[172]. This duplex RNA is recognized by Cas9, leading to processing into short crRNAs.

As an alternative, it is possible to create a chimeric RNA between the crRNA and the tracrRNA, referred to as single guide RNA (sgRNA)[178]. The single chimeric sgRNA sequence can be designed and directed with Cas9 to promote sequence-specific cleavage[179] (Figure 5A). However, not all positions in a genome can be targeted by Cas9. The target sequence of type II complexes must be flanked by a DNA motif called the protospacer-adjacent motif (PAM) (Figure 5A). "Protospacer" designates the part of phage DNA that will eventually be incorporated into the CRISPR array during CRISPR adaptation. The PAM is required to select novel spacers to be acquired and identify target sequences during the interference step to prevent self-targeting[180–182]. The PAM used by Cas9 from *Streptococcus pyogenes* (SpCas9) is an NGG motif on the 3` side of the target[183]. The PAM length determines the frequency of possible targets: on average, SpCas9 has one target every 8 bp in the *E. coli* genome if both DNA strands are considered. This depends on the targeted genome's characteristics: as SpCas9's canonical PAM is NGG, it is not as common in genomes with a low GC content, such as *B. subtilis*.

After binding to the DNA, the CRISPR effector starts to unwrap the DNA from the PAM side[184]. As the DNA unwinds, the guide RNA progressively forms a hybrid with the target DNA[185].

This structure is called the R loop. When the entire guide is annealed, a conformational shift occurs within Cas9, and a double-strand break (DSB) is introduced in the DNA[174,184,186,187]. This unique property of Cas9 has been used to select rare mutants in a population or develop sequence-specific antimicrobials. The resulting DSB is mainly repaired by (i) homologous recombination (HR) and (ii) non-homologous end joining (NHEJ) pathway (Figure 5A). An additional repair mechanism called alternative end-joining (AEJ; also referred to as microhomology-mediated repair, MMEJ)[188–190] has also been described in several bacteria.

1.6.1.1 DSB repair by homologous recombination (HR)

Type II CRISPR-Cas systems introduce a DSB at the same position in all copies of the target DNA molecule[191], and the concomitant lack of an intact DNA template should preclude the repair of these DSB by HR. In bacteria, DSBs are repaired by homologous recombination using an undamaged DNA template[192], usually a sister chromosome that is newly being formed by replication. This is specifically true during logarithmic growth when bacteria undergo multifork replication[4,31,193,194]. A repair template is usually provided via a plasmid system containing a selection marker to create chromosomal deletions or insertions via CRISPR-Cas9 in bacteria. Such template contains flanking homologous regions of the cleavage site to mend the Cas9 DBS via Homologous recombination[195,196].

The AddAB and RecBCD helicase-nucleases are related enzymes prevalent among bacteria and instrumental in repairing DNA double-strand breaks and genetic recombination[197]. The well-studied RecBCD complex recognizes and processes DNA ends and loads multiple RecA proteins onto resected single-stranded DNA, facilitating homologous recombination leading to the accurate repair of the chromosomal DNA break[198].

1.6.1.2 DBS repair by non-homologous end joining (NHEJ)

Although ubiquitously found in eukaryotes, NHEJ is not universally present in bacteria, *Bacillus subtilis* is one of the few bacterial species that encodes a NHEJ system[199] and does not contain an endogenous CRISPR system. Per definition, NHEJ repairs DSB without requiring a homologous repair template[200] and can mend the DBS generated by Cas9. In bacteria, the NHEJ system entails two core proteins: the DNA-end binding protein Ku and an ATP-dependant DNA ligase LigD[201]. Ku binds at the DSB and recruits the ligase to repair the break[202,203]. LigD usually perform the ligation, but Ku can also recruit other ligases in the absence of LigD[200]. It is widely

accepted that NHEJ aids DSB repair in bacteria when only one single copy of the genome is available, either after sporulation or during extended periods of stationary phase[204,205]. NHEJ repair was also shown to participate in stationary-phase mutagenesis during carbon starvation in *P. putida*[206], resulting in up to 50% error rates in certain bacteria[202].

1.6.2 CRISPRi

The nuclease activity of CRISPR effectors can be eliminated by mutating the catalytic residues for type II and V systems to prevent gene expression without cutting the target DNA[207–209]. In particular, the CRISPRi (short for CRISPR interference) approach uses a Cas9 protein without the endonuclease activity (dead-Cas9) to create gene knockdowns. It has been an especially valuable tool to control gene expression and study essential genes in a wide range of bacteria[210–214] (Figure 5B). The binding of dCas9 to the promoter region of a gene can efficiently block its transcription[208,209] (Figure 5B), and targeting dCas9 to any protein-recognized DNA sequence may hinder protein-DNA interactions specific to that region.

The RNA polymerase (RNAP) can actively displace dCas9 and continue elongation to produce a full mRNA transcript depending on the strength of the interaction between the dCas9/sgRNA complex and the target[214]. When the target is a promoter sequence, any DNA strand can be targeted, and the repression will be equally strong for type II systems[208,215]. In contrast, when the target is inside the coding sequence, target orientation is crucial. For dCas9, repression is only effective when the sgRNA pairs with the non-template strand. If dCas9 binds to the template strand, the repressive effect is much weaker[215].

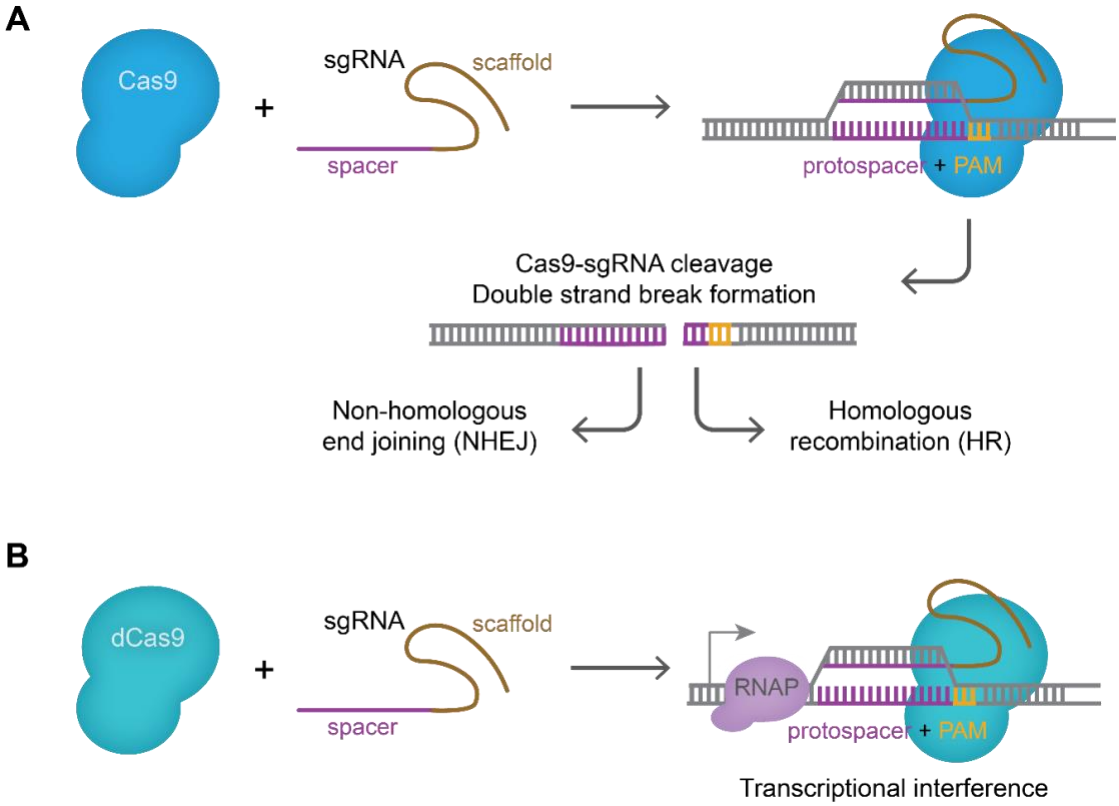

Figure 5. Cas9-sgRNA editing and dCas9 transcriptional interference.
(A) Cas9 (blue) binds to the sgRNA that is composed of a scaffold (brown) and a spacer (purple) sequence that is complementary to the protospacer sequence in the host. The protospacer sequence is upstream of a PAM (yellow) sequence. When the complex Cas9-sgRNA cleave both DNA strands in the host, the repair mechanisms are either NHEJ or HR. (B) dCas9 (light blue) is Cas9 without the nuclease activity. When it is in complex with the sgRNA, it bInds to the protospacer sequence creating a block in the DNA, blocking RNA polymerase (RNAP in lilac) from transcribing.

CRISPRi studies on replication initiation have unveiled different bacterial responses to replication arrest. For instance, one study performed in *E. coli* developed a system for controlling the bacterial cell cycle based on CRISPR/dCas9 binding to *dnaA* boxes[154]. The authors observed that the system could block replication initiation and that cells stay metabolically active and accumulate cell mass upon arrest. Other studies in *E. coli* targeted specific genes related to cell growth and replication to aim to have a non-growing producer strain to enhance protein production[142,145].

In *B. subtilis,* the phenotypes observed when knocking down *dnaA* led to two different observations of cell bending and growth halting[212], while in *S. pneumonia*, the main observation was the appearance of anucleated cells[213]. Different phenotypes in these studies can be explained by the mechanistic differences between DNA replication regulation, cell division, growth and cell cycle progression in other species, and the organization and location of *oriC*.

2. Aims

The effect of replication arrest in *B. subtilis* has been studied with different methods: antibiotic addition, ts mutants, nutrient scarcity, among others. However, these approaches are not ideal for performing a global characterization of non-replicating cells because they cannot be performed under physiological conditions, induce stress responses, or create heterogeneous populations of bacteria.

This work aims to characterize life without replication in *B. subtilis*, and to determine the general physiological adaptations upon replication arrest, by including a global proteomic characterization. Furthermore, we aim to evaluate responses to the lack of DNA replication initiation in a homogeneous population using two methods. One by deleting the replication initiation genes and the *oriC,* and the second one by creating a replication block in *oriC* so that DnaA cannot initiate replication.

3. Materials and methods

3.1 Contributions

The methods used in this thesis were performed, if not specified, by myself (V.M.) or by myself together with Katja Smidt (K.S.). I also performed some of the experimental work and data analysis with the help of some researchers. Dr. Knut Finstermeier (K.F.) for the design of the optimal protospacer, Timothy Sullivan (T.S.) for the election of the sgRNA for the CRISPRi approach, Dr. Fabian Cornejo (F.A.C.) for the proteomics data analysis, and Christian Frese (C.F.) for the proteomics sample preparation and data analysis. Several strains were created in collaboration with Silke Hackenschmidt (S.H.) from TU Darmstadt.

3.2 Bacterial strains, plasmids and oligonucleotides

Bacterial strains, plasmids and oligonucleotides used in this study are listed in Table 1, Table 2 and Table 3, respectively.

Table 1. Bacterial strains used in this study

Strain	Relevant characteristics[a]	Source
***Escherichia coli* strains – Hosts for cloning**		
RDN204 (Top10)	K12 strain, F⁻ *mcrA* Δ*(mrr-hsdRMS-mcrBC)* φ80d*lacZ*Δ*M15* Δ*lacX74 recA1 araD139* Δ*(ara-leu)7697 galU galK* λ⁻ *rpsL endA1 nupG*; SmR	Invitrogen
NEB 5-alpha	K12 strain, *fhuA2*::IS2 Δ*(mmuP-mhpD)169* Δ*phoA8 glnX44* φ80d[Δ*lacZ58(M15)*] *rfbD1 gyrA96 luxS11 recA1 endA1 rph*^{WT} *thiE1 hsd*R17	NEB, Anton & Raleigh, 2016[216]
TransforMax™ EPI300™	K12 strain, F⁻ *mcrA* Δ*(mrr-hsdRMS-mcrBC)* φ80d*lacZ*ΔM15 Δ*lacX74 recA1 endA1 araD139* Δ*(ara-leu)7697 galU galK* λ⁻ *rpsL nupG araC–*P_{BAD}*–trfA203-dhfr-1*; SmR, TmpR	Lucigen
***Bacillus subtilis* strains**		
EC3017	PY79, wildtype, *trpC2* prototroph	Youngman et al, 1984[217]
EC3136	EC3017 Δ*sigF*::lox72	S.H. TU Darmstadt
EC2829	EC3136Δ*skf*::lox72	S.H. TU Darmstadt
EC2833	EC2829*chr*(nt 4033341)::P_{degQ36}-*gfpmut2*(Δnt549-717)-artPS	S.H. TU Darmstadt

EC2835	EC2833*chr*(nt 3081):*mKate2*-artPS-*gfpmut2*(Δnt1-58)	S.H. TU Darmstadt
EC2836	EC2829 (pEC2420)	This work
EC2837	EC2833 (pEC2420)	This work
EC2838	EC2835 (pEC2420)	This work
EC2839	EC2829 (pEC2424)	This work
EC2840	EC2833 (pEC2424)	This work
EC2841	EC2835 (pEC2424)	This work
EC3274	EC3136 *amyE*::P_{degQ36}-*gfpmut2* SpcR	S.H. TU Darmstadt
EC3275	EC3136 *amyE*::$P_{hyperspank}$-*gfpmut2* SpcR	S.H. TU Darmstadt
EC3276	EC2833 3081:: P_{manP}-*cas9,* lox71-P_{spc}-*spcR*-lox66_artPS_ *(gfpmut2*(Δnt1-548)-*kan*R, AmpR	This work
EC3277	EC2829 *amyE*::P_{degq36}*gfpmut2,* KanR	This work
EC3137	EC3017 *lacA*::P_{xyl}-*dcas9,* ErmR	This work
EC3139	EC3136 *lacA*::P_{xyl}-*dcas9,* ErmR	This work
EC3146	EC3137 *amyE*::P_{veg}-sgRNA^{box1-2} ; CmR, ErmR	This work
EC3147	EC3137 *amyE*::P_{veg}-sgRNA^{box6-7}; CmR, ErmR	This work
EC3149	EC3137 *amyE*::P_{veg}-sgRNA^{box3-4}; CmR, ErmR	This work
EC3157	EC3139 *amyE*::P_{veg}-sgRNA^{box1-2}; CmR, ErmR	This work
EC3159	EC3139 *amyE*::P_{veg}-sgRNA^{box6-7}; CmR, ErmR	This work
EC3174	EC3139 *amyE*::P_{veg}-sgRNA^{box3-4}; CmR, ErmR	This work
EC3237	PY79 P_{dnaAN}*gfp-dnaN;* CmR	This work Adapted from [218]
EC3259	EC3017 *amyE*::P_{veg}-sgRNA^{box6-7} (SpcR), *lacA*::P_{xyl}-*dcas9*(ErmR), *gfp-dnaN*; CmR	This work
EC3266	EC3017 *amyE*::P_{yneA}-*gfp-yneA* (CmR)	This work Adapted from [219]
EC3270	EC3017 *amyE*:: P_{yneA}-*gfp-yneA* (CmR); *thrC*::P_{veg}-sgRNA^{box6-7} (SpcR)	This work
EC3272	EC3017 *amyE*:: P_{yneA}-*gfp-yneA* (CmR); *lacA*::P_{xyl}-*dcas9*(ErmR); *thrC*::P_{veg}-sgRNA^{box6-7} (SpcR)	This work

[a] Description given in the main text

[b] **Abbreviations:** Δnt refers to the deletion of nucleotides in the GFP sequence, the numbers correspond to the nucleotide positions deleted. artPS is an artificial protospacer that corresponds to the 20nt sequence CCCGTGGGTCTAGTCTAGCC, design of the sequence is explained in methods below. chr: this corresponds to chromosomal position, numbers indicate the nucleotide where insertion took place. Antibiotic resistances are represented as: AmpR – ampicillin, CmR – chloramphenicol, KanR – kanamycin, SpR – spectynomycin, ErmR – erythromycin.

Table 2. Plasmids used in this study

Plasmid[a]	Relevant characteristics[b]	Source

pEC2420 (pJOE8999)	*B. subtilis* replicative plasmid P_{manP}-*cas9*, P_{vanABK}-*sgRNAscaffold-opp*, *ColE1 ori*, *pE194*^{ts}, AmpR, KanR	Gift from Josef Altenbuchner[220]
pEC2424	P_{manP}-*cas9*, P_{vanAB}-sgRNA^{artPS} -, *ColE1 ori*, *pE194*^{ts} *ori*, AmpR, KanR	This work
pEC2418 (pUp)	pCC1, CmR ΩHR1^{int}–P_{degQ36}–*gfpmut2*(Δnt549-717)_artPS_AmpR_HR2^{int}	Genscript
pEC2419 (pDown)	ColE1 *ori*, KanR .ΩHR1^{int}–*mKate2*_lox71-P_{spc}-*spc*R-lox66_artPS_*gfpmut2*(Δnt1-58)_AmpR_HR2^{int}	Genscript
pEC2732 (p11103)	*B. subtilis amyE* integrative vector pDR111:: P_{degq36}-*gfpmut2* SpcR	S.H. TU Darmstadt
pEC2731	ΩHR1^{int}–P_{manP}-*cas9*,lox71-P_{spc}-*spc*R-lox66_artPS_*gfpmut2*(Δnt1-58)*kan*R_AmpR_HR2^{int}	Genscript
pEC2888	*B. subtilis amyE* integrative vector pDR111:: P_{degq36}-*gfpmut2kan*R SpcR	This work
pEC2728 (pJMP1)	*B. subtilis lacA*/*ganA* integrative vector *pAX01*ΩP_{xyl}-*dcas9*	Addgene #79873[221]
pEC2728 (pJMP2)	*B. subtilis amyE* integrative vector *pDG1662*ΩP_{veg}-*sgRNA_RR1*	Addgene #79874[221]
pEC2730 (pJMP3)	*B. subtilis thrC* integrative vector *pDG1731* ΩP_{veg}-*sgRNA_RR1*	Addgene #79875[221]
pEC2741	*B. subtilis amyE* integrative vector *pDG1662*ΩP_{veg}-*sgRNA*$^{box1box1-2}$	This work
pEC2742	*B. subtilis amyE* integrative vector *pDG1662*ΩP_{veg}-*sgRNA*$^{box6-7}$	This work
pEC2743	*B. subtilis amyE* integrative vector *pDG1662*ΩP_{veg}-*sgRNA*$^{box3-4}$	This work
pEC2892	*B. subtilis thrC* integrative vector *pDG1731* ΩP_{veg}-*sgRNA*$^{box6-7}$	This work

[a] Description given in the main text

[b] **Abbreviations:** Opp - strong terminator, sgRNA scaffold: sgRNA handle, explained in introduction and results sections. pE194ts refers to temperature sensitive replicon for replication in Bacillus subtilis, sgRNAartPS: sgRNA designed to target a unique artificial protospacer. HR1int and HR2int are integrative homologous regions of around 500bp, Φ(gfpmut2(Δnt1-58)kanR) is a translational fusion.

Table 3. Oligonucleotides used in this study

Oligo	Sequence 5'-3'	F/R	Purpose/ Target
OLEC8856	TACGCCCGTGGGTCTAGTCTAGCC	F	pEC2424
OLEC8857	AAACGGCTAGACTAGACCCACGGG	R	pEC2424
OLEC8794	GCACCGACTCGGTGCCAC	R	pEC2424 (SEQ)

OLEC8478	CCAAAATATATGCTGGATGCA	F	pEC2419 (SEQ)
OLEC8479	CAGACTGAATCACATCGGCTA	R	pEC2419 (SEQ)
OLEC8480	CGTGAAAAAAGACCACTGACA	F	pEC2420 (SEQ)
OLEC8481	AAACGAGAGCTTGCAATGGT	R	pEC2420 (SEQ)
OLEC7893	CAGGTAGTAATTCCTCTAAGTCATAATTTC	F	pEC2732 pEC2888 (SEQ)
OLEC8476	AAAATCGTCTCCCTCCGTTT	R	pEC2732 pEC2888 (SEQ)
OLEC11790	CGCAATTAATGTGAGTTAGG	F	pEC2888
OLEC11791	TTTGTATAGTTCATCCATGCC	R	pEC2888
OLEC11792	AGCTGCTGGGATTACACATGGCATGGATGAACTA TACAAAATGAGAATAGTGAATGGACC	F	pEC2888
OLEC11793	GTAGCGACCGGCGCTCAGGATCCTAACTCACATTA ATTGCGTCAAAATGGTATGCGTTTTG	R	pEC2888
OLEC11108	CTTGAAGTTACGGTTATAAATAGGAGTGAAGTTG TCCC	F	pEC2741 pEC2742 pEC2743
OLEC11109	GCTCTAAAACAAAAGTTATTCACACTTTCCACATTT ATTGTACAACACGAGCCCATTTTTG	R	pEC2741
OLEC11112	GGAAAGTGTGAATAACTTTTGTTTTAGAGCTAGAA ATAGCAAGTTAAAATAAGG	F	pEC2741
OLEC11115	CTTCACTCCTATTTATAACCGTAACTTCAAGTGG	R	pEC2741 pEC2742 pEC2743
OLEC11110	GCTCTAAAACCAAATCCACAGGCCCTACTAACATTT ATTGTACAACACGAGCCCATTTTTG	R	pEC2742
OLEC11113	TAGTAGGGCCTGTGGATTTGGTTTTAGAGCTAGA AATAGCAAGTTAAAATAAGG	F	pEC2742
OLEC11111	GCTCTAAAACCATGTGGATAGGCTGTGTTTACATT TATTGTACAACACGAGCCCATTTTTG	R	pEC2743
OLEC11114	AAACACAGCCTATCCACATGGTTTTAGAGCTAGAA ATAGCAAGTTAAAATAAGG	F	pEC2743
OLEC11116	GTCTGATCGGATCCTAGAAGC	F	pEC2741 pEC2742 pEC2743 (SEQ)
OLEC11117	CTGATTTAATCTGTATCAGGCTG	R	pEC2741 pEC2742 pEC2743 (SEQ)
OLEC8696	TAGATGACAACCAGGAACTT	F	SEQ *oriC*
OLEC8697	CCGTATAAGTTCTTTGTCATT	R	SEQ *oriC*

OLEC8474	GGAGATGATTGAGGAAAG	R	SEQ *cas9*
OLEC8475	AACATAGAGACAAACCAA	F	SEQ *cas9*
OLEC8870	TATTTTCTGCTTGTTCAC	R	SEQ *cas9*
OLEC8872	TATCAGTAGAATCTACCA	R	SEQ *cas9*
OLEC11498	GTATTCACTCTGCCAAGTTG	F	SEQ int *amyE*
OLEC11499	AACTGCTTCCAACAAAACCC	R	SEQ int *amyE*
OLEC11500	AAAAGAATCCGCCCATATCG	F	SEQ int *lacA*
OLEC11501	GAAGGGCTAAGAGAACAAGG	R	SEQ int *lacA*
OLEC11879	CCAGTAAATGAAGTCCATGG	F	SEQ
OLEC12597	GGTTATTGGGATAAGTTAGAGC	R	SEQ
OLEC11491	GATCAATCGGGGAAAGTGTG	F	qPCR *ori-ter* ratio
OLEC11492	GTAGGGCCTGTGGATTTGTG	R	qPCR *ori-ter* ratio
OLEC11493	TCCATATCCTCGCTCCTACG	F	qPCR *ori-ter* ratio
OLEC11494	ATTCTGCTGATGTGCAATGG	R	qPCR *ori-ter* ratio

[a] F/R - Forward/Reverse. All oligonucleotides were ordered from Sigma-Aldrich

SEQ: Sequencing oligos to confirm cloning

3.3 DNA manipulation and cloning

3.3.1 PCR

PCRs were performed with Phusion DNA polymerase (Thermo Scientific Fisher) or PrimeStar GXL DNA polymerase (Takara) according to manufacturer's instructions.

50 µl PCR reactions were prepared and incubated according to the manufacturer's instructions, using around 100 ng template DNA per reaction in PCR tubes (Sigma-Aldrich). Primer annealing temperatures were calculated using NEB Tm calculator online. Amplicons were checked by agarose gel electrophoresis using 1x TAE agarose gels (DNA fragments < 1 kbp: 1.5% agarose; DNA fragments > 1 kbp: 1% agarose). For this, 10 µl of the reaction was mixed with 2 µl 6x loading dye (Thermo Scientific Fisher) and ran at 100 V for 45 min to 1h depending on the length of the amplicon. Agarose gels were incubated in ethidium bromide (0.5 µg/ml in dH_2O water) for 15 min and DNA was visualized on a Molecular Imager GelDoc XR+ System (Bio-Rad) using the protocol for ethidium bromide stained nucleic acids.

In some cases, where PCR product was amplified for a plasmid, 2 µl Fast digest DpnI (NEB) enzyme was added to mix upon amplification to degrade the template DNA. The incubation was at 37°C for at least 1h followed by an inactivation at 85°C for 5 min.

3.3.2 Cloning

For cloning, amplicons were purified using the QIAquick PCR purification Kit (Qiagen) or by gel extraction with the QIAquick Gel Extraction Kit (Qiagen) after gel electrophoresis and following the manufacturer's instructions and eluted in 20 µl dH_2O water. All DNA concentrations were measured on a NanoDropTM One spectrophotometer (Thermo Fisher Scientific). The sequencing of the PCR-generated DNA fragments and plasmids was performed by Sanger Sequencing at Microsynth, Switzerland, using oligonucleotides listed in Table 3.

3.3.3 Plasmid construction

All plasmids were constructed by Gibson assembly method[222] using the Gibson Assembly master mix kit (New England Biolabs) in *E. coli* DH5 (NEB) or Top10 (Invitrogen) with the exception of plasmid pEC2424 which was constructed by Golden Gate assembly as previously described[223].

Golden Gate Assembly is used for cloning one or more inserts into a vector by designing overlapping ends that contain Type IIS restriction sites which can join the desired DNA together after cleavage by the non-palindromic restriction enzyme, followed by ligation to bind the DNA together. To construct plasmid pEC2424, the artificial protospacer targeting sgRNA was obtained by oligo annealing of primers OLEC8856 and OLEC8857, which contained BsaI sites. For a one pot reaction, a PCR tube was set with 0.5 µL of T4 DNA Ligase (Thermo Fisher Scientific), 2 µl of 10X T4 DNA Ligase Buffer (Thermo Fisher Scientific), 0.5 µL of BsaI enzyme (Thermo Fisher Scientific), 100 ng of vector in equimolar concentration with the insert and completed with dH_2O to a volume of 20ul. The vector is pEC2420 (pJOE8999), a kind gift from Prof. Altenbucher from University of Stuttgart.

The reaction was placed on the thermocycler and the program was set up as follows: 5 minute at 37°C (activation of the enzyme) were followed by 5 minutes at 16°C (activation of the ligase) for 45 cycles. Then a cycle of 15 minutes at 55°C (inactivation of the enzyme) was followed by 20 min at 85°C (inactivation of the ligase). After the Golden Gate Assembly, the whole volume (20 µl) was transformed into competent *E. coli* cells.

3.3.4 Generation of chemically-competent *E. coli* cells

E. coli cloning host strain was streaked on LB plates (plus antibiotics, when needed) from a -80 °C glycerol stock culture. LB plates were incubated overnight at 37°C and a single colony was inoculated into 10 ml LB medium (plus antibiotics, when needed) in 50 ml flasks and incubation continued at 37 °C shaking overnight. The next day, 500 µl were transferred into 50 ml fresh LB medium (plus antibiotics if needed, in 250 ml flask) and the culture was incubated at 37 °C shaking until an $OD_{600\ nm}$ of 0.4 (BioSpectrometer® kinetic, Eppendorf). Cells were transferred into 50 ml centrifugation tubes, centrifuged (4 °C, 4000 g, 10 min) and the pellet was resuspended in 25 ml ice-cold 0.1 M $CaCl_2$. After incubation in ice for 30 min, cells were centrifuged at 4°C for 10 min, 4000 g and resuspended in 4 ml ice-cold 0.1 M $CaCl_2$, 20% glycerol. Competent cells were aliquoted (100 µl) in 1.5 ml Eppendorf tubes, snap-frozen in liquid nitrogen and stored at - 80°C.

3.3.5 Bacterial transformation in *E. coli*

For transformation, competent cells were thawed on ice, and 1 µl plasmid DNA (20 to 50 ng total DNA concentration) was added. Cells were incubated on ice for 30 min before heat-shock was performed at 42°C for 45 s. Cells were incubated on ice for 3 min and recovered by adding 900 µl LB medium and incubation at 37°C for 60 min with mild agitation. Finally, 100 µl of the transformation approach was plated onto LB plates supplemented with respective antibiotics. The residual cells were centrifuged (4000 g, 10 min), the resulting pellet resuspended in 50 µl LB and plated onto LB plates plus respective antibiotics. Plates were incubated overnight at 37°C and stored at 4°C until further usage.

3.3.6 Bacterial transformation in *B. subtilis*

Strains were constructed using natural competence transformation with SMM medium as previously described[224,225]. 3ml of LB medium were inoculated with a single colony of *B. subtilis* and incubated at 37 °C (or 30 °C when needed) overnight (≥15 h). 500 ul of the overnight culture were diluted 5ml in *SMM competence medium* (14 g/L potassium phosphate dibasic, 6 g/L potassium phosphate monobasic, 2 g/L ammonium sulfate, 1 g/L sodium citrate dihydrate, 6mM magnesium sulfate, 0.5 % w/v glucose, 1 mg/ml tryptophan, 0.02% w/v casaminoacids, 0.22 ug/ml ferric ammonium citrate) were inoculated with 500ul of an overnight culture and incubated at 37 °C, then grown in a 100ml flask at 37°C with constant shaking (200 rpm) until cells reached OD_{600}

$_{nm}$≥0.8. Then added 5 mL *starvation medium* (14 g/L potassium phosphate dibasic, 6 g/L potassium phosphate monobasic, 2 g/L ammonium sulfate, 1 g/L sodium citrate dihydrate, 6mM magnesium sulfate, 0.5 % w/v glucose) and incubated for another 2 h. 1ml of culture were then mixed with DNA (≥400 ng of plasmid DNA or PCR product, 5 µg genomic DNA in a 15 ml falcon tube and incubated at 37 °C with constant shaking (200 rpm) for 1 h. After 1 h, cells were plated on LB agar containing selective antibiotics (10 µg/mL kanamycin, MLS (1 µg/mL erythromycin and 15 µg/mL lincomycin), 5 µg/mL chloramphenicol or 100 µg/mL spectinomycin).

In the case of strains EC3237 and EC3266, the transformations were performed using purified genomic DNA from strains YCN036 (*amyE*::P$_{yneA}$*yneA*-gfp)[219] and strain MS104 (P$_{dnaN}$*gfp-dnaN)*[218] (a kind gift from Prof. Heath Murray) and transformed into the *B. subtilis* host strain of interest.

3.4 Bacterial cell methods

3.4.1 Bacteria cell culture

Table 1 contains all strains used in this work. *B. subtilis* and the derivative strains were cultured in Luria-Bertani (LB Broth Miller, Becton Dickinson) medium containing: 10 g/L peptone, 5 g/L yeast extract, 10 g/L NaCl (and 15 g/L agar for solid medium). The above-mentioned components were dissolved in distilled water (dH2O), the pH was adjusted at 7.0 and the medium was autoclaved.

B. subtilis strains were grown in LB broth with constant shaking of 180-200rpm/min and at 37°C (or 30°C when indicated). The growth on solid medium was conducted on LB agar), which was supplemented with glucose (Carl Roth), mannose (Sigma) or xylose (Sigma) when indicated. *E. coli* strains were grown at 37°C, shaking (180 rpm/min) and LB broth medium. For the growth of *E. coli* on solid medium, LB agar was used.

For the growth of *B. subtilis*, the strains were grown at 37°C, or 30°C when indicated in experiment on a LB agar plate streaked from bacteria glycerol stocks stored at - 80°C. Subsequently cultures were grown from single colonies by inoculating in 10 ml (for protein extraction, growth curve analysis and serial-dilutions experiments). The cultures were then diluted (depending on the experiment, see below) and the growth was monitored by measuring the optical density at 600 nanometers ($OD_{600\ nm}$). When needed, antibiotics were added to the media at the following final concentrations: 10 µg/ml kanamycin (CorningTM) and 1 µg/ml erythromycin (Sigma-Aldrich); 15

µg/ml lyncomycin (CorningTM) and 150 µg/ml spectynomycin (Sigma-Aldrich) for *E. coli*. When necessary, glucose (Carl Roth), mannose (Sigma Aldrich) or xylose (Sigma Aldrich) were supplemented to the medium. Mannose was added to a final concentration of 0,2% (w/w) to induce the conditional promoter (P_{xyl}) and xylose was added to a final concentration of 1% (w/w) to induce the conditional promoter (P_{manP}). Glucose was used at a final concentration of 0.5% or 1% (w/w) and was used to repress the conditional mannose inducible promoter (P_{manP}) and xylose inducible promoter (P_{xyl}). To preserve the strains, aliquots of the all the bacterial strains utilized were prepared in 30% glycerol, snap feezed with liquid nitrogen and stored at - 80°C until use.

3.4.2 Growth curves

Cultures were grown from single colonies from fresh LB plates grown overnight at 37 ºC or 30°C when needed. The growth comparison of the *B. subtilis* WT and mutant strains was performed by diluting the overnight cultures to an $OD_{600\ nm}$ (BioSpectrometer® kinetic, Eppendorf) of 0.025 in 20 ml of LB medium in 100 ml-flask containing appropriate antibiotics and/or supplemented inductors when needed. The cultures were incubated at 30 °C or 37 °C in shaking waterbaths MaxQTM 7000 (Thermo Fisher) and constant shaking (200 rpm/min). The growth curves were performed in biological triplicates and the standard deviations were reported.

3.4.3 Cas9 induction, survival measurement

Plasmid system

Bacterial viability upon Cas9 expression was monitored by determining colony-forming units (CFU)/ml over time. Strains EC2836, EC2837, EC2838, EC2839, EC2840 were taken from a -80°C glycerol stock and streaked onto LB plates containing 1% (w/v) glucose (Carl Roth) and kanamycin (12 µg/ml), and incubated at 30°C overnight. Single colonies were picked and inoculated in 10 ml LB containing 1% glucose (w/v) and kanamycin (12 µg/ml) at 30°C overnight with constant shaking (180 rpm). Overnight cultures were back-diluted to $OD_{600\ nm}$ 0.01 in 20ml LB + 1% glucose and kanamycin (12 µg/ml) in 100ml flasks and further incubated at 37°C, 180 rpm until cell reached mid-logarithmic growth phase $OD_{600\ nm}$ 0.3-0.4. Cells were spun down at room temperature, 4000g for 5 min and split in two and resuspended in two conditions: one with

LB with 1% (w/v) glucose to repress Cas9 expression, and one with LB with 0.2% (w/v) mannose that induces Cas9 expression and incubated at 30°C at 180rpm. 100 µl samples were taken at 0, 1, 3, and 20 h and then 10-fold serially diluted in LB. 10 µl of each dilution was spotted onto LB agar plates containing 1% (w/v) glucose to inhibit additional expression of Cas9 and incubated overnight at 30°C. The number of CFU/ml were registered.

Chromosomal system

Bacterial viability upon Cas9 expression was monitored by determining colony-forming units (CFU)/ml over time. Strains EC3136 and EC3276 were taken from a -80°C glycerol stock and streaked onto LB plates containing 1% (w/v) glucose (Carl Roth) and for strain EC3276 in LB with 1% (w/v) glucose (Carl Roth) and spectinomycin (150 µg/ml), and incubated at 37°C overnight. Single colonies were picked and inoculated in 10 ml LB containing 1% glucose (w/v) at 37°C overnight with constant shaking (180 rpm). Overnight cultures were back-diluted to $OD_{600\ nm}$ 0.01 in 20ml LB + 1% glucose in 100ml flasks and further incubated at 37°C, 180 rpm until cell reached mid-logarithmic growth phase $OD_{600\ nm}$ 0.3-0.4. Pellets were washed, centrifuged, split in two and resuspended in fresh medium with either glucose or mannose as in *Plasmid system* and incubated at 180rpm, at 37°C. 100 µl samples were taken at 0, 1, 3, and 20 h and then 10-fold serially diluted in LB. 10 µl of each dilution was spotted onto LB agar plates containing 1% (w/v) glucose to inhibit additional expression of Cas9 and incubated overnight at 37°C. The number of CFU/ml were registered.

CRISPRi system

To validate the inhibition of replication by CRISPRi, strains EC3017, EC3136, EC3137, EC3139, EC3146, EC3147, EC3149, EC3157, EC3159 and EC3174 were taken from a -80°C glycerol stock and streaked onto LB plates supplemented with chloramphenicol (5 µg/ml), MLS (1 µg/ml erythromycin and 25 µg/ml lincomycin) and 1% (w/v) glucose when required. Single colonies were picked and inoculated in 10 ml LB containing 1% glucose (w/v) at 37°C overnight with constant shaking (180 rpm). Overnight cultures were diluted to $OD_{600\ nm}$ 0.01 in 20 ml LB with 1% glucose in 100ml flasks and further incubated at 37°C, 180 rpm until $OD_{600\ nm}$ 0.25 (+/- 0.025). To ensure cells are in early exponential phase, cultures were then back-diluted 1:10 in a total volume of 120 ml LB and 1% glucose (w/v) in 1L flasks, incubated at 37°C, 180 rpm until $OD_{600\ nm}$ 0.1 (+/- 0.025). Cells were pelleted at 4000g, at room temperature for 5 min and resuspended

in LB supplemented with either 1% glucose (w/v) or 1% xylose (w/v). Cells were incubated at 37 °C, 180 rpm and 100 µl samples were taken at 0, 1, 3 and 20 h and then 10-fold serially diluted in LB. 10 µl of each dilution was spotted onto LB agar plates containing 1% (w/v) glucose to inhibit additional expression of dCas9 and incubated overnight at 37°C. The number of CFU/ml were registered.

Cas9 editing confirmatory PCR in batch culture

To confirm the deletion of *oriC* and visualize the different editing events happening in both *Plasmid system* and *Chromosomal system*, confirmatory PCRs were performed. In both cases, cells were grown as explained in **Cas9 induction** section. 15 ml samples were taken after 3 hours of induction of Cas9 expression and spun down at 4°C, 13000 g for 10 minutes. Genomic DNA was purified with Nucleospin DNA extraction Kit (macherey-nagel) according to the manufacturers instruction and PCRs were performed with Phusion polymerase and external oligos (OLEC8479 and OLEC8480).

3.4.4 Flow cytometry

Cells were grown at 30 °C (*Plasmid system*) or 37 °C (*Chromosomal system*) in LB. Induction of Cas9 expression with 0,2% (w/v) of mannose was initiated when cells reached the mid exponential growth phase (OD_{600} nm~0.3). Cell samples were prepared by washing 1ml of culture twice with 1x PBS (phosphate-buffered saline, NaCl 137 mM, KCl 27 mM, Na_2HPO4 10mM, KH_2PO4 1.8 mM, pH 7.4) at 400 g for 10 min, RT Pellets were resuspended in PBS and data was collected with the use of a SH800S Cell Sorter (Sony) and analyzed either using Sony SH800S software or FlowJo (Treestar, San Carlos, CA). Further details are extended in Chapter3: Results.

3.4.5 Microscopy

Images were acquired with an Inverted Microscope (Leica DMi8, DFC9000 GT VSC-D6212 camera), and a 100X phase contrast objective (HC LP APO 100X/1.40 oil) with a SOLA Light Engine (Lumencor) light source. Filter sets used for different experiments were as follows: camera: 55%, exposure of 200ms for GFP and TXR filters. The images were captured using LasX software (Leica) and further processed analyzed in ImageJ[226].

3.4.6 Life and dead staining

B. subtilis live and dead staining was performed following the manufacturer's instructions (LIVE/DEAD™ BacLight™ Bacterial Viability Kit; Thermofisher) and taking 1,5 µl of final bacteria suspension spotted onto a 1,5% (w/v) low melting point agarose (Sigma-Aldrich) pads in TAE (40 mM Tris-acetate, 1 mM EDTA, pH 8.0). Microscopy image acquisition was set as follows: camera: 55%, exposure of 200ms for GFP and TXR filters.

3.4.7 OPP labelling

Protein synthesis was determined by measuring incorporation of the puromycin analog O-propargyl-puromycin (OPP), which is visualized and quantified in single cells by an addition of a fluorophore using click chemistry[227]. OPP incorporation leads to an accumulation of fluorescently tagged nascent polypeptide chains that directly corresponds to the rate of translation (Liu et al., 2012). To measure protein synthesis upon CRISPRi in the origin of replication, O-propargyl-puromycin (OPP) labelling assay was performed as previously described[228]. Click-iT Plus OPP Protein Synthesis Assay Kit (Invitrogen) was used to label cells with OPP following manufacturer's instructions. 450 µL of cells at given time points were transferred to disposable glass tubes. Click-iT® OPP (Component A) was diluted to the cell aliquots to a 13 µM final working concentration. Labelling was performed at 37 ºC and 180rpm for 20 min. Cells were harvested by centrifugation at room temperature and 13000 g for 1 min and resuspended in 100 µL of 3.7% formaldehyde (w/v) in PBS for fixation. Cells were fixed for 10 min at room temperature, harvested by centrifugation at 4000g for 2 minutes, and permeabilized using 100 µL of 0.5% Triton X-100 in PBS for and incubating for 15 min at room temperature. Cells were then labelled using 100µL of 1X Click-iT cocktail for 20 min in the dark. Cells were harvested by centrifugation at room temperature at 4000g for 5 minutes and washed one time using Click-iT rinse buffer and then re-suspended in 40 µL of 1X PBS for imaging.

3.4.8 DNA damage response assay

The *B. subtilis* strain EC3272 was created to evaluate DNA damage response (DDR). DNA damage leads to induction of LexA repressed genes such as *yneA*, which was fused to the GFP-encoding gene and integrated into the ectopic *amyE* locus[219]. Experiments were performed as described for the CFU/ml experiments. Early growing cultures ($OD_{600\ nm}$ 0.1) were treated with 1% (w/v) glucose to repress or with 1% (w/v) xylose to induce expression of dCas9 for 3 hours. Cells treated with 3 µg/ml mitomycin for 3 hours were used as positive controls. 1 ml of each culture was

washed twice (4000 g, room temperature for 5 minutes) and suspended in 1X PBS (phosphate-buffered saline, NaCl 137 mM, KCl 27 mM, Na_2HPO4 10mM, KH_2PO_4 1.8 mM, pH 7.4); 2µl were placed on 1,5% agarose in TAE pads.

3.4.9 Western blot

To prepare cell extracts, cells were collected after centrifugation (11000 g, 4°C, 10 minutes) and pellets were washed twice with 1X PBS pH 7.4 and lysed by bead beating with 0.1 mm glass beads (BioSpec) in a FastPrep instruments (MP Biomedicals™ FastPrep-24™ 5G) using 500 µl of disruption buffer (50 mM Tris-HCl pH 7.5, 10 mM EDTA, 150 mM NaCl, 0.1% Triton X-100, Protease inhibitor Complete 1X, Roche)) to obtain cytoplasmic proteins. The suspension was centrifuged (4000 x g, 4°C 10 minutes), the supernatant was collected and the total protein concentration was measured using the Bradford assay (Pierce BCA protein assay, Thermo Scientific Fisher) according to manufacturer's instructions, using series-dilutions of BSA as calibration standard.

When protein concentration was lower that the Bradford standard, a TCA protein precipitation protocol was used. In short, 125ul Trichloroacetic acid (TCA) were added to 500ul of protein extracts in a 1.5ml Eppendorf tube. Solutions were incubated for 10 minutes at 4°C followed by a centrifugation of 11000 g for 5 minutes. Supernatant was discarded leaving protein pellet intact. Pellet was washed with 200ul cold acetone and spin down at 11000 g for 5 min. The later steps were repeated for a total of 2 acetone washes. Pellets were dried by placing tubes with open lid in chemical hood for 30 minutes to drive-off acetone. Resuspension was done in 20ul water + 20 ul 2x SDS-PAGE buffer (specifications) and boiled for 20 minute at 95°C in a heat block before loading sample into polyacrylamide gel.

Protein concentration was normalized to 10 µg and separated on a 15% SDS-PAGE gel (sodium dodecyl sulphate – polyacrylamide gel electrophoresis; 180 V for 1 hour) blotted via wet transfer (transfer buffer, 39 mM glycine, 48 mM Tris, 0.037% SDS and 20% (v/v) methanol; 2 hours at 50 volts) on a PVDF membrane (0.2 uM Pore Size; BioRad) for Western blot analysis. Membrane blocking was performed by overnight incubation at 4°C in 5 % Skim Milk (Sigma) in 1X TBST (TBST 10X: 100 mM Tris, 1.5 M NaCl, 0.5% Tween 20, pH 8). Next, the membrane was incubated for at least 1 hour at 4°C with a rabbit monoclonal antibody (1/5000 dilution) in 1X TBST 5% Skim Milk (Sigma-Aldrich Chemie GmbH), then washed 3 times for 5 minutes in the same buffer and incubated with an anti-rabbit antibody () in 1X TBST for 1 hour at 4°C. The SigA-antibody

(Rabbit Polyclonal, 1/5000 dilution) was used as loading control measured on the same membrane. The Western blot was developed (Clarity Western ECL Substrate; Bio-Rad) and signals were recorded using the Molecular Imager Gel-Doc system (Bio-rad) and analyzed in ImageJ[226].

3.4.10 Determination of origin-to-terminus ratio by q-PCR

Strains EC3017 and EC3147 were grown overnight at 37°C and 180rpm. Overnight cultures were diluted to $OD_{600\ nm}$ 0.01 in 10ml LB + 1% glucose in 50ml flasks and further incubated at 37°C, 180 rpm until $OD_{600\ nm}$ 0.25 (+/- 0.025). To ensure cells are in early exponential phase, cultures were then back-diluted 1:10 in a total volume of 120 ml LB and 1% glucose (w/v) in 1L flasks, incubated at 37°C, 180 rpm until $OD_{600\ nm}$ 0.1 (+/- 0.025). Cells were pelleted at 4000g, at room temperature for 5 min, split in two and resuspended either in LB supplemented with 1% glucose (w/v) or 1% xylose (w/v) and incubated at 37°C, 180 rpm. 15 ml samples were taken at different timepoints (0, 1, 3, 5 and 20 hours), spun down at 11000 g, 4°C for 5 min followed by a genomic DNA extraction with Nucleospin DNA extraction Kit (macherey-nagel) according to the manufacturer's instructions and resuspended in 30 µl dH_2O.

The primer pair targeting the origin region was OLEC11491 and OLEC11492, and for the terminus was OLEC11493 and OLEC11494. qPCR reactions of 20 ul contained 2.5ng of DNA, 200nM of each primer and 10 ul of 2X Power SYBR™ Green PCR-Master-Mix (Applied Biosciences™), and amplifications were performed on a QuantStudio™ 5 Real-Time PCR system (Applied Biosciences) according to the following protocol: 95°C for 3 min, followed by 40 cycles of 95°C for 30 s, 60°C for 30 s, and 72°C for 30 sec. Ori-ter ratios were analysed using comparative cycle threshold (Ct) analysis; the 2ΔΔCt method[229]. A fixed sample of the wild type strain grown into late stationary phase, where the population would be expected to have an ori-ter ratio corresponding to 1, was used for normalisation in every cycling run.

3.4.11 Replisome localization by GFP-DnaN

To colocalize the replisome, strains with protein DnaN fused to a GFP were constructed and fluorescent foci observed in the microscope. Strains EC3237 and EC3259 were taken from a -80°C glycerol stock and streaked onto LB plates supplemented with chloramphenicol (5 µg/ml), MLS (1 µg/ml erythromycin and 25 µg/ml lincomycin) and 1% (w/v) glucose. Single colonies were picked and inoculated in 10 ml LB containing 1% glucose (w/v) at 37°C overnight with

constant shaking (180 rpm). Overnight cultures were diluted to $OD_{600\,nm}$ 0.01 in 20 ml LB with 1% glucose in 100 ml flasks and further incubated at 37°C, 180 rpm until $OD_{600\,nm}$ 0.25 (+/- 0.025). To ensure cells are in early exponential phase, cultures were then back-diluted 1:10 in a total volume of 20 ml LB and 1% glucose (w/v) in 100 ml flasks, incubated at 37°C, 180 rpm until $OD_{600\,nm}$ 0.1 (+/- 0.025). Cells were pelleted at 4000g, at room temperature for 5 min and resuspended in LB supplemented with either 1% glucose (w/v) or 1% xylose (w/v). Cells were incubated at 37 °C, 180 rpm and 200 µl samples from timepoint 0, 3 and 5h were spun down at RT, 4000g for 5 minutes and pellets were washed twice with 1X PBS and resuspended in a final volume of 500 µl 1X PBS from which 1,5 µl were spotted onto 1,5% agarose pads and observed in microscope in the GFP channel with indications as explained **Microscopy**.

3.5 Bioinformatics and statistical analysis

3.5.1 Artificial protospacer design

Protospacer designs with a length of 20 bp result in 420 bp ≈ 1 trillion unique possible nucleotide combinations. Exploring this space exceeds computational resources. To circumvent this issue, protospacers have been assembled from smaller segments. At first, we identified the frequency of all possible 5-mers in the reference sequences and its reverse complement. Utilizing prior knowledge about the position specific impact of mismatches of nucleotides in a protospacer[178], we prepared a mismatch matrix by pre-calculating all possible combinations of 5-mers applying position-specific and nucleotide-specific mismatch activity scores[178]. Next, the frequency of all 4-mers in the reference sequence was determined and protospacers with a length of 20 bp were assembled selecting low frequency 4-mers. Protospacer designs were filtered for common 5-mers by incremental inclusion of low frequency 5-mers until a 100-fold design counts in excess were created, resulting in at least 18,825 accepted designs (≤ 0.098%). A second filter was used to exclude common 5-mers in the reverse-complement of the reference sequence by incremental inclusion of rare 5-mers until at least 70-fold surplus designs (9429 designs) were accepted (≤ 0.075%). We allowed for a maximum GC content of 65% and subsequently analyzed homopolymer content among candidate protospacers and excluded designs containing homopolymer lengths >4.

We then sought to determine off-target activity within the reference sequence using the precalculated mismatch matrix, followed by a folding structure analysis of Protospacer designs

using the Vienna RNAfold package for predictions[230]. To maximize design diversity, we filtered against very similar designs based on hamming distances. We then evaluated the list of the remaining candidates and ranked them to minimize self-folding and off-target activity and maximized on-target activity. Furthermore, high GC content in the last 5 bp was slightly favored by multiplying ranking scores with 0.8 if the GC content of the last 5 bp was ≤60%. We finally calculated similarity of design sequences by utilizing Hamming distance and clustering by Ward.

3.5.2 Proteomics

3.5.2.1 Sample collection

Strains EC3017 and EC3147 were taken from a -80°C glycerol stock and streaked onto LB plates containing 1% glucose (w/v) for EC3017 and 5 µg/ml Cm, MLS (1 µg/ml erythromycin and 15 µg/ml lincomycin) and 1% glucose (w/v) for EC3147 and incubated at 37°C overnight. Single colonies were picked and inoculated in 10 ml LB containing 1% glucose (w/v) at 37°C overnight with constant shaking (200 rpm). Overnight cultures were diluted to $OD_{600\ nm}$ 0.01 in 20ml LB + 1% glucose in 100ml flasks and further incubated at 37°C, 180 rpm until $OD_{600\ nm}$ 0.25 (+/- 0.025). To ensure cells are in early exponential phase, cultures were then back-diluted 1:10 in a total volume of 120 ml LB and 1% glucose (w/v) in 1L flasks, incubated at 37°C, 180 rpm until $OD_{600\ nm}$ 0.1 (+/- 0.025). Cells were pelleted at 4000g, at room temperature for 5 min and resuspended in LB supplemented with 1% xylose (w/v). Cells were incubated at 37 °C, 180 rpm and 20 ml samples were taken at different timepoints per treatment (0, 3, 4, 5 and 6 hours) followed by a centrifugation at 11000 g, 4°C for 5 min. Pellets were resuspended in 20ml 1X PBS (precooled at 4°C). Cell were washed thrice in 1X PBS (precooled at 4°C) at 11000g at 4°C for 5 min and the pellets were immediately frozen using liquid nitrogen. Samples were kept at -80°C for further processing.

Cells were lysed with 500 µl 2x lysis buffer (final concentration: 2% SDS, 20 mM TCEP, 80 mM CAA (Chloroacetamide, Sigma-Aldrich), 100 mM HEPES pH 8 (VWR), 0.5x protease inhibitors (Roche) in tubes containing using 25 mg 0.1mm silica beads (BeadBeater® Glass beads, 0,1 mm (Roth) and were disrupted using a FastPrep-24TM 5G Homogenizer (MP Biomedicals) as follows: 3 cycles of 45 seconds and 4m/sec. Samples were spun down at 11000g, 10 min to separate the soluble from the insoluble fraction. The supernatant was heated at 95°C for 5 min and then cooled down to room temperature. The protein concentration was determined using Pierce™ BCA

Protein Assay Kit ((ThermoFisher Scientific) and followed by a nucleic acid digestion with Benzonase (Sigma-Aldrich) for 30 minutes at 37°C; which was performed by adding 0.5 Units of Benzonase per 1 µg of protein. Samples were kept at -20°C for further analyses.

3.5.2.2 Sample preparation

All samples were subjected to SP3 sample preparation[223] on an Agilent BRAVO liquid handling robot. Ten µg of a 1:1 mixture of hydrophilic and hydrophobic carboxyl-coated paramagnetic beads (SeraMag, #24152105050250 and #44152105050250, GE Healtcare) were added for each µg of protein. Protein binding was induced by addition of acetonitrile to a final concentration of 50% (v/v). Samples were incubated for 10 minutes at room temperature. The tubes were placed on a magnetic rack and beads were allowed to settle for three minutes. The supernatant was discarded and beads were rinsed three times with 200 µL of 80% ethanol without removing the tubes from the rack. Beads were resuspended in digestion buffer containing 50 mM triethylammmoniumbicarbonate and both Trypsin (Serva) and Lys-C (Wako) in a 1:50 enzyme to protein ratio. Protein digestion was carried out for 14 hours at 37°C in a PCR cycler. Afterwards the supernatant was recovered dried down in a vacuum concentrator.

3.5.2.3 Peptide labelling and fractionation

TMT 11plex (Pierce, #A37725) was used for peptide multiplexing and quantification. Briefly, equal amounts of peptides were resuspended in 50 mM HEPES pH 8.5. Additionally, 10% from each sample was pooled to create a common sample as internal standard. TMT reagents were allowed to equilibrate to room temperature for 30 minutes and were dissolved in anhydrous acetonitrile to a final concentration of 59 mM. To each sample TMT was added to a final concentration of 11.8 mM and tubes were incubated at 25°C for 60 minutes with mixing at 500 rpm on a ThermoMixer. Labeling was quenched by addition of hydroxylamine to a final concentration of 0.4%. Samples were mixed, desalted using solid phase extraction (Seppak 1cc/50mg, Waters), dried down in a vacuum concentrator and resuspended in 20 µL 2% acetonitrile. Basic reversed phase fractionation was performed on a quaternary Agilent 1290 Infinity II UPLC system equipped with a Kinetex Evo-C18 column (150 x 2.1 mm, 2.6µm, 100 Å, Phenomenex) that was operated at 40°C. Solvent A consisted of HPLC grade water, solvent B consisted of 100% acetonitrile, and solvent C consisted of 25 mM ammoniumbicarbonate in water. Fractionation was carried out at a constant flow rate of 100 µl/min using a linear gradient from 2-

25% acetonitrile within 50 minutes, followed by column washing and equilibration. Over the whole gradient solvent C was kept constant at 10%. In total 32 fractions were collected in conical 96well plates. The organic solvent was removed in a vacuum concentrator for 30 minutes and fractions were concatenated into 8 final samples. Peptides were acidified with formic acid, desalted using OASIS HLB 96well cartridges (Waters, #186001828BA), dried down and resuspended in 2% acetonitrile, 0.1% trifluoroacetic acid (TFA) prior MS analysis.

3.5.2.4 Mass spectrometry

All samples were analyzed on a Orbitrap Exploris (Thermo Scientific) that was coupled to a 3000 RSLC nano UPLC (Thermo Scientific). Samples were loaded on a pepmap trap cartridge (300 µm i.d. x 5 mm, C18, Thermo) with 2% acetonitrile, 0.1% TFA at a flow rate of 20 µL/min. Peptides were separated over a 50 cm analytical column (Picofrit, 360 µm O.D., 75 µm I.D., 10 µm tip opening, non-coated, New Objective) that was packed in-house with Poroshell 120 EC-C18, 2.7 µm (Agilent). Solvent A consists of 0.1% formic acid in water. Elution was carried out at a constant flow rate of 250 nL/min using a 180 minute method: 8-33% solvent B (0.1% formic acid in 80% acetonitrile) within 120 minutes, 33-48% solvent B within 25 minutes, 48-98% buffer B within 1 minute, followed by column washing and equilibration. Data acquisition on the Orbitrap Exploris was carried out using a data-dependent method in positive ion mode. MS survey scans were acquired from 375-1500 m/z in profile mode at a resolution of 120,000. AGC target was set to 100% at a maximum injection time of 50 ms. The ten most abundant peptides were isolated within a 0.4 m/z window and subjected to HCD fragmentation at a normalized collision energy of 36%. The MS2 AGC target was set to 200%, allowing a maximum injection time of 54 ms. Product ions were detected in the Orbitrap at a resolution of 30,000. TurboTMT acquisition as enabled. Precursors were dynamically excluded for 45 s.

3.5.2.5 Proteomics data analysis

Raw files were processed with Proteome Discoverer 2.4 (Thermo Scientific). Briefly, peak lists were extracted from raw files and searched using SEQUEST HT against a Uniprot *Bacillus subtilis* database (version 190614, taxonomy ID 224308) and a database containing sequences of common contaminants (derived from Maxquant v.1.6.0.1). Trypsin/P was set as enzyme specificity, allowing a maximum of two missed cleavages. The minimum peptide length was set to 7 amino acids. Carbamidomethylation on cysteine was set as fixed modification. Protein N-

terminal acetylation, oxidation of methionine, and TMT on lysines and peptide n-termini were allowed as variable modifications. Mass tolerances for MS1 and MS2 were set to 10 ppm and 0.02 Da, respectively. Peptide-spectrum-matches (PSMs) were filtered to a 1% FDR level using Percolator employing a target/decoy approach. Only rank 1 peptides were allowed. TMT reporter ion intensities were quantified within 20 ppm windows and quan value correction was used to correct for reagent isotope impurities. Only unique peptides were used for protein quantification. PSM with a co-isolation value of >50% were rejected. Further data processing was carried out in R and Perseus (v. 1.6.2.3). All contaminant proteins were filtered out. A three step normalization procedure was applied. First, the sum of the reporter ion intensities for each TMT channel was normalized to the average grand total to correct for pipetting errors. Next, the common internal standard in each TMT 11plex set was used for internal reference scaling[231] in order to correct for batch effects. Afterwards the data was normalized applying trimmed mean of M values (TMM) using the edgeR package. Statistical analysis was performed using two-sample t-tests and multiple sample ANOVA tests. Resulting p-values were corrected for multiple testing using a permutation-based FDR approach or by the method of Benjamini-Hochberg. Hierarchical clustering was performed on the z-scored averaged intensities using Euclidian distances.

The mass spectrometry proteomic data is available in the supplementary data in the CD attached to this thesis (Attached as a document in pdf format, readable in Perseus[232]).

3. Results

The role of replication inhibition in bacteria has been widely explored[23,115,136]. However, the impact of replication arrest is not well studied because it is an essential process and there are several methodological limitations to study it, which includes the difficult enrichment of non-propagating cells. To investigate the cellular and physiological effects of replication arrest in *B. subtilis*, we aimed to create a stable strain that cannot initiate replication using an inducible CRISPR-Cas9 system and enrich this population by fluorescent-activated cell sorting (FACS). We decided to use a CRISPR-Cas9 system to selectively investigate the effects of bacterial replication arrest in a clean deletion of the *oriC*, avoiding the use of thermosensitive mutants that can lead to temperature mediated proteome remodelling and also the emergence of suppressor mutants. In this strain, Cas9 expression should remove the *oriC* and part of the replication initiation machinery and concurrently reconstitute and express GFP. Using flow cytometry, we should be able to enrich the cells without *oriC* to further characterize them.

To enable the study of replication-arrest in *B. subtilis* vegetative cells, we used a sporulation-deficient mutant. It has been shown that when the growth rate of *B. subtilis* slows down, the concentration of a response regulator protein, Spo0A, increases, and the bacteria are more likely to form spores[1]. For this reason, we wanted to avoid the cell was going to escape replication arrest by sporulation. Sporulation begins with phosphorylation of Spo0A[232]. Since this transcription factor regulates many other stationary phase processes, including biofilm formation, genetic competence, and degradative enzyme production[233], we left the *spo0A* gene intact. Instead, we used a strain lacking the *sigF* gene, which is the first forespore-specific transcription factor that controls genes for the early stages of prespore development and is not required for other differentiation processes[234–236].

3.1 Construction of a suitable strain for CRISPR-Cas9-based genome editing

We genetically modified the *B. subtilis* ⊿*sigF* strain by inserting identical, synthetic protospacers flanking the *oriC* region. The protospacers are 20 bp sequences designed to ensure that the selected

sgRNA target have no significant matches elsewhere in the genome, thereby minimizing off-target and maximizing on-target activity during CRISPR editing (See Materials and Methods – Artificial protospacer design).

3.1.1 Plasmid-based CRISPR-Cas9 system for deletion of *oriC*

The general strategy to create *oriC*-less cells is depicted in Figure 6. We first explored an established plasmid system for CRISPR editing in *B. subtilis*[220]. This vector consists of: (i) a temperature-sensitive replicon from pE194ts for replication in *B. subtilis*, (ii) a minimal pMB1 (derivative) origin of replication in *E. coli*, (iii) a kanamycin resistance cassette for selection in *B. subtilis*, (iv) a *cas9* under a mannose-inducible promoter P_{manP}, that is activated in *B. subtilis* by the native transcriptional activator of the mannose operon, ManR, in the presence of mannose and the absence of glucose[237], and (v) a sgRNA under a constitutive semisynthetic promoter P_{vanABK}. The sgRNA was adjusted to target the identical, synthetic protospacers located up and downstream of the *oriC*.

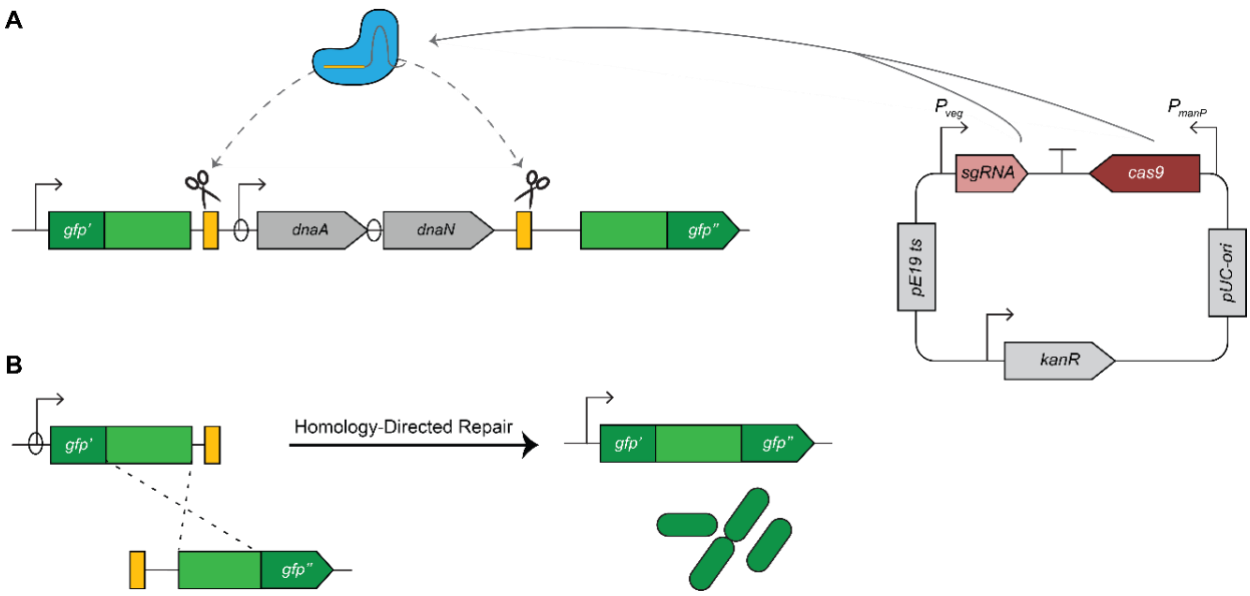

Figure 6. Plasmid system rationale for *oriC* deletion using CRISPR-Cas9 system
Schematic of the modified *oriC* integrated into the *B. subtilis* genome. (A) A green fluorescent protein (GFP in green) is split up- and downstream of the *oriC*. The first half of the *gfp* sequence upstream of the *oriC* is transcribed from a constitutive promoter. The transcript does not result in a functional protein due to the missing back region (GFP"). The native *oriC* is also flanked by synthetic protospacers (yellow). (B) Two double-strand breaks occur in the genomic DNA after induction of Cas9 (blue) and spacer-targeting sgRNAs expression. Only cells that will have repaired these double-strand breaks by homologous

recombination can become fluorescent. Homologous regions provide the homologous repair template in the split *gfp* up and downstream (light green). Cells that successfully repair the double-strand break transcribe a complete GFP coding sequence resulting in fluorescence.

The protospacers are recognized and cleaved by an inducible Cas9-sgRNA complex present in a replicative plasmid (Figure 6A). Since we anticipate that cells without *oriC* would be incapable of DNA replication and propagation, it is not possible to select colonies. Therefore, we designed a system in which GFP is only expressed when the *oriC* is removed by Cas9 cleavage and subsequent DNA repair by homologous recombination (Figure 6B). We inserted split versions of the GFP sequences up and downstream of the *oriC*-containing operon – *dnaAN*. The upstream part is under the control of a strong constitutive promoter P_{degQ36}^{238} and only expressed fully functional GFP when reconstituted upon successful CRISPR-Cas9 editing. To provide homology templates to repair the double strand breaks by the endogenous homologous repair system, we inserted 500bp homologous regions that are part of the GFP sequence down and upstream of the split version GFP. This experimental approach facilitates the selection of the GFP^+ cells from the replicating cells, making them ideal candidates to study the effect of replication arrest.

We observed leakiness of the Cas9 promoter during the cloning procedure that hindered us from selecting for the desired parental strain with a modified *oriC* and CRISPR plasmid. This issue was circumvented by selecting colonies in LB containing glucose to avoid basal Cas9 expression before induction of expression. Therefore, in all experiments using this system, overnight cultures and pre-induction cultures are grown in the presence of 1% (w/v) of glucose.

3.1.2 Evaluation of the plasmid-based CRISPR-Cas9 system

To confirm that the plasmid-based CRISPR-Cas9 system was functional, we performed cell survival experiments under Cas9 expression alone (Plasmid A) or together with a sgRNA (Plasmid B) in different strains (Figure 7A). The strains evaluated were: 1. Strain without modifications in the *oriC* (wild-type), 2. Strain with modifications only upstream of the *oriC*, carrying one protospacer and lacking a template for homologous repair, and 3. Strain with fully modified *oriC* (Figure 7A).

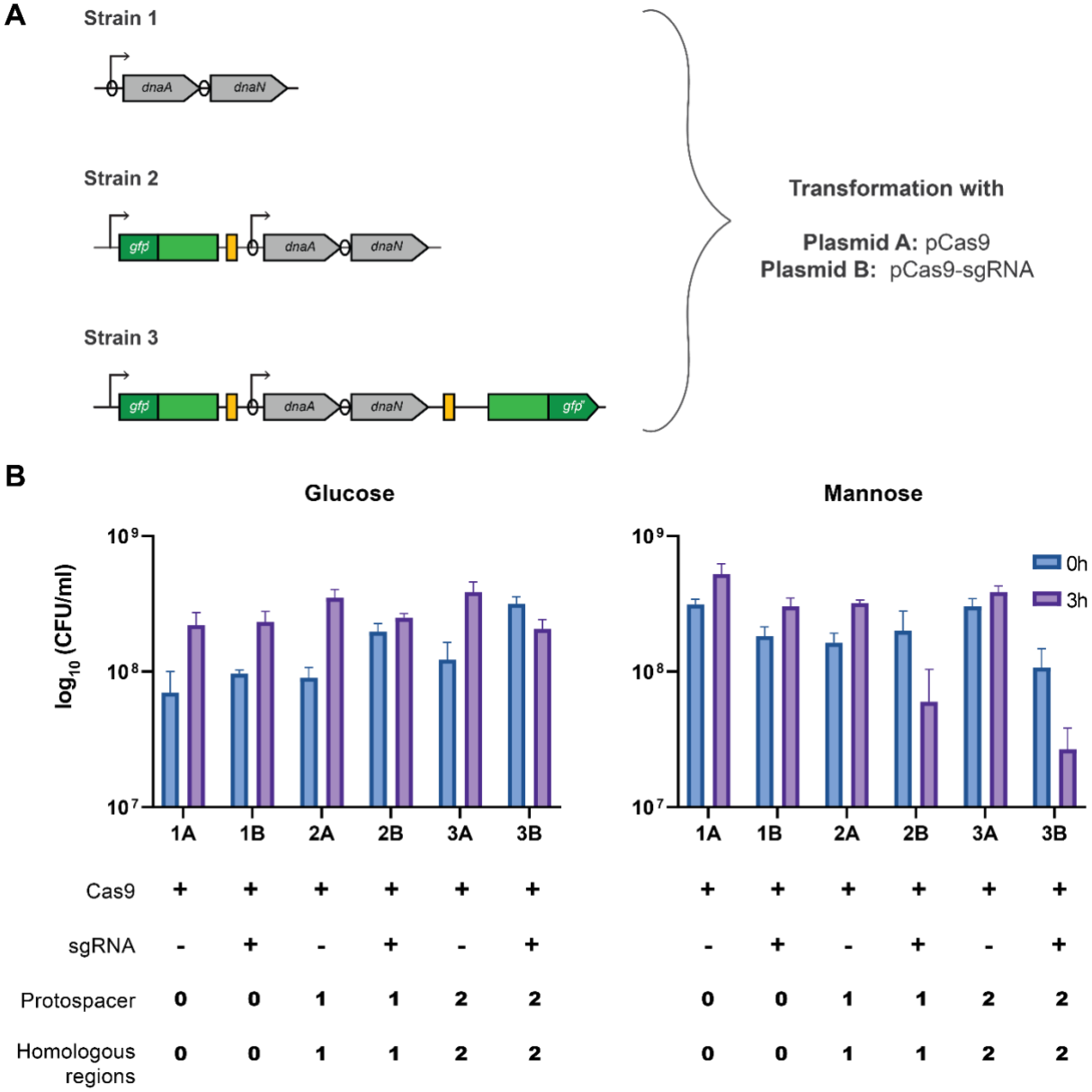

Figure 7. Survival after Cas9 induction. (A) Strains used for this assay correspond to Strain 1, which contains the native *oriC*. Strain 2 with the integration of only one module containing partial *gfp* sequence (green) and an artificial protospacer (yellow). Strain 3 contains the fully modified *oriC* with integrations of partial sequences of *gfp* (green) upstream and downstream of the native replication locus and two protospacer sequences (yellow) flanking the *oriC*. Strains were named according to (A) and A or B refers to the plasmid they contained: either one containing only Cas9 (plasmid A) or one with Cas9 and sgRNA (plasmid B). (B) Cell survival after growing cell in Cas9 repression or induction conditions in Glucose 0.5% (w/v) or Mannose 0.2% (w/v), respectively. Cells were plated in LB amended with glucose to stop inhibition. Blue bars indicate time 0 and orange bars indicate time after 3 hours (180 minutes) of induction of Cas9 and/or sgRNA expression. Serial dilutions were made and colonies counted in the lowest countable dilution. The figure shows experiments with three biological replicates and three technical replicates per biological replicate.

The CRISPR system was induced when cells reached mid-logarithmic growth phase (OD_{600nm} 0.3-0.4) by the addition of mannose. Colony-forming units (CFU/ml) were measured at timepoint 0 and 3 hours to determine the effect of Cas9 on cell survival. As expected, strains that

grew in the presence of glucose, did not have a big effect on cell survival (Figure 7B). Except for the strain 3B that contained the fully modified *oriC* and the Cas9/sgRNA plasmid and had a small CFU drop, which may be due to leaky expression of Cas9 (Figure 7B).

However, strains treated with mannose displayed a different trend. In the control strain without modification of the *oriC* region, the growth constantly increased even after 3 hours of Cas9 expression (Figure 7C). Conversely, we detected a drop in CFU/ml for cells carrying a partial modification of the *oriC*, due to the Cas9-induced double-strand break in the protospacer sequence without providing a homologous repair template (Figure 7C: Strain 2B). Finally, the fully modified *oriC* region displayed a stronger CFU/ml drop, most likely due to the two instead of one possible sites for Cas9-induced double-strand breaks in the chromosome (Figure 7C: Strain 3B).

Finally, when Cas9 and protospacer were present but sgRNA was absent, we had no drop in CFU/ml, indicating that Cas9 expression alone is not toxic for the cells. Similarly, when Cas9 and sgRNA were present, but no artificial protospacer was integrated, the CFU/ml did not drop, suggesting that no off-targeting events occurred. These two observations demonstrate the feasibility to use the system to perform further experiments.

GFP fluorescent cells appear 3 hours after expression of the plasmid-based CRISPR system

Using fluorescence microscopy, we detected GFP fluorescence to verify the correct plasmid-based CRISPR editing and subsequent DNA repair process in the cells of the modified strain (hereafter, Bsu-pCRISPR). The CRISPR system was induced when cells reached mid-logarithmic growth phase. Since the plasmid has a thermosensitive replicon, all experiments were conducted at 30°C. We imaged cells by every 30 minutes upon mannose induction and found the first GFP^+ cells after 3 hours (Figure 8A). However, GFP fluorescence could not be detected by plate reader on a population level because of the limited amount of GFP cells.

A close collaboration with Prof. Matthew Cabeen at Oklahoma University allowed the analysis of the frequency of GFP^+ events in a mixed population grown in a microfluidic chamber. This system also allowed a better observation of the single cell events. It was found out that, on average, the amount of GFP^+ events is 1.9% (Figure S2). Additionally, they performed time-lapse microscopy in mannose-induced cells for 10 hours and observed that cells that become GFP fluorescent and later undergo cell lysis, and second, cells that become GFP fluorescent and

continue having fluorescence for the 10 hours of the experiment (Figure S1A). This indicates that cells that die could have a defective DNA repair process while in the other cells it was successful.

Since GFP fluorescence was not homogeneous in the whole population, we could not perform a clean PCR of the edited cells. Thus, we performed a confirmatory PCR with primers annealing outside of the *oriC* region in the batch culture after 3 hours of treatment with mannose. Results of the PCR displayed two bands: one large fragment indicating the modified length of the *oriC* before Cas9-induced editing (≈ 6Kb) and a shorter fragment (≈ 1.3Kb) indicating that the Cas9 induced removal of the *oriC* region and subsequent DNA repair through the endogenous homologous recombination system has occurred (Figure 8C). Since in the PCR, the short fragments are overrepresented because they can be amplified more times during the extension part of the cycle, we cannot give a quantitative interpretation of this result but rather an observation of the events taking place in the batch.

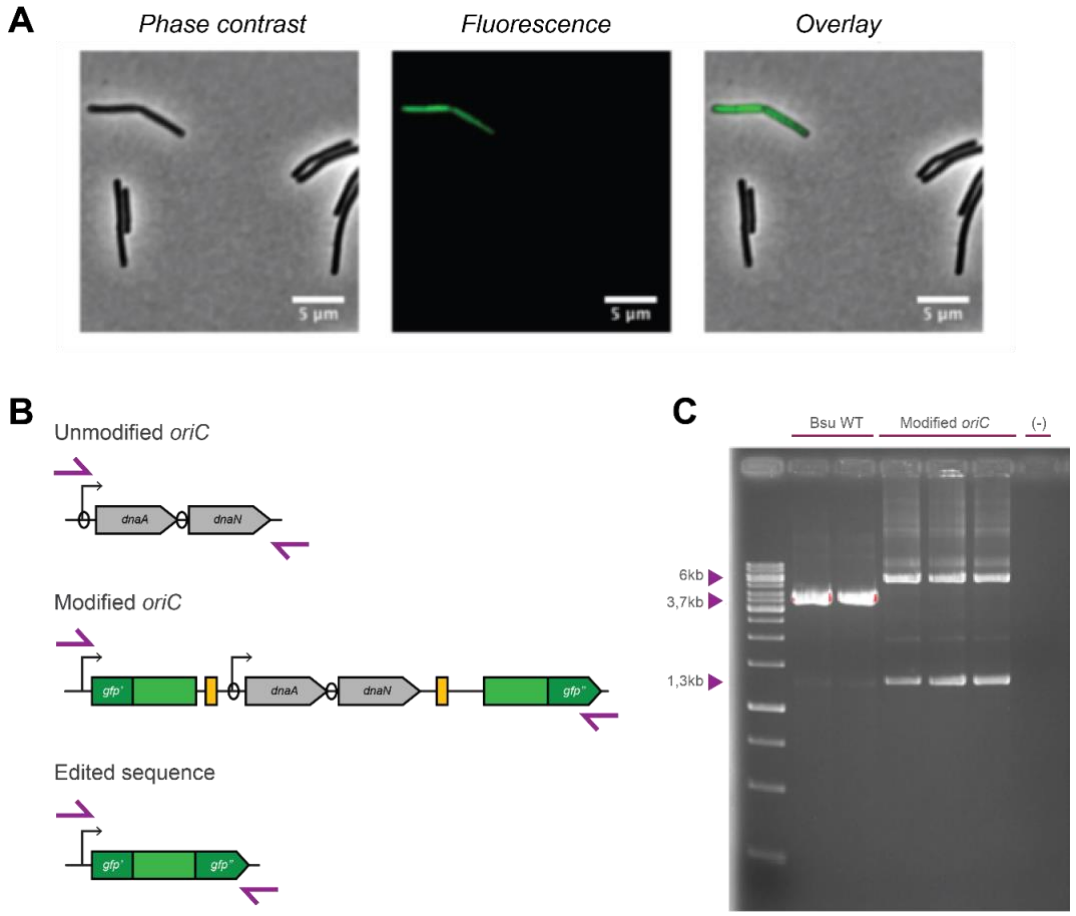

Figure 8. Bsu-pCRISPR-mediated *oriC* deletion occurs in a low frequency

Strain with total modification of the *oriC* containing a plasmid with Cas9 and sgRNA, after Cas9 induction. Pictures were taken at 100x with exposure time to GFP channel of 50ms. (A) Cells after Cas9 induction with Mannose 0.2% for 3 hours. Green cells represent cell with correct repair after Cas9 cleavage. (B) We used primers (purple) flanking the replication initiation locus, as a control, we used the wild-type PY79 strain and expected a PCR product of around 3.7 kb. We expected to see two bands for the strain with the

modified *oriC*, one showing the full length of the modified *oriC* around 6 kb and one of the editing events of around 1.3 kb. (C) Agarose gel of the PCR shows the edited and unedited band in the strain with modified *oriC*, indicating a mixed population also shown in (A).

To quantify the percentage of GFP+ cells in Bsu-pCRISPR, we performed a flow cytometry analysis (Figure 9A and 4B). We establish a gating strategy with the positive control that consists of a GFP-containing strain under the control of the promoter P_{degQ36} integrated into the *amyE* locus and a negative control that consists of a wild-type *B. subtilis* strain (Figure 9B). To validate the gating strategy's proper functioning, we sorted positive events and observed them in the microscope (Figure 9C), and confirmed they corresponded to the desired population. Flow cytometry analysis of GFP-containing cells indicated that only 0.8-1% of the population successfully deleted the *oriC* and reconstituted the GFP (Figure 9B). Although we successfully deleted the replication initiation machinery, we could not recover enough cells to perform further analysis in clean recovered cells.

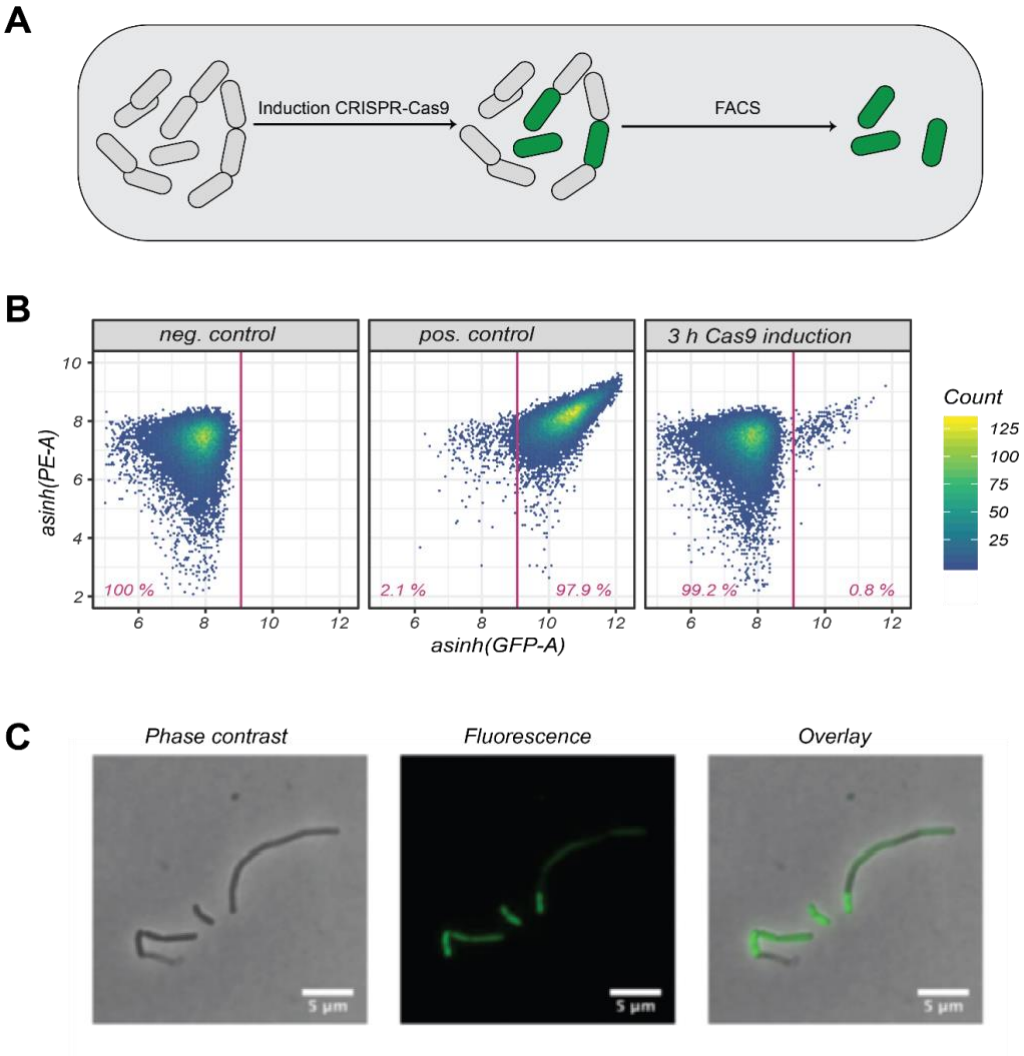

Figure 9. Proportion of GFP⁺ cells recovered by FACS

(A) Rationale of the FACS sorting strategy. Non-induced cells (grey) are induced at exponential phase with CRISPR-Cas9 system to eliminate the replication initiation machinery; the result is a mix population of

positive events (green) and negative events (grey). After FACS sorting, we expect to enrich edited cells. (B) Representative FACS plot of the sorting strategy used for the isolation of CRISPR-edited cells with active GFP fluorescence. The GFP positive events are located in the right half of each figure. As a positive control, we used a strain constantly inducing GFP from the native promoter P_{degQ16} that was also used in the modified strain. After 3 hours of induction, 0.8% of the events were GFP positive. Picture shown from a representative event of two biological replicates with three technical replicates. (C) Fluorescence microscopy of the cells after FACS run shows some cells with bright fluorescence and some that have lost it. This is a representative picture of one sorting run.

We next wanted to assess the ability GFP sorted cells to propagate. For that, we sorted the GFP positive events and subjected these selected cells for time-lapse microscopy for 5 hours. We found no sign of replication in cells from the positive selection. As expected, cells in the WT, continued growing (Figure 10). Since sorting of positive events is long, we should consider possible effects of the sorting process on the cell physiology.

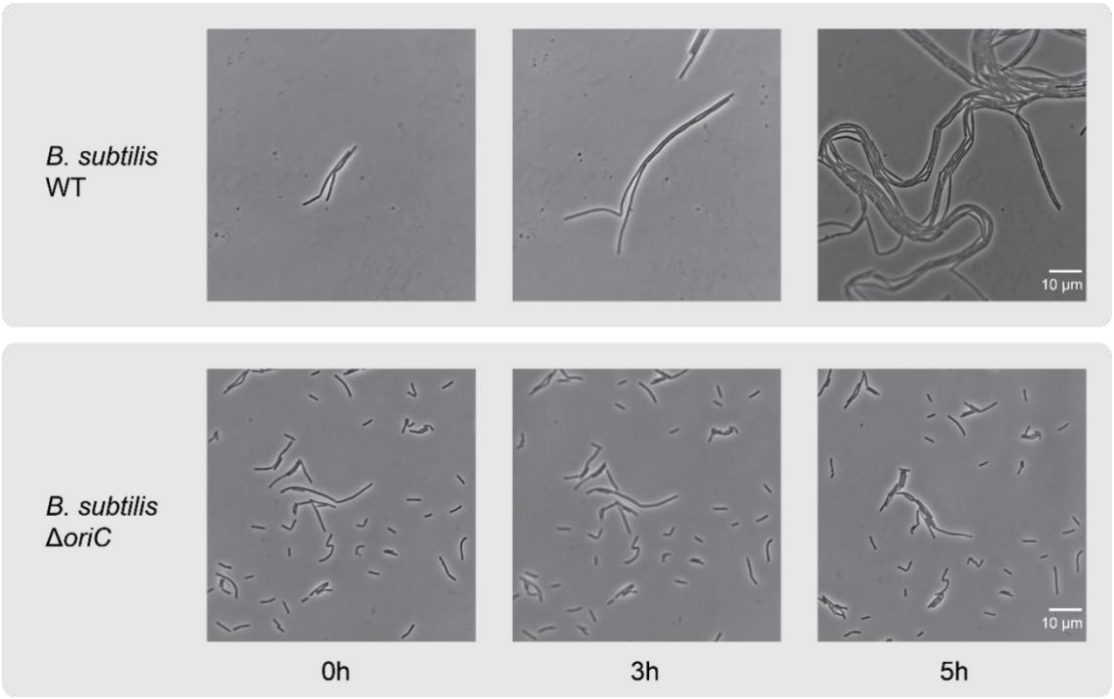

Figure 10. Visualization of population dynamics after FACS recovery.
Shown are snapshots from a movie of WT strain and GFP+ events from the strain with modified *oriC* and the CRISPR system in a plasmid. Images are in phase contrast and intervals of the video were taken every 30 min.

To observe the chromosome integrity of GFP fluorescent cells, cells were stained with SYTO63. Cells with red fluorescent (SYTO63) show the DNA content of the cells. Surprisingly, when analysed at the DNA content level, we found that some GFP fluorescent cells had lowered or absent DNA content after 3 and 20 hours of mannose induction (Figure 11).

We hypothesize that the absence of the chromosome could occur either because the chromosome is not segregated or partially segregated and ultimately truncated by septum formation where the chromosomal DNA is eventually degraded, a process called the guillotine effect[239].

From these results, we infer that DNA degradation is one of the CRISPR editing outcomes. Due to the active multifork replication, each newborn cell contains more than one *oriC*, therefore between 4 or more DSB caused by CRISPR have to be repaired. This enhanced burden on DSB could result in the degradation of the chromosomal DNA. To further investigate if the chromosome of these cells gets degraded, one could think of using SSB protein fused to GFP as a reporter for nucleoid stability (Ref).

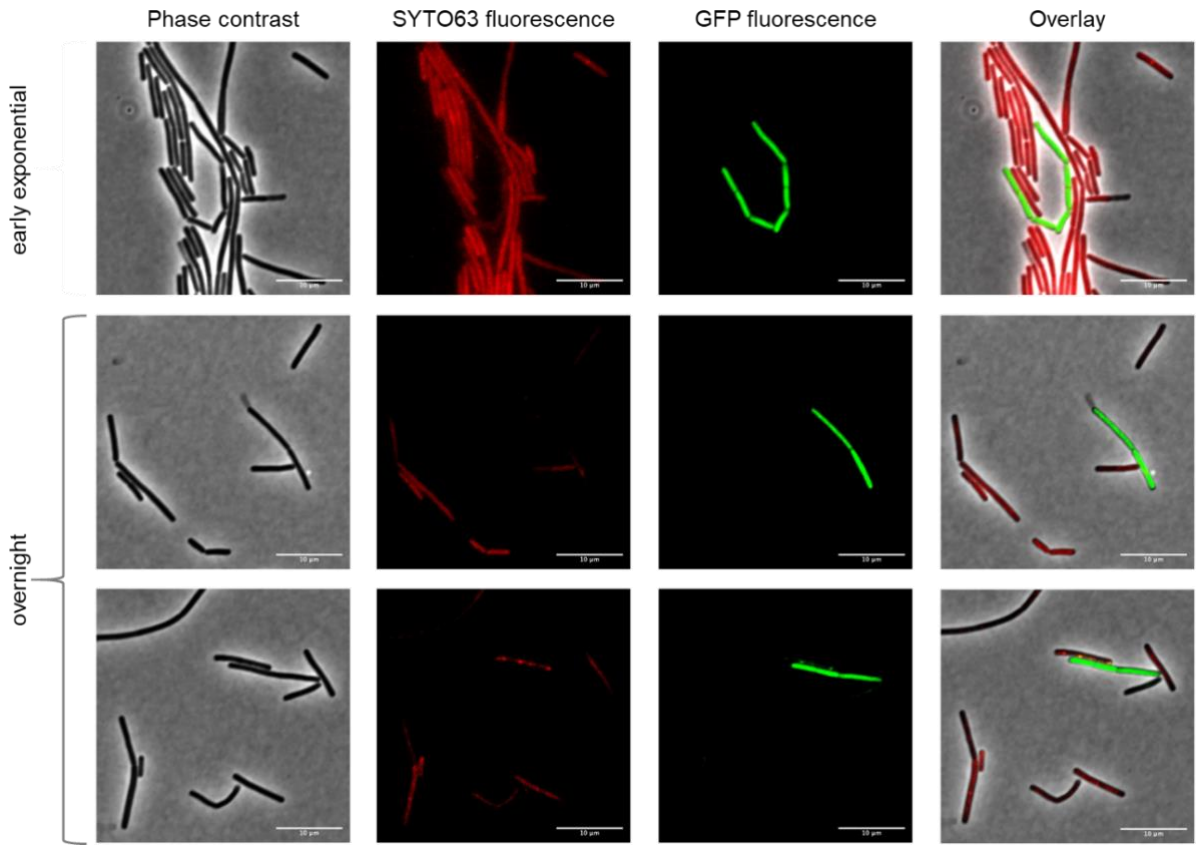

Figure 11. DNA loss is observed in some GFP⁺ cells
Selected events in the early exponential and stationary phase of the cultures. DNA content is seen in red fluorescence and edited events in green fluorescence. Some editing events did not have a clear chromosome content and are depicted here. Pictures represent selected events that show lack of chromosome.

In summary, three factors hindered our capacity to perform further proteomics analysis and clean PCRs: (1) the timing of the sorting was long due to low proportion of GFP cells (2) the

sorting effect on cells during the timing of recovery, which affects cell physiology and (3) the total number of recovered cells was insufficient.

The results with the plasmid system demonstrate that our experimental approach is feasible to delete part of the replication initiation machinery but is inefficient for adequate global downstream analysis. Moreover, the usage of this specific plasmid system imposes several challenges, such as dependence on antibiotic addition and restrictive temperature to perform experiments. Therefore, we wanted to alleviate these constraints by integrating the CRISPR system in the genome.

3.1.2 Chromosome-based CRISPR-Cas9 system for deletion of *oriC*

To optimize the CRISPR system previously described, we designed a chromosome-based CRISPR-Cas9 editing system. With this system, we aimed to have a more attenuated Cas9 expression by inserting the CRISPR system next to the P_{dnaAN} operon. Additionally, we inserted the system inside the regions to be removed so that after editing is taking place, the CRISPR system gets excised too. Finally, this system would allow flexibility in temperature changes and antibiotic usage.

This system contains two modules: one module includes a sequence upstream of the *oriC* with a split GFP, a homologous region, and a protospacer (Figure 12). The second module contains the Cas9-sgRNA editing system, split GFP-fused to a kanamycin resistance (KanR) cassette, a homologous region, and a protospacer downstream of *oriC*. We used kanamycin as a second selection to detect *oriC*-deleted cells, as only non—replicating cells will reconstitute KanR and become resistant. Therefore, the addition of kanamycin to the media should kill all replicating cells. We also included the an array of *chi-sites* in the space between the protospacer and the homologous regions to protect DNA strands from degradation, since it has been observed that *chi-sites* reduce DSB processing in a RecA-dependent manner and prevent excessive loss of DNA around the break[240].

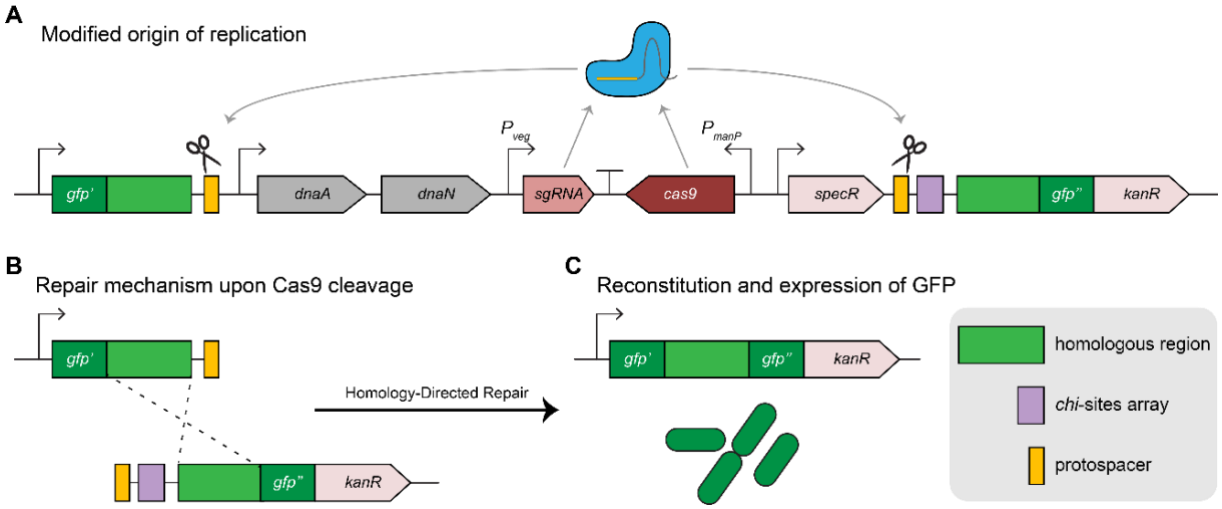

Figure 12. Chromosomal system rationale

Schematic of the modified *oriC* integrated into the *B. subtilis* genome. (A) A green fluorescent protein (GFP in green) transcriptionally fused to a kanamycin-resistant cassette (KanR) is split. The first half of the *gfp* sequence upstream of the *oriC* is transcribed from a constitutive promoter. The transcript does not result in a functional protein due to the missing back region. The native *oriC* is also flanked by synthetic protospacers (yellow). Additionally, there is a chromosomal CRISPR editing system downstream of the replication initiation locus, where sgRNA is under the control of a constitutive promoter and *cas9* is under the control of a mannose promoter. Moreover, there is an integrated chi-site array (purple) located downstream of the CRISPR system. (B)Two double-strand breaks occur in the genomic DNA after induction of Cas9 (blue) and spacer-targeting sgRNAs expression. Only cells that will have repaired these double-strand breaks by homologous recombination can become fluorescent. Homologous regions provide the homologous repair template in the split *gfp* up and downstream (light green). Cells that successfully repair the double-strand break transcribe a complete GFP coding sequence resulting in fluorescence.

To evaluate the efficiency and functionality of the chromosomal system, we induced Cas9 expression in the cells in the mid-logarithmic growth phase (correspondent to OD_{600nm}=0.3-0.4), and after 3 hours, we visualized the first marginal GFP-fluorescent cells under the microscope (Figure 13A).

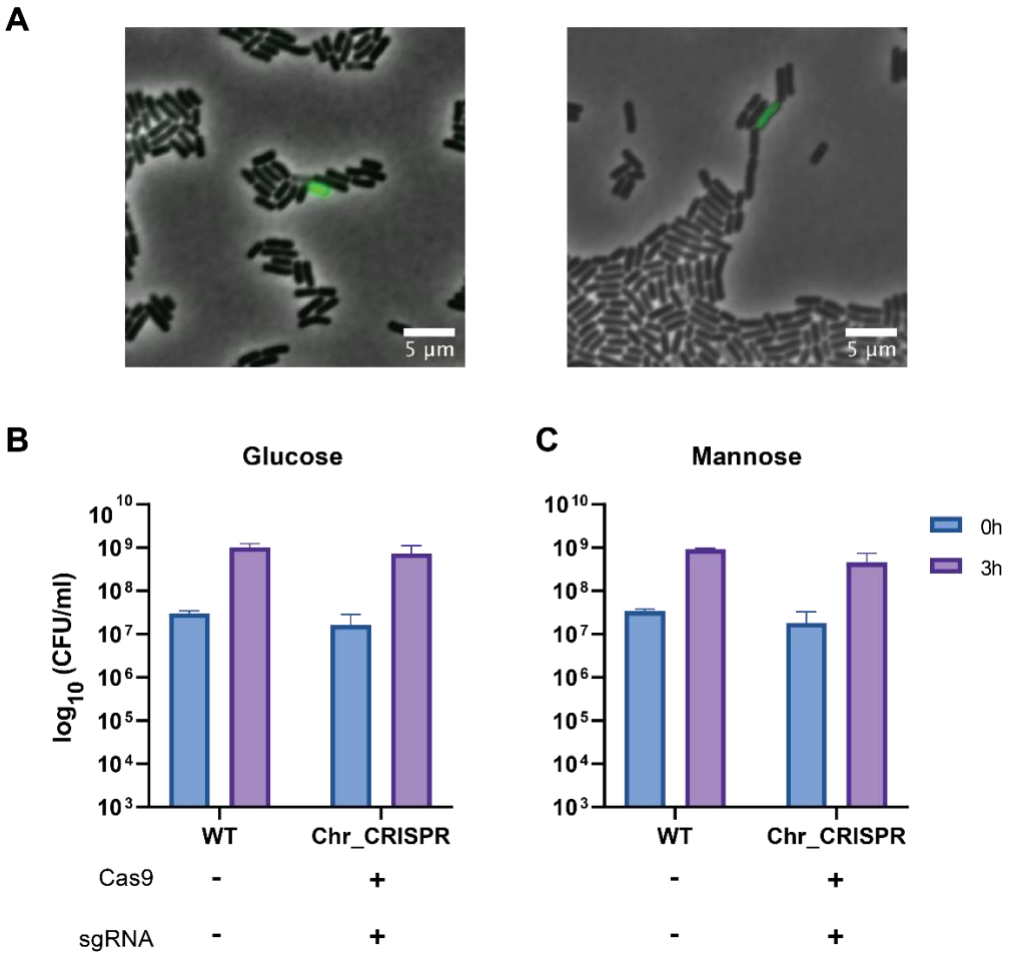

Figure 13. Effects of replication initiation machinery deletion on *B. subtilis* with the chromosomal system.

(A) Fluorescence microscopy of modified strains were induced with the CRISPR system (addition of mannose) in exponential phase. Experiment performed in triplicates; the image is a representative selection of the GFP+ events. (B) Colony survival after growing modified strain in Cas9 repression or induction conditions in Glucose 1% (w/v) or Mannose 0.5% (w/v), respectively. Cells were plated in glucose to stop inhibition. Blue bars indicate time 0, and orange bars indicate time after 3 hours of Cas9 induction. Serial dilutions were plated, and colonies counted in the lowest countable dilution. Figure corresponds to three biological replicates and three technical replicates per biological replicate. The error bars indicate the standard deviation of the mean.

As expected for the strains which grew in the presence of glucose, there were no effects on cell survival (Figure 13B). Strains induced with mannose displayed a similar trend, and we detected no drop in CFU/ml. In contrast with the plasmid-based CRISPR-system where a drop in cell survival was shown (Figure 7A). The survival of the cells in the CRISPR system's presence might indicate a defective CRISPR system or the emergence of suppressor mutants. To test if the CRISPR system is defective, we selected colonies before and after experiments and sequenced their CRISPR-Cas9 system. We found no alterations in the sequence of either the Cas9, sgRNA

or their respective promoters, indicating that the CRISPR system was not mutated during the experiments. Therefore, most likely the strains growing contain suppressor mutations.

Additionally, we also tested if we could use kanamycin to kill the population of replicating cells and found it inefficient.

First, the fluorescence of the translational fusion of KanR-GFP was low, hindering the detection of positive events by FACS. After several FACS trials to recover the GFP-KanR$^+$ cells, we found it challenging to separate the populations. We confirmed a weaker fluorescence intensity by gating the positive control with a strain containing an integrated GFP-KanR fusion under the control of a P_{degQ36} promoter. Second, the effect of kanamycin in the cells was slow and did not trigger cell lysis during the experiments, which could have been ideal to separate cells. This suggested a low activity of both functions of KanR-GFP.

We then decided to confirm the editing events via PCR verifications in the bulk culture with primers annealing outside of the *oriC* region in the batch culture after 3 hours of treatment with mannose. We identified two bands; one corresponds to the entire modified *oriC* region (11.7 kb) and the second one to *oriC*-deleted cells (2.1 kb) (Figure 14A). We subjected the cells to either mannose or glucose growth conditions and run an agarose gel after 3 hours. We then cut the editing bands and analysed their DNA sequence sequenced by Sanger. To our surprise, there was around 18 to 20x more acquisition of mutations when the CRISPR system was induced compared to the repression conditions where 0 to 1 mutation were acquired in the different biological replicates (Figure 14B and 14C). These results could indicate Cas9 induces the acquisition of more mutations. However, these results represent the bulk's editing effects, and it does not mean a single cell has acquired 20 mutations. Therefore, the interpretation is difficult. However, a more in-depth analysis by next-generation sequencing could assess the mutation frequency more accurately.

It has been demonstrated that CRISPR effectors can have a toxic effect on bacteria if they are expressed to high levels. The impact of toxicity differs among different organisms, and the type of Cas9 used. The overexpression of *S. pyogenes* dCas9 (*Sp*dCas9) leads to growth defects[114] and morphological defects[241] in *E. coli*. Likewise, *Sp*dCas9 is toxic to mycobacteria, but this toxicity can be alleviated using a different Cas9 ortholog from *Streptococcus thermophilus*[242]. Similarly, *Sp*Cas9 is toxic to cyanobacteria[243], but Cas12a from *Francisella novicida* is not[244].

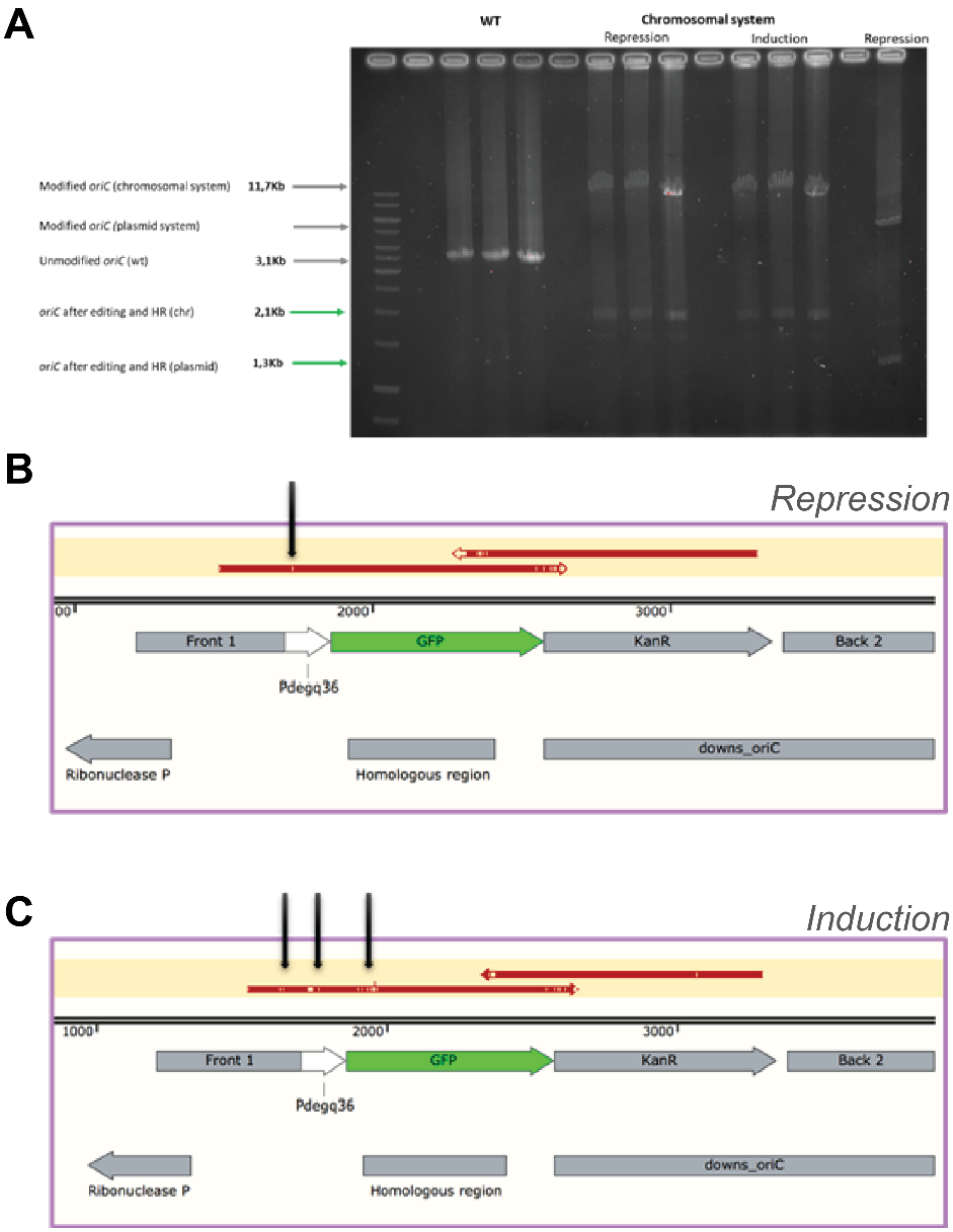

Figure 14. Editing events are detected in the modified origin of replication carrying the chromosomal CRISPR system.

(A) Agarose gel showing PCR amplified CRISPR arrays of WT, strain with modified *oriC* and chromosomal CRISPR system, and a control of a strain with modified *oriC* and plasmid CRISPR system. Strain with modified *oriC* and chromosomal CRISPR system was observed after 3 h of repression (glucose) or induction (mannose) conditions. Images are shown for three biological replicates. (B) Sanger sequencing alignment of the 2.1 kb bands in (A) in both repression and induction conditions. Black arrows indicate the acquisition of mutations compared to the expected edited sequence.

In conclusion, we established a system that enables deleting the *oriC* and selecting and enriching these mutants. Particularly, we constructed inducible CRISPR-Cas9 systems to perform a clean deletion of the DNA replication machinery, leading to a reconstitution of GFP. We found that the extrachromosomal system (plasmid-based) is less stable than the chromosomal system. We established a chromosomal system with a second antibiotic screen, chi-sites flanking regions to prevent strand degradation upon DBS. However, these added features were insufficient to increase the proportion of GFP^+ cells to perform multi-omics experiments. Our initial sequencing results from the batch PCR suggest that mutations in the HR are present, but no proportion could be calculated. As our focus is on the general characterization of replication-halted *B. subtilis* at the proteomic level, we emphasize that although both plasmid and the chromosomal system proved to work to produce CRISPR-mediated *oriC*-less cells, the percentage of recovery is insufficient to perform a global analysis, thus restricting the analysis of these cells to current single-cell methods, such as microfluidics. Therefore, we devised a new strategy to create a system independent of DBS that does not require HR, and switched to a CRISPRi (Section 3.2).

3.1 CRISPRi – Impeding the binding of DnaA to specific DnaA boxes

A recent study unravelled the molecular details of the origin of replication in *B. subtilis* and precisely pinpoints at DnaA boxes 6 and 7 as crucial for DNA unwinding and replication initiation[21]. Based on this observation, we decided to use a CRISPRi approach to target those specific DnaA boxes to stop replication initiation in a targeted manner, similarly to an approach that has been previously applied in *E. coli*[118]. To establish such a system, we used *B. subtilis* integrative plasmids from the Carol Gross lab where dCas9 is under the control of a xylose inducible promoter (P_{xyl}) and integrated into the *lacA* locus, and the sgRNA is under a strong constitutive promoter (P_{veg}) in the *amyE* locus[221] (Fig. 15A). The integrations were performed in *B. subtilis* PY79.

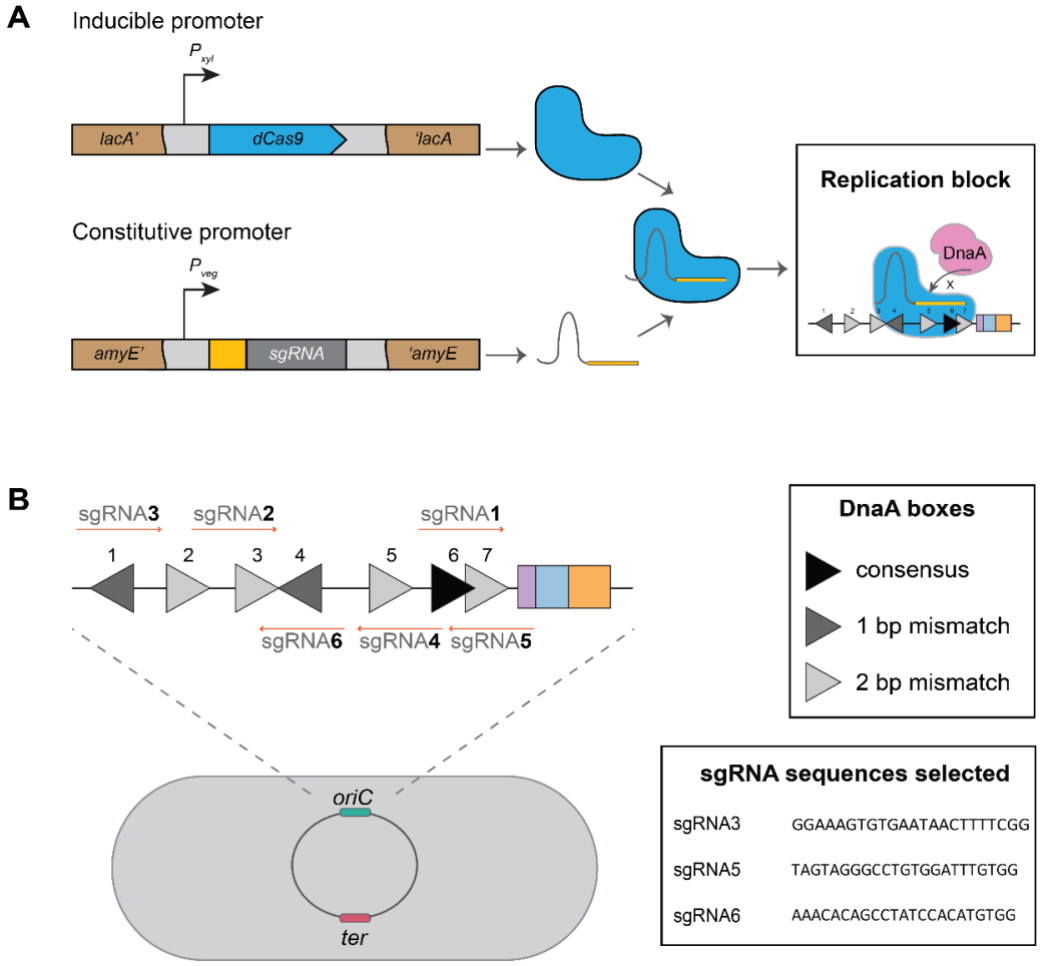

Figure 15. CRISPRi system strategy to produce replication arrest.
(A) *B. subtilis* xylose-inducible dCas9 (blue) is directed to specific DNA targets by constitutively expressed sgRNAs (yellow) under the P_{veg} promoter control. The dCas9-sgRNA complex blocks the binding of DnaA (pink) to the DnaA boxes (triangles). *dcas9* was stably integrated into the *lacA* locus, and the sgRNAs were integrated into the *amyE* locus. (B) DnaA boxes from *B. subtilis* and all the possible sgRNA targets according to the PAMs present (left side). The three spacer sequences to perform further experiments were selected by off-target scoring (right bottom corner).

We evaluated all the possible PAM sequences within the *oriC* region to use them as a target for the CRISPRi system (Fig. 15B). Three guides were chosen by off-target scoring (Table S1). Since we intended to target the DnaA boxes 6 and 7, we selected the sgRNA5 (here after, sgRNA^{box6-7}) to block access to these DNA boxes (Fig. 15B). Additionally, we selected the sgRNA3 (hereafter, sgRNA^{box1-2}) and the sgRNA6 (hereafter, sgRNA^{box3-4}) to target other DnaA boxes in the *oriC* region and evaluate the inhibition effects. We avoided a multiplexing approach because of the close proximity of the DnaA boxes, which could cause anti-cooperative behavior[245].

We first evaluated the growth of the respective strains carrying d*cas9* integrated into the *lacA* locus and the corresponding sgRNA integrated into the *amyE* locus (Fig. 16). These experiments were performed in LB with 1%(w/v) glucose to avoid basal levels of expression of dCas9. The presence of glucose in the media the xylose promoter[246], thereby preventing leaky expression from the *xylR* promoter.

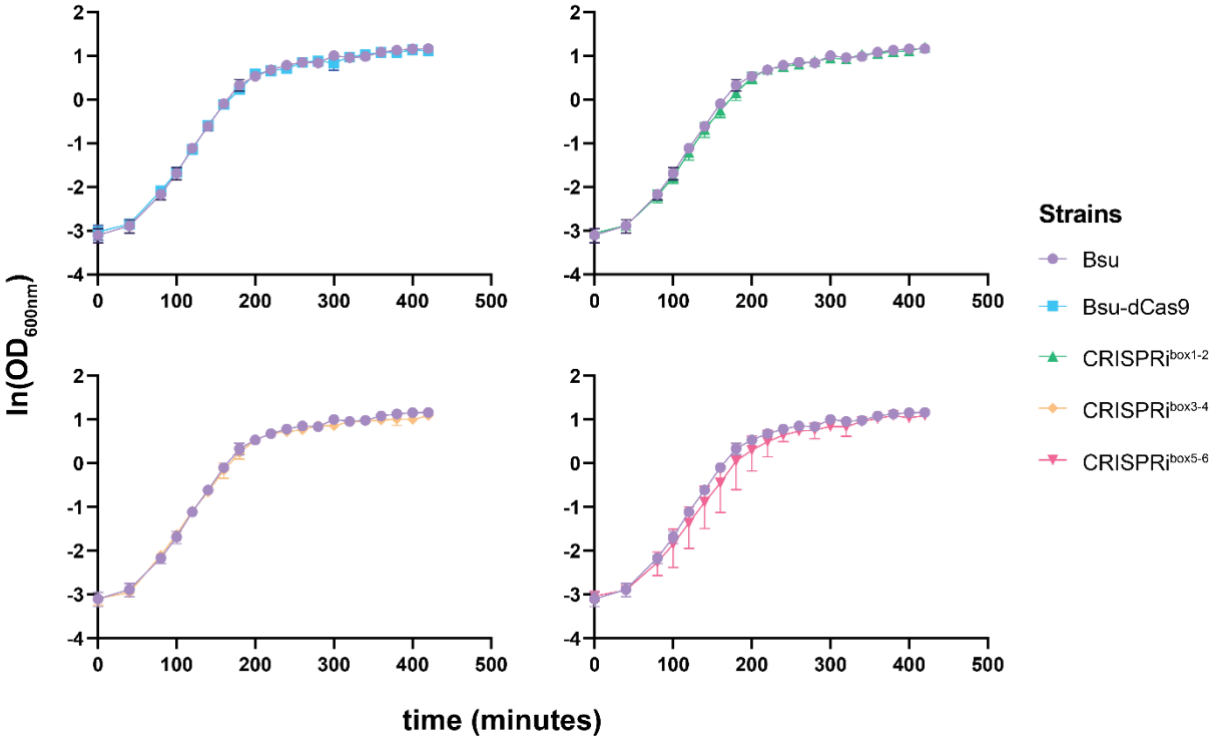

Figure 16. CRISPRi system does not affect the growth of *B. subtilis* in repressive conditions. Growth curves of *B. subtilis* wildtype and CRISPRi strains in LB amended with 1% glucose at 37 °C in shaking waterbath. The data represents the average of three biological replicates ± the standard deviation (except for strain CRISPRi^{box3-4} which only has 2 biological replicates). For clarity reasons, the growth curve of the wildtype strain (Bsu) is showed on every panel. K.S. contributed to the replication of the *B. subtilis* growth curves.

The respective strains containing dCas9 (here after, Bsu-dCas9), dCas9 and sgRNA^{box1-2} (here after, CRISPRi^{box1-2}) and dCas9 and sgRNA^{box6-7} (here after, CRISPRi^{box6-7}) displayed growth curves similar to the parental strain under P_{xyl} repression conditions (addition of glucose). Conversely, a strain encoding d*cas9* and sgRNA^{box3-4} (hereafter, CRISPRi^{box3-4}) displayed a slower growth compared to the parental strain and other mutant strains (Figure 11). These results demonstrated that integration of d*cas9* or the complete CRISPRi system alone does not dramatically affect growth.

To validate the inhibition of cell propagation by CRISPRi, we quantified the CFU/ml after dCas9 induction or repression. Our results show that all strains had a similar CFU/ml counts and that the expression of dCas9 alone had no effect on cell viability (Fig. 17A). Conversely, we observe a drop in viability when dCas9 and sgRNA^{box6-7} were expressed simultaneously, while cells expressing sgRNA^{box1-2} and sgRNA^{box3-4} along with dCas9 still were able to form colonies (Fig. 17B). Our results suggest that the decreased viability of CRISPRi^{box6-7} strain results from a competition between DnaA and dCas9 at the respective DnaA boxes, preventing replication initiation and resulting in drop in CFU/ml because replication arrest is taking place. Tight binding of sgRNA/dCas9 can prevent DnaA from sequence recognition, thus preventing initial DnaA-filament formation and the subsequent opening of the replication-bubble that initiates replication.

We also observed the recovery of the CFU/ml in the last timepoint (20h), indicating that some strains escaped the CRISPRi system, possibly by suppressor mutants (Figure 17).

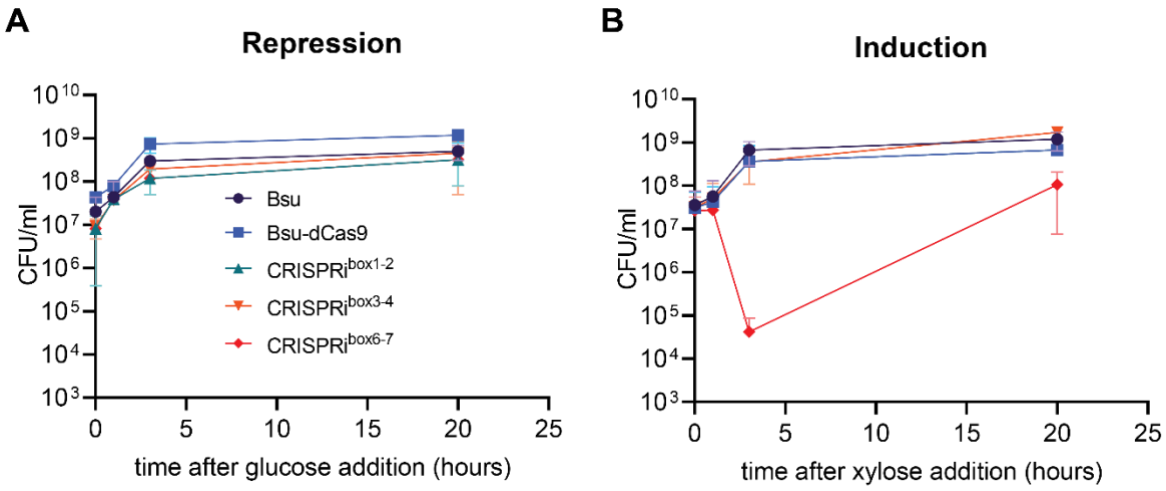

Figure 17. CRISPRi targeting DnaA boxes 6 and 7 induces a drop in colony-forming unit after 3 hours of induction in CRISPRi^{box6-7}

(A) Exponentially growing strains (OD=0.3) were divided in two (time zero); one half was treated with 1% glucose to repress dCas9. (B) The other half was treated with 1% xylose to induce the dCas9. Colony-

forming units (CFU/ml) were determined 0, 1, 2, 3, 5 and 20 h after treatment. Data points in (A) and (B) represent the mean of four independent cultures; error bars indicate standard deviations. K.S. contributed to the replicate generation.

As a strategy to have a more stable system and avoid suppressor mutants, we repeated our experiments with the wild-type and the CRISPRi$^{box6\text{-}7}$ strain and changed the induction to the early logarithmic phase ($OD_{600\ nm}$=0.01). Experiments were conducted in conditions in which dCas9 expression is induced with xylose 1% (w/w) or repressed with glucose. We then measured the CFU/ml at different timepoints (Figure 18).

As expected, under repression conditions, strain CRISPRi$^{box6\text{-}7}$ displayed similar CFU/ml counts as the wildtype through the course of the experiment, except for timepoint 20 h (Fig. 18A). This effect could be a consequence of glucose consumption and, therefore, leakiness of the *xylR* promoter. However, after 3 h of inducing dCas9 expression, we observed a significant change in the CFU/ml that is constant throughout the experiments (Fig. 18B).

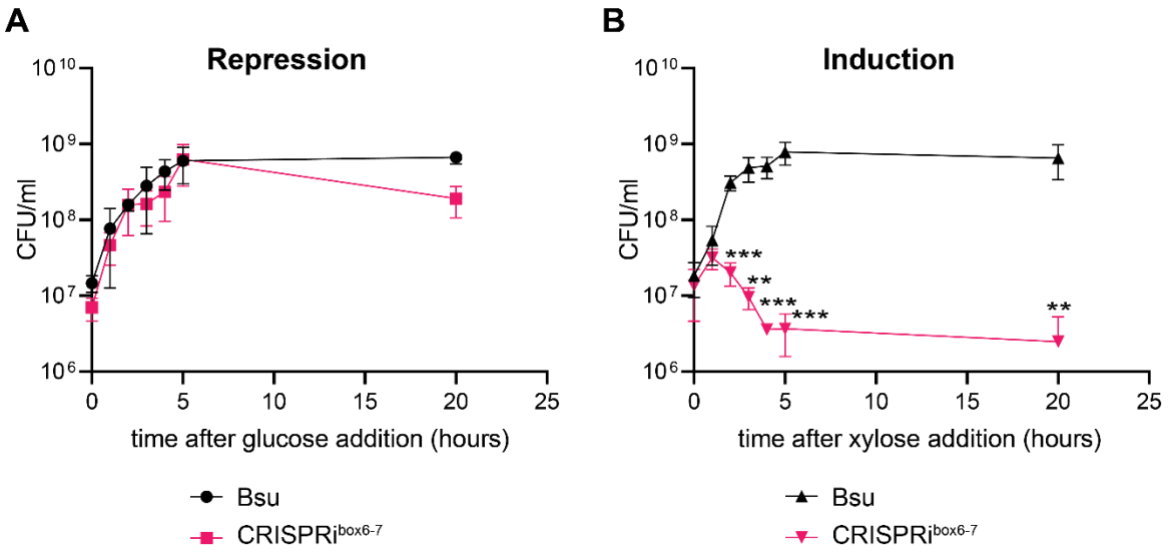

Figure 18. CRISPRi$^{box6\text{-}7}$ does not resume growth when induced at the early exponential growth phase.

(A) Early exponentially growing strains (OD ≈0.1) harbouring dCas9 under the control of xylose promoter and sgRNA constitutively expressed were divided in two (time zero); one half was treated with 1% glucose to repress dCas9. (B) The other half was treated with 1% xylose to induce dCas9. Colony-forming units (CFU/ml) were counted after 0, 1, 2, 3, 4, 5 and 20 h, and plated in LB with 1% glucose. Statistical significance was analysed using an unpaired t-test between the wildtype and the CRISPRi$^{box6\text{-}7}$ strain at t=0h (p=0.4704), 1h (p=0.1887), 2h (p=0.0002), 3h (p=0.0015), 4h (p=0.007), 5h (p=0.0009) and 20h (p=0.0063). Asterisks indicate significant differences compared to the WT.
Data points in (A) and (B) represent the mean of four independent replicates; error bars indicate standard deviations. K.S. contributed to the replicate generation.

Additionally, we observed dCas9 expression upon xylose induction at several timepoint and confirmed by mass spectrometry (Figure 21B) and Western blot that dCas9 is expressed

already after 1 hour of induction (Figure S3). However, the significant phenotypic change starts after 2 hours of induction (Figure 18B) and stabilizes after 4 h and remains constant until 20 h.

3.1.2 Replication is arrested in CRISPRi^{box6-7}

Next, we wanted to investigate whether: (1) cells are alive after CRISPRi is induced and (2) if replication has stopped.

Membrane integrity is intact under non-replicating conditions

To distinguish whether the non-replicating cells are non-viable (dead) as indicated by the CFU/ml count or if they are unable to propagate, we perform induced the CRISPRi system and analysed them by life/death staining using fluorescence microscopy. After incubating the cells for 3 h in either induction or repression conditions, we stained the cells with SYTO ® 9 (green) to label cells with an intact membrane and with propidium iodide (PI) to label cells with compromised membrane integrity (red).

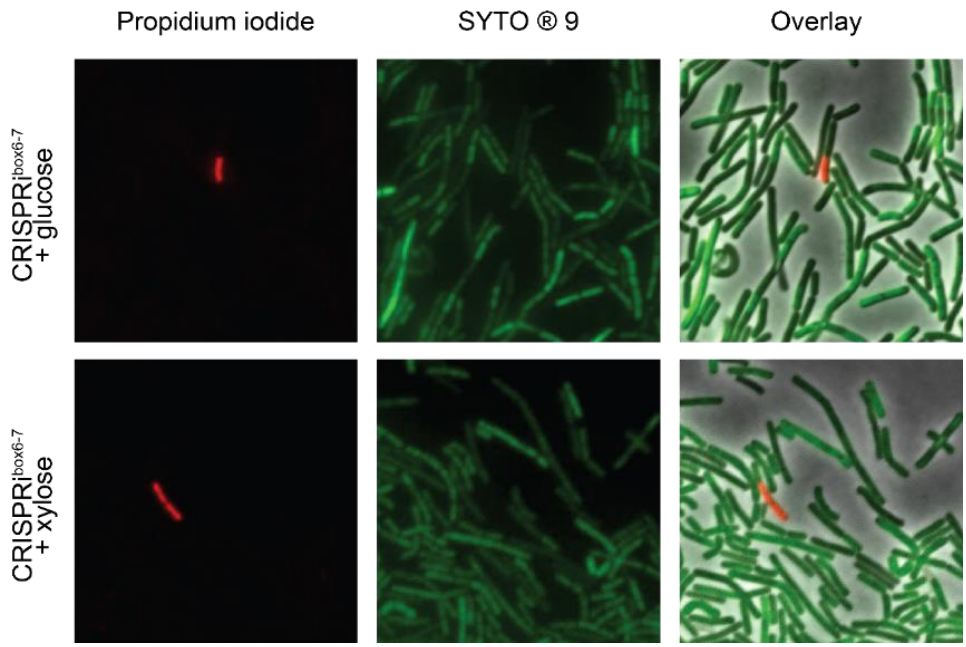

Figure 19. **Live-dead staining**

Cells after 3h of CRISPRi system expression mediated by xylose induction were prepared for dead (cell depicted in red)/live (cell depicted in green) analysis and observed by fluorescence and phase contrast (Ph) microscopy. Representative images are shown.

Nearly all cells in repression condition appeared green, indicating cells have intact membrane and are alive (Figure 19A). Similarly, after 3 h of induction (xylose) incubation, most cells also appeared green and very few displayed red fluorescence (Figure 19B). From these two

observations, we infered that inducing CRISPRi expression results in replication arrest but does not lead to cell death.

DnaN localization indicates replication fork disassembly

We used a green fluorescent protein fused to DnaN at its endogenous genomic locus to assess whether DnaN colocalizes with the replisome, to evaluate the progression of DNA replication in the cell[83]. The GFP-DnaN fusion protein forms bright foci that assemble and disassemble inside the cells, signalling the start and completion of DNA replication, respectively. Previous studies have shown that DnaN foci are not present in the cell in the absence of replication, while actively replicating cells contain between one to four DnaN foci[83,247].

The dynamic localization of GFP-DnaN was captured by fluorescence microscopy at 2, 3 and 5 h with induction of dCas9 expression (Fig. 20A). The wild-type strain displayed bright foci indicating that the replication forks are assembled, and the cells are undergoing rounds of replication. Remarkably, in strain CRISPRi$^{box6\text{-}7}$, foci diffusion is already observed after 2 hours of xylose induction, suggesting that replication is no longer initiated in these cells.

Marker-frequency analysis of the ori:ter confirms replication arrest

Since DnaA binding to the boxes 6 and 7 promotes initiation of DNA replication, and dCas9-sgRNA hampers this interaction, we wondered whether the rate of DNA replication was changed in the CRISPR$^{box6\text{-}7}$ strain under induction conditions. To test this hypothesis, we quantified the copy number ratio between chromosomal origin and terminus regions (ori:ter ratios) using real-time quantitative PCR (Figure 20C). In the wild-type strain, during exponential growth in nutrient-rich conditions, the ori:ter ratio are expected to be more than 1, as most cells have started new rounds or undergoing multifork DNA replication (Figure 20B). Consistently, the block in the DnaA boxes resulted in a decreased DNA replication initiation rate with an ori:ter ratio after 3 hours of induction of 0.88 vs 2.89 for WT cells.

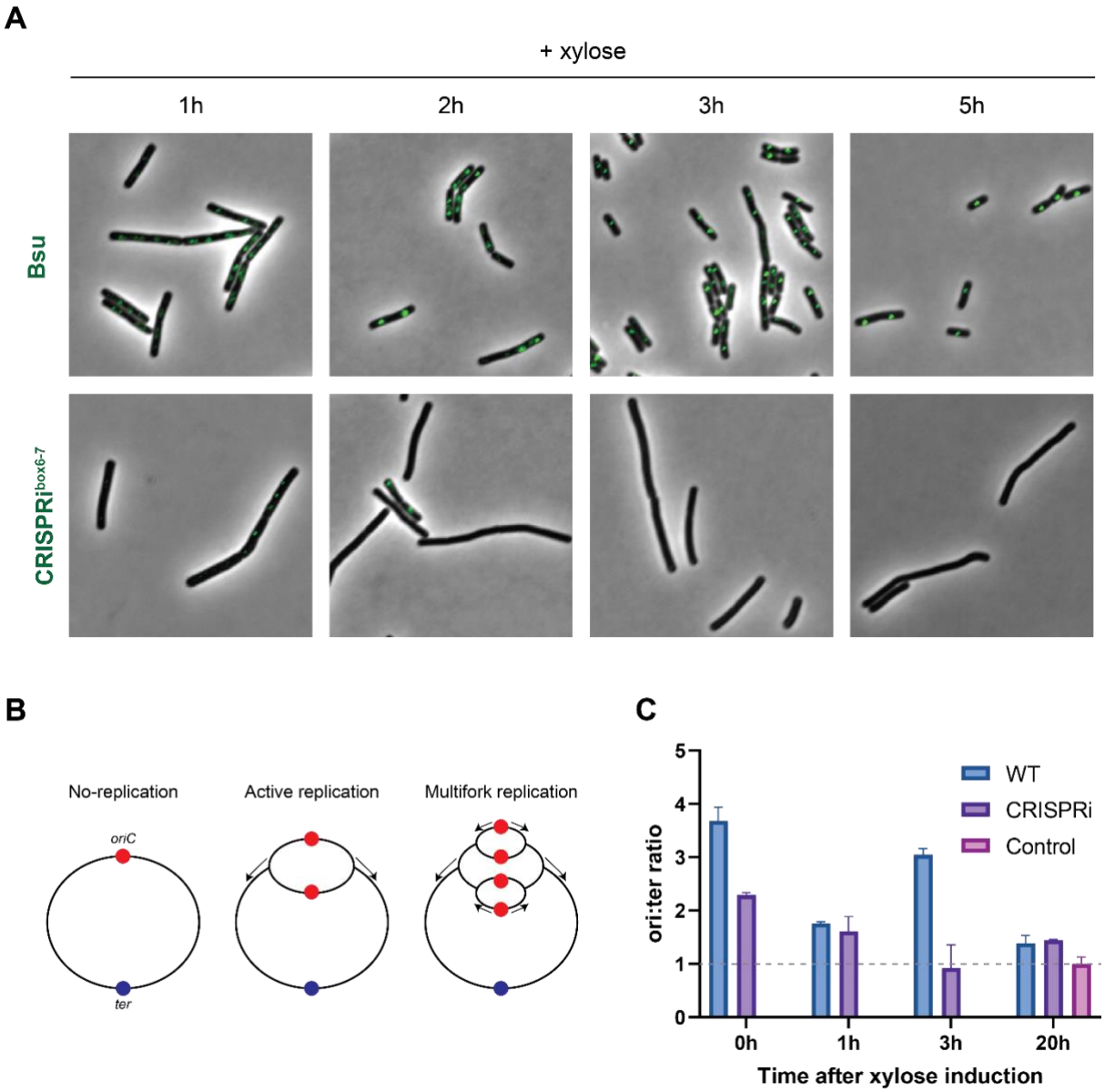

Figure 20 Replication is inhibited in the CRISPRi^{box6-7} strain.
(A) Localization of GFP-DnaN upon xylose mediated dCas9 induction. Epifluorescence microscopy of *B. subtilis* cells expressing GFP-DnaN undergoing CRISPRi replication arrest. Strains were grown in LB + 1% glucose until OD_{600nm} 0.1, washed and resuspended in LB + xylose 1%. Cells were immediately subjected to microscopic analysis at 1, 2 , 3 and 5 h after xylose addition. (B) Explanation of replication states in bacteria. In nutrient-rich conditions, chromosomes undergo multifork replication and have more than one *oriC* (red) per cell; therefore, their *ori* to *ter* (blue) ratio is higher than in non-replicating conditions. (C) ori:ter ratios as determined by RT-qPCR for wild type and CRISPRi^{box6-7} cells. Replication block leads to a clear reduction in the ori:ter ratio. *B. subtillis* cells in the stationary phase were used as control. Data points in (C) represent the means of two independent replicates; error bars indicate standard deviations of the mean.

Global proteome changes after CRISPRi mediated replication arrest

Next, we wanted to better understand the global response of *B. subtilis* to the CRISPRi-mediated replication arrest, we decided to perform quantitative mass spectrometry (MS) analysis. Based on the survival experiments in Fig 18, we determined that time points 0, 3, 4, 5 and 6 hours after xylose addition will be taken for MS analysis to follow replication arrest mediated by CRISPRi.

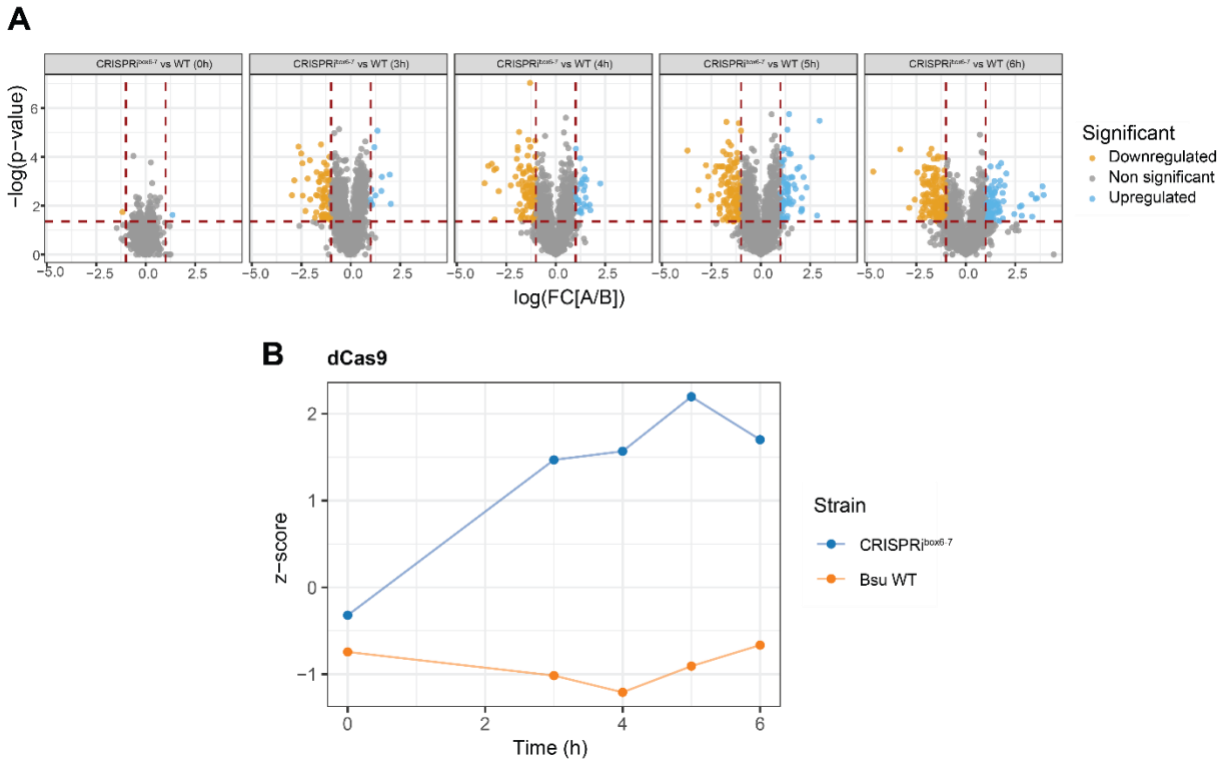

Figure 21. *B. subtilis* proteomic response to replication arrest
(A) Volcano plot of the WT strain versus the CRISPRi^{box6-7} strain, showing the statistical significance (*p*-value) versus magnitude of change (fold of change), each protein is represented as a dot. Proteins with statistically significant differential expression (≥1.5-fold, $p<0.05$) located in the top right and left quadrants. Differential expression analysis was performed by C.F. and F.A.C. and analysed by F.A.C. and V.M. (B) Trends are shown for the differentially expressed dCas9 protein. The yellow lines represent the median Z-scores for the set of proteins of the wildtype across all timepoints upon xylose induction, whereas the blue lines indicate the one of the CRISPRi^{box6-7} strain. Underlying data analysis and presentation was supported by FAC.

To explore the proteome changes in *B. subtilis* after the replication block, we quantitatively analysed the overall proteome changes between the wild-type and the CRISPRi^{box6-7} strains growing in LB+1% xylose using TMT labelling. Since the wild-type strain does not carry the CRISPRi system, we first asked, how similar are the protein profiles between wild-type and the CRISPRi^{box6-7} strains at the beginning of the experiment (t=0h). The differential protein abundance analysis revealed that at timepoint 0, the two proteomes were similar, showing only two proteins with different abundances (Figure 21A). As expected, after 3 hours of dCas9 expression, we detected

an increase differentially abundant proteins between the two strains. The differential abundance ranges from 63 less and 11 more proteins after 3 hours of xylose induction to 133 less and 67 more abundant proteins after 6 hours of xylose induction (Figure 21A). This indicates that over time, there is an increment of differential protein abundance. The protein expression analysis at different timepoint was performed with an absolute $\log_2$ fold change ($\log_2$ FC) ≥ 1 and an adjusted *p*-value < 0.05 (Figure 21A).

The levels of the proteins of the replication machinery are not changing upon CRISPRi replication initiation block

It could be assumed that due to the CRISPRi induction and the replication block, replication-associated proteins are mostly downregulated. However, GSEA analysis (Figure 22) does not indicate that this process is enriched or depleted. Next, we analysed the cellular levels of individual replication proteins throughout the experiments. We created profile plots of all the proteins under the functional category Replication retrieved from SubtiWiki[1]. As shown in Figure 23, a comparison between CRISPR$^{box6\text{-}7}$ and wild-type strain indicate that most replication proteins remain at similar cellular levels. ~~One possible explanation for the constant protein abundance between these two strains could be that wild-type cells start reaching stationary phase therefore their replication proteins are not that active as in exponential phase.~~ Moreover, Figure 20C shows that at 3h, WT cells are more actively replicating that the halted CRISPRi$^{box6\text{-}7}$ strain. It is interesting to notice that the levels of replication proteins do not change that much, even in absence of replication.

To evaluate the dynamics of gene interference with this CRISPRi system, we followed the cellular protein levels for DnaN (Figure 22 – profile plot). *dnaN* is located downstream of the targeted DnaA boxes and is part of the *dnaAN* promoter. Hence, one would expect a reduced expression of DnaN when dCas9 binds to the respective DnaA box. We detected a decrease of the DnaN levels over time in CRISPR$^{box6\text{-}7}$ compared to the wild-type (Figure 23), consistent with dCas9 is binding to the DnaA boxes, thereby impeding the downstream transcription of DnaN. Moreover, dCas9 was present during the experiments in the CRISPR$^{box6\text{-}7}$ strain (Fig. 21B).

As stated, above, DnaN was downregulated because the DnaA boxes are directly located upstream of this gene, impeding its transcription. In the case of DnaA, which is located upstream of the targeted DnaA boxes, we observe there is a slight decrease compared to the WT (Figure

23), which can be a consequence of being located in the same operon where the CRISPRi block is taking place[216].

Interestingly, the other highly abundant protein in the WT at timepoints 3, 4 and 5 hours was SsbB and downregulated after 6 hours (Figure 22). In *B. subtilis*, SsbB (YwpH)[253,254] is a single-stranded DNA (ssDNA) binding protein (SSB)[255], and like other SSBs, its expression is elevated during SOS response and interact with RecA[254]. Its expression is ComK dependent, and the gene product is required for natural transformation[254]. The expression of SsbB in WT conditions could indicate cell undergo SOS response when reaching stationary phase, while in replication-arrest conditions such a system might not be activated.

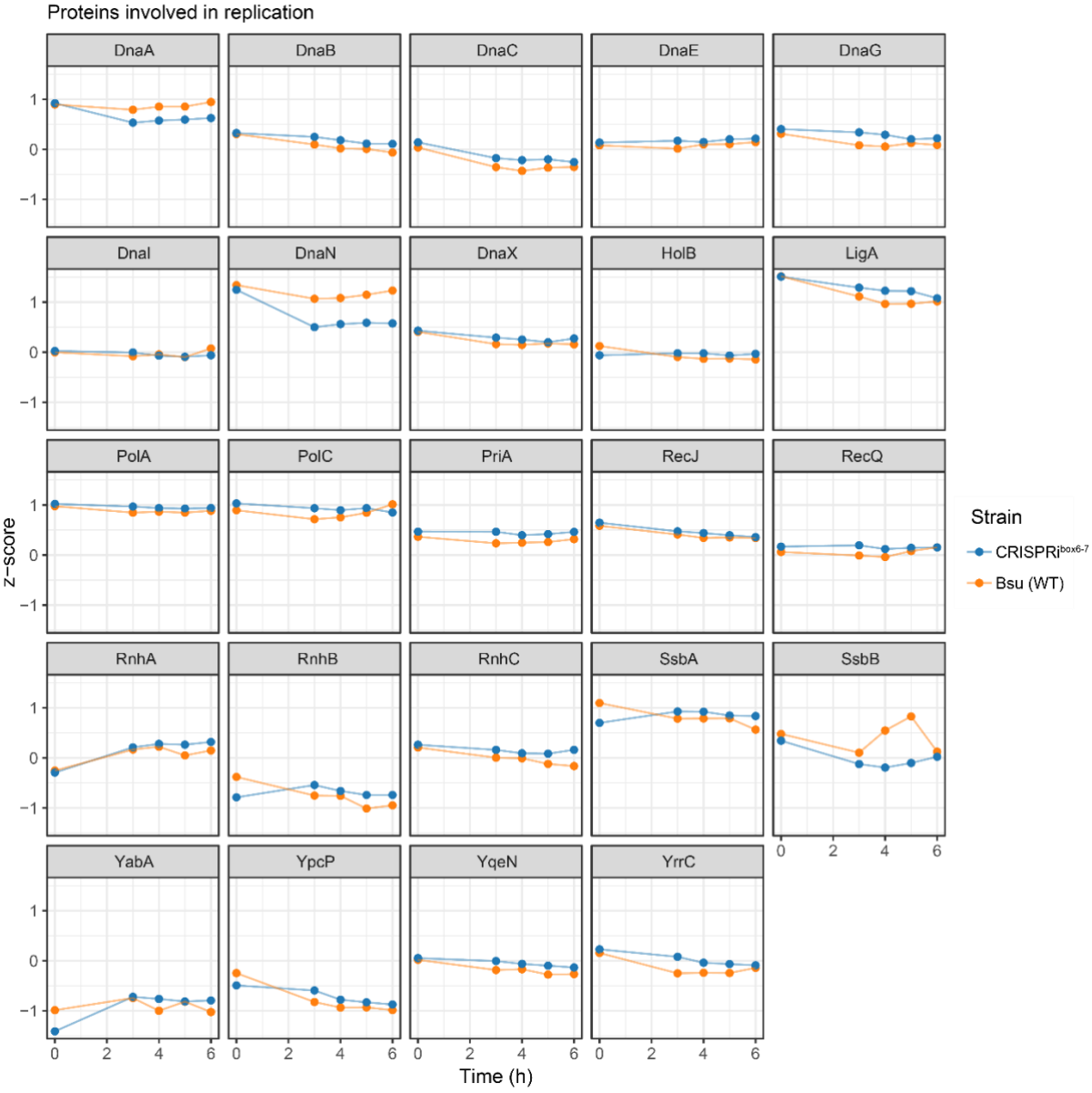

Figure 22. Replication proteins show a similar abundance profile in replication arrested and wild-type cells.

Abundance profile are shown for the differentially expressed proteins belonging to the functional category *Replication*, obtained from SubtiWiki. The yellow lines represent the average z-score for the set of proteins of the wildtype across all timepoints, whereas the blue lines indicate the one of the CRISPRi^{box6-7} strain. Experiments analyzed from three biological samples. Underlying data analysis and presentation was supported by FAC.

Functional process analysis from the proteomic data

To obtain a global view of up- and downregulated functional processes upon CRISPRi induction, we performed a Gene set enrichment analysis (GSEA)[248,249] and identified enrichment in the KEGG pathways, Gene Ontology, UniProt Keywords, InterPro, and SMART categories using the DAVID database[250–252] (Figure 22).

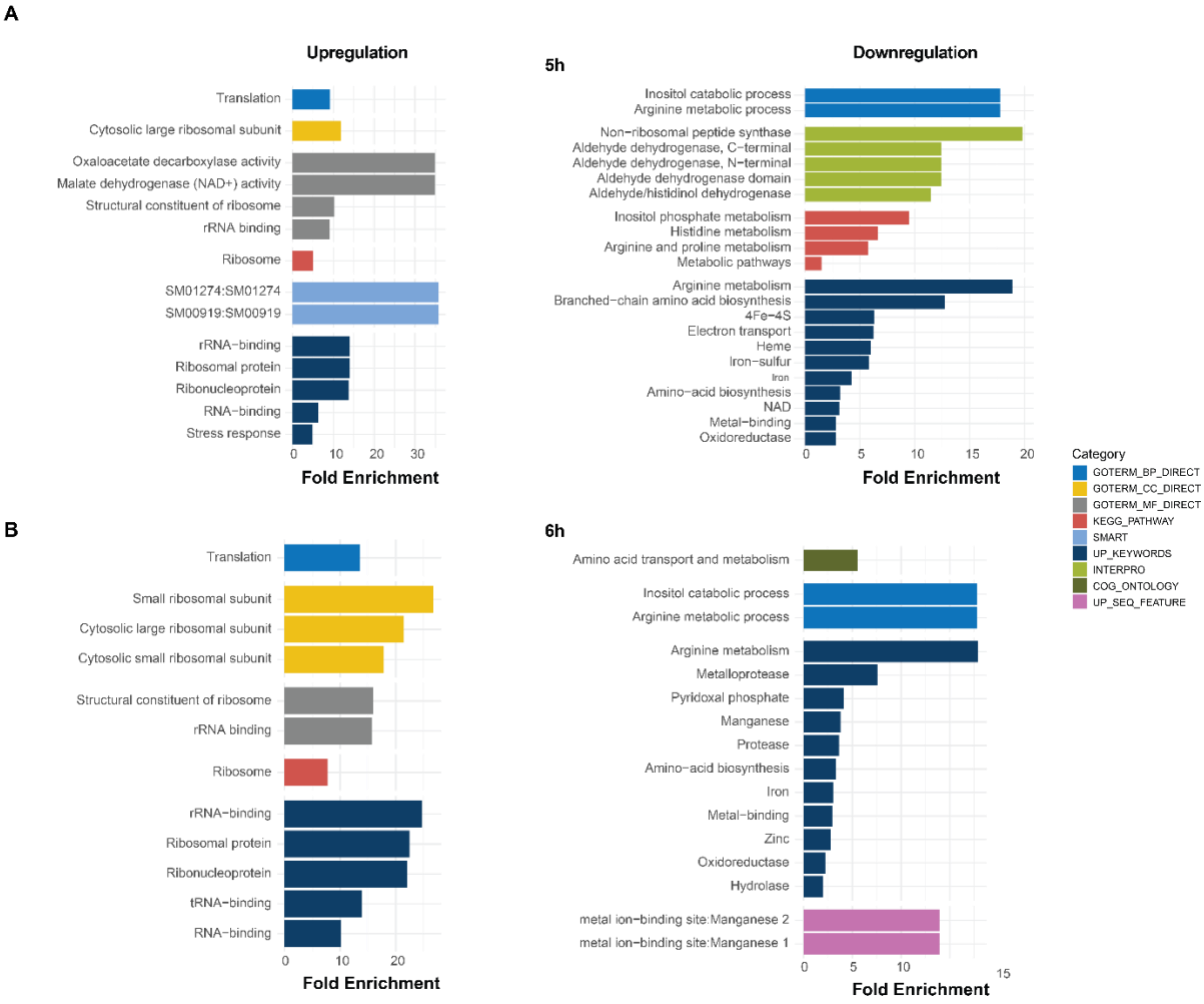

Figure 23. Down- and upregulated pathways after replication inhibition in CRISPRi^{box6-7}.
The fold enrichment value represents the fraction of quantified proteins belonging to a particular category compared to the total number of proteins assigned to that category in the genome. Underlying data analysis and presentation was supported by FAC.

After 3 hours of CRISPRi expression, proteins with reduced abundance mainly belonged to the inositol metabolism. Similarly, proteins related to the inositol catabolic process are less abundant going along with nitrate assimilation and nitrogen metabolism after 4 hours of CRISPRi induction (Figure S4.). Interestingly, proteins linked to translation, small and large ribosomal subunits, and other ribosome constituents were more abundant after 5 and 6 hours of CRISPRi induction (Figure 22). Altogether, our results suggest that CRISPRi-mediated replication initiation arrest upregulates translation, whereas inositol, nitrogen and arginine metabolism pathways are downregulated.

SOS response is not triggered under replication arrest

One of the possible consequences of inducing replication arrest in a rich medium is the occurrence of replication-transcription conflicts at stalled replication forks that can result in DNA damage. To evaluate DNA-damage response (DDR), we integrated a *gfp* translational fusion of the *yneA* gene in the *amyE* locus. DNA damage leads to the induction of LexA repressed genes such as *yneA*[219]. We grew the WT and CRISPRi$^{box6\text{-}7}$ strains until early exponential phase and divided them into three groups: one grew in the presence of either LB + 1% glucose, one in 1% xylose or one in mitomycin.

The presence of GFP fluorescence in both WT and CRISPRi$^{box6\text{-}7}$ in xylose conditions is rare ranging from 0.09 to 0.37% depending on the timepoint (Figure 24) compared to the mitomycin treatment where 98-100% of cells are fluorescent. This observation indicates SOS response is not induced under replication arrest, which coincides with the protein abundance profile retrieved from the MS data, where this process is not enriched in the CRISPR$^{box6\text{-}7}$ strain.

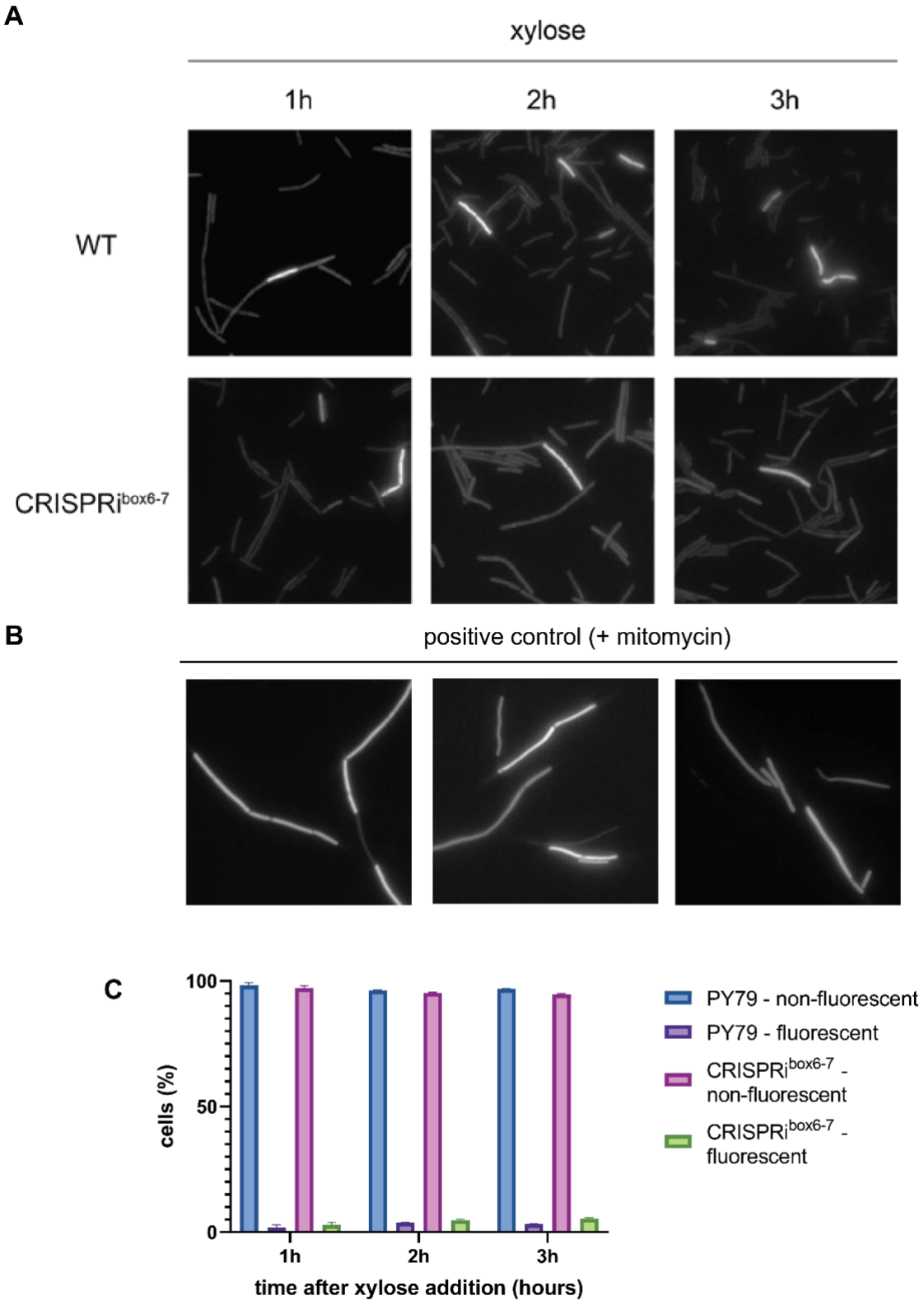

Figure 24. SOS response is not enhanced under replication arrest.
(A) Representative pictures of WT and CRISPRi^{box6-7} strains containing the *yneA-gfp* ectopic integrations and grown LB with 1% xylose. Pictures are aliquots taken from medium constantly growing at 37°C. (B) WT containing the *yneA-gfp* ectopic integration and growth in LB with mitomycin. (C) Percentage of fluorescent and non-fluorescent cells in cells in (A). At least 120 cells were count from two different biological replicates. KS supported strain generation and one replicate of this experiment.

Replication arrest with CRISPRi affects cell elongation

To determine if replication arrest affects the protein expression of other related processes like cell division, cell shape and DNA segregation, we assessed the protein changes of these specific processes (Figure 25). We observed that most proteins have similar cellular levels compared to the WT. However, we found an up-regulation of LytE (Figure 25A), a cell wall hydrolase involved in cell elongation and separation[256], whose activity requires functional MreB and MreBH[257,258]. The profiles of MreB and MreBH also show a slight up-regulation, which might suggest that this protein is expressed.

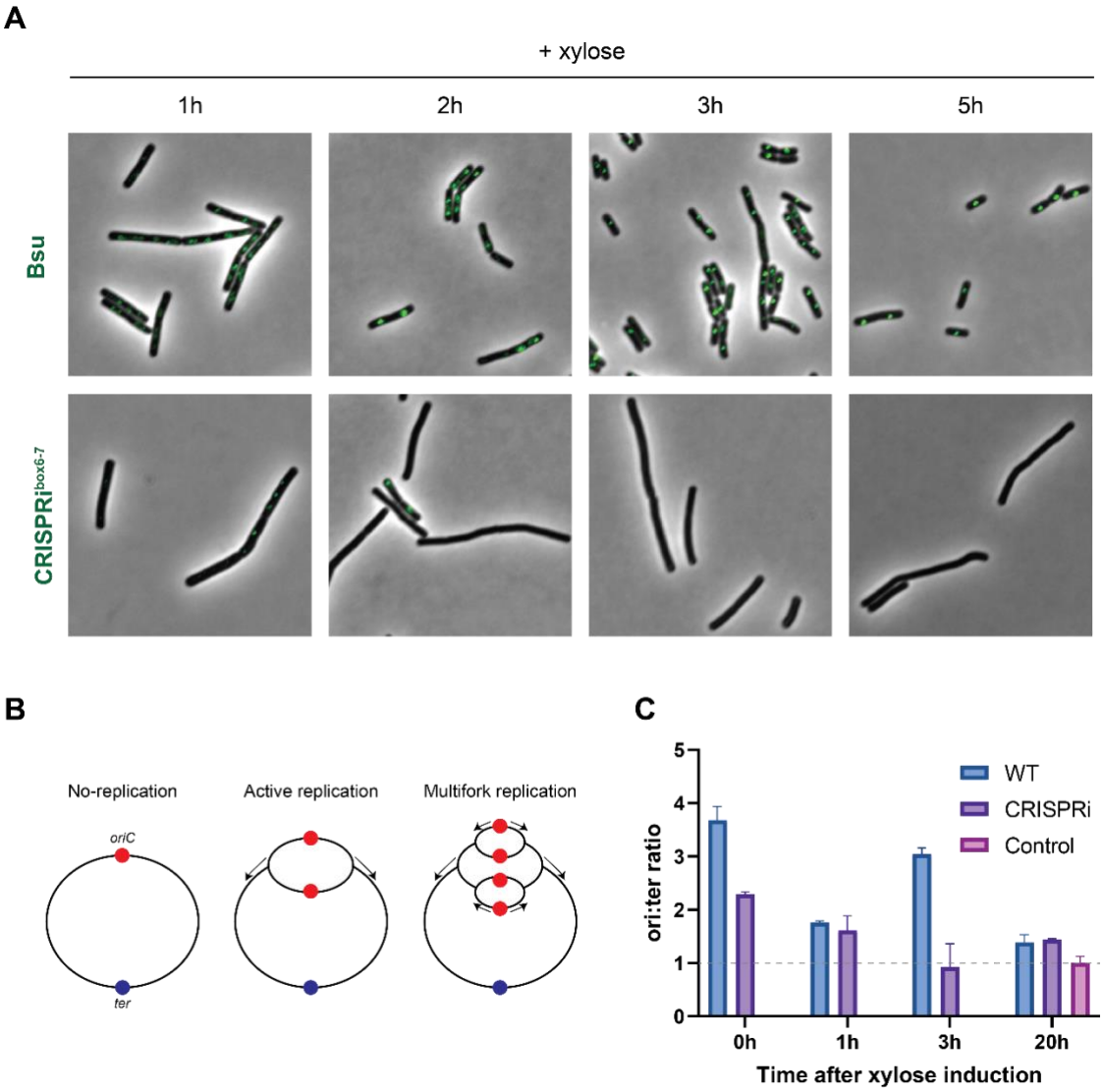

Figure 25. Cell elongation associated proteins are more abundant in replication halted cell
A) Heatmap of $\log_2$ fold change of proteins related to division, cell shape and DNA segregation processes (retrieved from SubtiWiki). Underlying data analysis and presentation was supported by FAC. (B) measurements of cell length and width in WT (Bsu) and CRISPRi^{box6-7} during growth in LB with 1% xylose. At least 80 individual cells were counted per condition. Data represents the means of two independent replicates; error bars indicate standard deviation of the mean.

To confirm if cell shape is affected upon replication arrest by CRISPRi, we measured the cell length of WT and CRISPRi^{box6-7} strains during LB with 1% xylose growth. Overall, cell width remains similar across the experiments while cell length is larger in the CRISPRi strain around 3 to 5 hours of induction of the CRISPRi system (Figure 25B). These results indicate evidence of a cell elongation during replication arrest.

Protein synthesis is increased upon inhibition of replication initiation

CRISPRi^{box6-7} showed an enrichment in translation-related proteins upon 5 hours of xylose induction compared to the WT (Figure 22). Therefore, we assayed global new protein synthesis during CRISPRi induction by measuring the incorporation of the puromycin analog O-propargyl-puromycin (OPP). Nascent peptide chains can be visualized and quantified in single cells by the addition of a fluorophore using click chemistry. Incorporation of OPP produces an accumulation of fluorescently tagged nascent polypeptide chains that correlates with the translation activity[227] (Figure 26).

WT and CRISPRi^{box6-7} strains were grown in glucose to repress CRISPRi induction or in xylose to mediate its expression at early exponential phase as previously described and after 4 hours of incubation, cells were labelled with OPP and observed under the microscope (Figure 26).

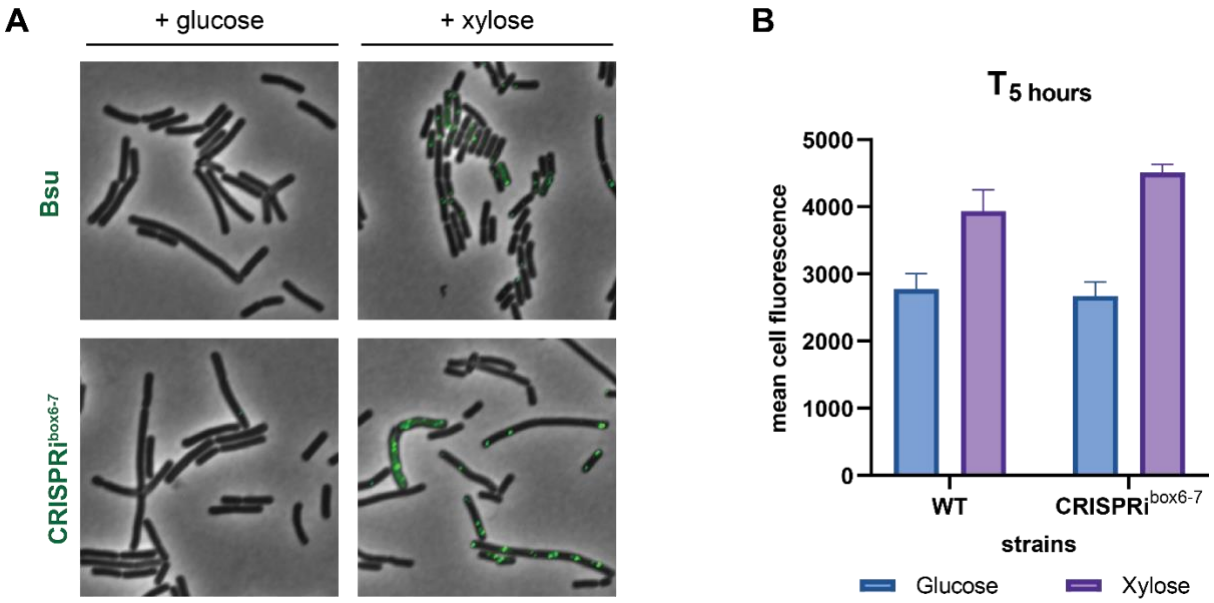

Figure 26. New protein synthesis in strains CRISPRi^{box6-7} and WT under glucose and xylose treatments.
(A) WT and CRISPRi^{box6-7} strains were growth until early exponential phase growth and growth in LB with 1% glucose. Aliquots from the batch culture were labelled with OPP after 5 hours of growth in either xylose or glucose. (B) Mean cell fluorescence of (A). Error bars indicate standard deviation. At least 100 cells were counted from two biological replicates.

Cell grown in glucose displayed bright green fluorescence at timepoint 0h that steadily decrease upon 3 and 5 h of growth (Figure 26A). This might be explained because the cells reach the point of nutrient limitation and start entering stationary phase. During xylose induction, WT cells also show decrease fluorescence over time, whereas CRISPRi$^{box6\text{-}7}$ exhibited bright foci after 5 hours of xylose induction, indicating even a higher rate of translation than the WT (Figure 26B).

Stringent response is downregulated under replication arrest

The stringent response in bacteria is a complex response in reaction to amino-acid starvation, fatty acid limitation, iron limitation, heat shock and other stress conditions[259–264]. Due to the depletion of iron metabolism and proteins related to amino acid synthesis like arginine, histidine and proline observed upon replication arrest (Figure 22), we asked if replication arrest elicits stringent response. Since the CodY repressor, also responds to an intracellular decrease in amino acid content, we analysed the protein abundance of all proteins associated to the Stringent Response and CodY regulator (Figure 27 and Supplementary figure S6).

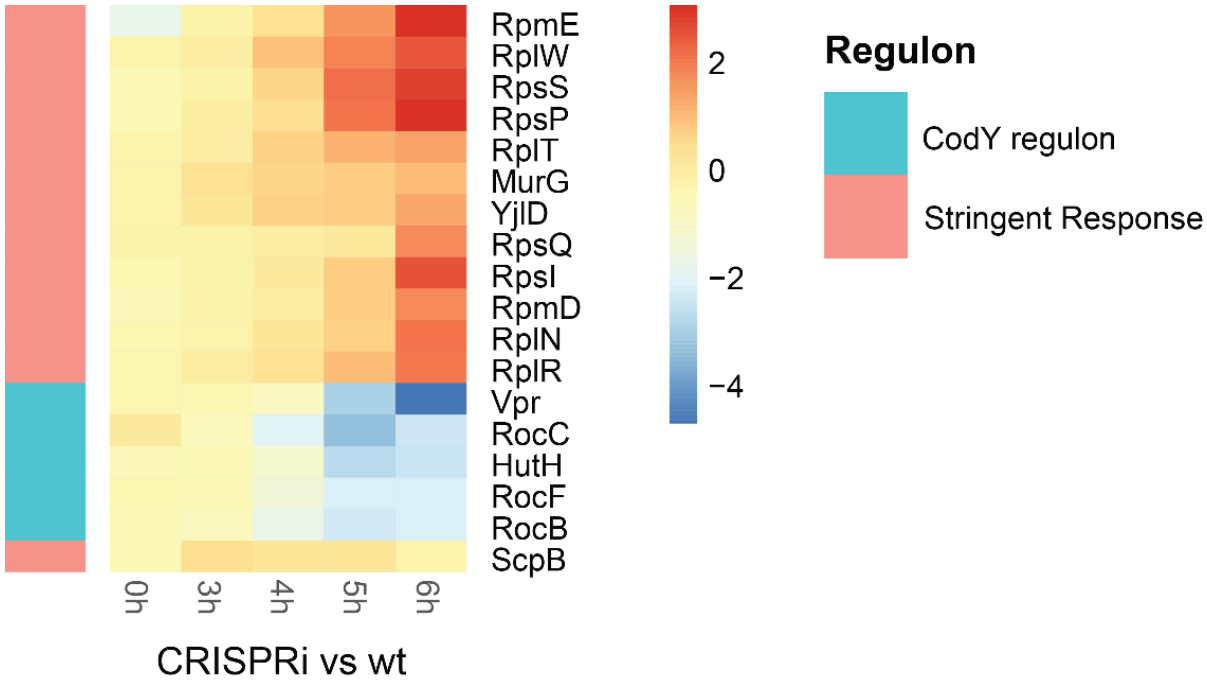

Figure 27. The ribosomal proteins related to the stringent response regulon of *B. subtilis* are upregulated.
Heatmap show proteins related to the stringent response and the CodY regulons. Shape and DNA segregation retrieved from SubtiWiki. Values represent $\log_2$ fold changes of transcript levels relative to wild type cells. Heatmap scale indicates protein abundance. N = 3. Underlying data analysis and presentation was supported by FAC.

We observed an increased level of proteins whose expression is negatively regulated during stringent response, especially ribosomal proteins (RpmE, RplW, RpsS, RpsP, RplT, RpsQ, RpsI, RpmD, RplN RplR) and decreased levels of CodY regulated proteins related to peptidoglycan biosynthesis (MurG), respiration (Nhd - YjlD), protein degradation (Vpr) and arginine utilization (RocB, RocC, RocF) (Figure 27). Indicating that there is no stringent response and that CodY is active in the CRISPRi$^{box6\text{-}7}$ strain. In addition, we did not observe an induction of YvyD levels in WT and CRISPRi$^{box6\text{-}7}$ (Supplement data file 1), which is also consistent with the absence of the stringent response[266,267]. However, there might be an induction of stringent response in the WT due to nutrient exhaustion at later timepoints.

In summary, we successfully designed and used a CRISPRi system to target DnaA boxes 6 and 7 to create a replication arrest in *B. subtilis* cells and described the impact of replication arrest on changes in the global proteome. We show that targeting DnaA boxes 6 and 7 repress colony formation, unlike targeting DnaA boxes 1 and 2 (sgRNA3) and DnaA boxes 3 and 4 (sgRNA6) where cells retained the capacity to propagate (Figure 17). Additionally, the cells have their membrane integrity intact, indicating they are alive (Figure 19). The replisome is disintegrated, indicating the absence of new replication rounds (Figure 20A). The ori:ter ratio is close to 1, demonstrating that replication is not active (Figure 20C). Additionally, global proteome analysis and OPP labelling show that translation is upregulated after replication arrest (Figure 23 and 26). Finally, stress responses such as SOS and SR seem not to be activated (Figure 24 and 27). Taken together, replication arrest in *B. subtilis* presents attractive features which could also be used for industrial applications and needs to be further evaluated.

4. Discussion

In this project, we used three different strategies to evaluate the response to replication initiation arrest in *B. subtilis*: a plasmid approach using CRISPR-Cas9, a chromosomal approach using CRISPR-Cas9, and a CRISPRi system targeting the DnaA boxes.

5.1 CRISPR-Cas9 deletion approaches

We were able to establish a plasmid-based and a chromosome-based CRISPR-Cas9 methods to enable the deletion of *dnaA-oriC-dnaN* and evaluate its phenotype. In these two approaches, the repair template was integrated into the chromosome along with inserted artificial protospacers flanking the origin of replication (Figure 6 and 12). Using these methods, we could generate *dnaA-oriC-dnaN* deletions that were observed by fluorescence microscopy and confirmed by PCR and Sanger sequencing (Figure 8 and 14). Previous *B. subtilis* editing methods have provided the CRISPR system (Cas9 and sgRNA) in a plasmid or chromosomally, while the repair template was located in a plasmid[220,267–273]. Moreover, these approaches have all relied on the availability of PAM sequences in the genome to find suitable protospacers, leaving them vulnerable to off-target effects. Here, we demonstrated that targeting CRISPR-Cas9 deletion with the integration of artificial protospacers flanking the area of interest and GFP reconstitution to select positive clones is possible but very inefficient.

However, it might become a more successful tool to delete other essential genes, sets of genes, or sequences and evaluate their phenotype at the single-cell level. For instance, with our approach, it is possible to investigate the effect of deleting the essential cell wall hydrolases in *B. subtilis*, LytE, and CwlO in a controlled manner by inducting the CRISPR system, without requiring the addition of beta-lactams that could have a more systemic effect due to their binding to different penicillin-binding proteins (PBPs).

5.1.1 Evaluation of the CRISPR-Cas9 deletion setup

The setups were suitable for easy genetic screen and phenotypic evaluation of the non-propagating cells. A limiting factor of the setups to evaluate the obtained phenotypes was the lack of a good selection screen to enrich the non-replicating cells and the insufficient frequency of events to get enough cells for global analysis. Elevated non-replicating cell counts would provide

a more feasible approach to evaluate the response to the deletion of sequences essential for replication. However, we found that using the plasmid system (Figure 6), the DSB caused in the cell containing only one protospacer and without a repair template did not result in a significant decrease in cell viability (Figure 7). Cleavage of targets lacking repair template by Cas9 is frequently lethal in bacteria[191,274]. DSB cleavage drives editing via homologous recombination (HR) or, in some bacteria, by non-homologous end joining (NHEJ) as well[200,275], a previously identified and characterized system in *Bacillus subtilis*[199]. The minimal NHEJ system in most bacteria consists of a DNA ligase (LigD) and DNA-end-binding enzyme (Ku)[189]. One possible explanation for the lack of lethality in our experiments in *B. subtilis* is that repair of the cleavage sites could be happening via NHEJ. For instance, *Streptomyces coelicolor* possesses an endogenous NHEJ system and was demonstrated to effectively repair Cas9-mediated DSB-introduced indels at the target position when no repair template was provided[275]. Additionally, the integration of the NHEJ system from *Mycobacterium tuberculosis* (MtbNHEJ) into *E. coli* can insert indels at the Cas9-introduced DSB sites[191,276]. *B. subtilis* NHEJ system has been tested in *E. coli* but functioned at lower efficiencies than the MtbNHEJ or *Mycobacterium smegmatis* NHEJ[277].

In another study in *B. subtilis*, the deletion of *ligD* facilitated the repair by HR-mediated strand breaks in an editing setup based on nCas9 (nickase Cas9)[278], a Cas9 modified to cleave only one DNA strand. Based on this observation, it might be possible to use a *ligD* knockout to improve the deletion efficiency and select positive clones of a nCas9 approach. Additionally, we are planning an analysis of mutations at the cleavage sites of the surviving clones and in the batch culture by Next-Generation Sequencing to determine the frequency of mutations and try to analyze if NHEJ is responsible for the repair of Cas9-induced DSBs. Another possible scenario for repairing Cas9-induced DSBs is that because the break was performed so close to the *oriC* during the exponential growth phase, the ongoing replication provided a parental strand that served as a repair template for HR. Repair of DBS can also occur via HR with the sister chromosome[191], especially during the logarithmic growth phase when more than one copy of the chromosome is in the cell during replication[204].

Most studies involving the generation of mutants in bacteria rely on the recovery of edited colonies carrying a selection system. Therefore, the editing efficiency is calculated using the number of edited colonies vs. unedited ones. The calculations of transformation efficiency and editing frequency, although valid, cannot take into account the editing events that result in cell lethality or non-propagating phenotypes. Therefore, the molecular details of the Cas9 editing events at the single-cell level remain elusive. In our case, we targeted the replication machinery of

B. subtilis; therefore, the editing event resulted in a non-propagating cell. We found that editing frequency occurs in around 0.4-1% of the cells (Supplementary figure 2).

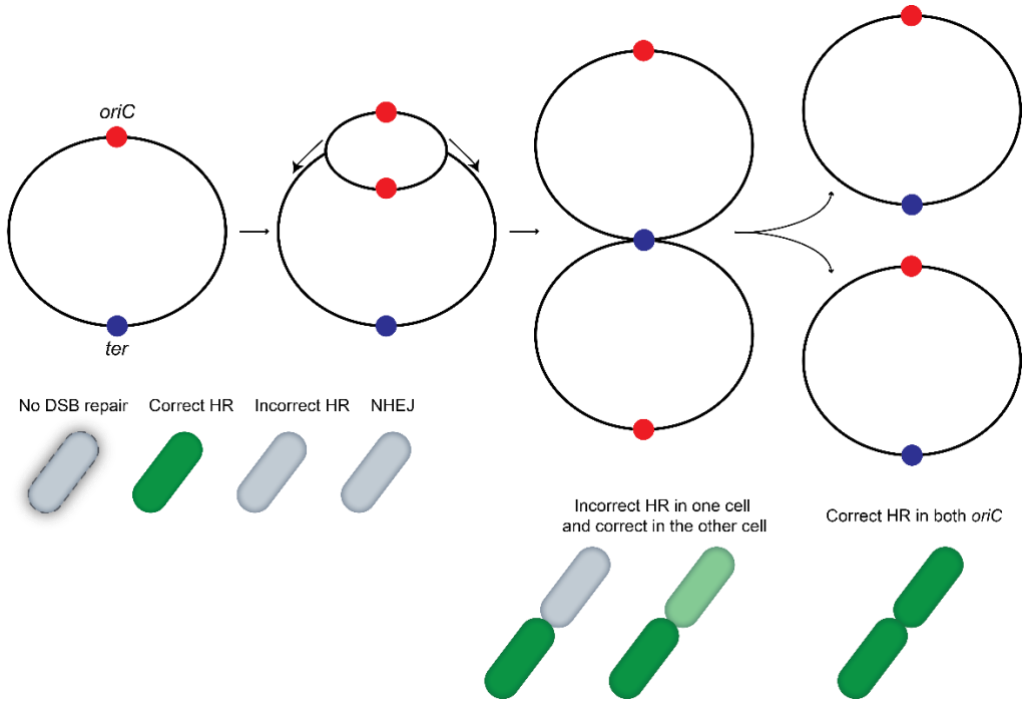

Figure 28. Possible editing outcomes in actively replicating bacterium.
Schematic figure showing the different stages from replication to cell division. *oriC* (red) and *ter* (blue dot) locations are indicated in each chromosome. When bacteria are actively replicating, *oriC* is higher than 1 in the cell. CRISPR-editing of the *oriC* can happen when there is one *oriC* or more *oriC*, and the outcomes of this process can lead to different phenotypes depending on the repair mechanism used by the cell and the growth phase.

The low frequency of editing events in both chromosomal and plasmid system made us hypothesize that there several possible explanations for this observation: (i) occurence of suppressor mutants, which are ameliorating the effect of targeting an essential cellular process, (ii) DSB repair is prone to mutations, which could inactivate the repaired GFP, (iii) homologous recombination is inefficient, and/or (iv) repair by NHEJ. So far, CRISPR approaches in bacteria have been mainly used for deletions and insertions with a homologous repair template provided in trans in *E. coli*[183,279–281,281,282], *B. subtilis*[220,267,273], *Streptomyces spp.*[283], and many others[284]. For our purpose, the only way to efficiently reconstitute GFP was to provide the repair template in cis. We cannot exclude that having a limited amount of homologous repair template chromosomally versus delivering it in a plasmid in more copies does not affect the overall HR efficiency.

When analyzing the cells by fluorescence microscopy, we found that cell chains contained GFP positive and negative cells; this can be affected by: (i) incorrect HDR in one cell and correct

in the adjacent one (Figure 28), (ii) repairing the breaks by NHEJ, (iii) mutated CRISPR system or (iv) suppressor mutations.

It is important to consider that cells are actively replicating at the time of induction (mid-logarithmic phase), which means that they might contain more than one *oriC* in the cell. This antecedent indicates that instead of mending two breaks, it can be up to 8 breaks per cell. This process can decrease the possibility of obtaining a more considerable rate of GFP fluorescent cells, and could also provide a reason for the observed chromosome degradations (Figure 11)

5.1.2 Comparison of the plasmid and the chromosomal CRISPR-Cas9 approaches

We observed that the GFP+ events obtained with the chromosomal system are nearly two times lower than with the already inefficient plasmid system. One possible explanation for this is that the translational fusion of GFP with kanamycin has lower GFP intensity and lower enzyme activity. Hence, we might have encountered more difficulties in identifying these cells by FACS or fluorescence microscopy.

In both cases, *B. subtilis* cells grow in chains, which hinders the capacity of the FACS to separate positive events from negative ones if cells are attached. This event induces false positives because a positive cell could be tethered to a negative one and sorted in the process; and false negatives, since some chains could be discarded if they contain a non-fluorescent cell. Hence, GFP negative cells overgrow non-replicating GFP positive cells, rendering a global analysis of these cells more difficult.

In general, the number of cells recovered in both plasmid and chromosomal CRISPR systems is too low to perform global multi-omic analysis. Additionally, stress caused by the "sorting" cannot be excluded due to the low frequency of the events that increase the sorting time. For these reasons, this experimental approach by CRISPR, although allowing to produce *oriC*-less cells in low numbers, cannot be used for global analysis. However, this method is compatible with the use of microfluidics; in fact, our collaborators have demonstrated that these cells can be observed in the chamber for an extended period (Figures S1).

We also observed the acquisition of suppressor mutations during induction by mannose addition in a batch culture with the CRISPR system on the chromosome. Although suppressor mutants can arise because of targeting an essential process like replication, we have also observed that mutations are acquired when Cas9 is induced in the system (Figure 14). Moreover, Cas9

toxicity independent of its target has been previously described in bacteria[153,215] and might increase the number of suppressor mutants in our system. For this reason, checking the frequency of acquisition of mutations at the repair sites or within the Cas9 system and at the genomic level within the batch culture could provide more information about how cells survive the editing of an essential sequence and interfere with a possible Cas9 toxicity.

Table 4. Comparison of the plasmid and chromosomal system as gene editing strategies

Features	Plasmid system	Chromosomal system
Cell recovery FACS	0.8-1%	0.41 – 0.68%
Phenotype microscope	Non-dividing	Non-dividing
Strain stability	Unstable	Stable strain
Experimental conditions	30°C	37°C (wide range)
Repair mechanism	HDR Probably NHEJ	HDR Probably NHEJ
Advantage	High GFP fluorescence intensity	No need of antibiotic Temperature flexible
Disadvantage	Impaired growth Need antibiotic	Low GFP fluorescence intensity because of fusion with KanR

Taken these results together, we conclude that this approach might be used for analyzing different relevant short-lived phenotypes that arise from targeting other essential processes such as peptidoglycan biosynthesis, division, and protein secretion, among many others. The described CRISPR-Cas9 methods are unsuitable for a global analysis due to the low frequency of events but might become a tool when applied in microfluidic devices. We also identified various bottlenecks in this setup, such as low editing efficiency and acquisition of mutations during induction conditions, that are worth addressing when applying this method in the future.

5.2 CRISPRi-mediated replication arrest

An adapted approach to study the role of inhibited replication initiation in *B. subtilis*

In nature, bacteria can survive long periods in non-growing states; this is the norm rather than the exception. *B. subtilis* can survive for many months living in pure water with a very slow-

growing rate, a process called oligotrophic growth state[109]. The phenotypical characterization of non-growing and slow-growing states has been performed in different organisms[109,141,285–287].

Information on the role of *oriC* in replication initiation and its proteome remodelling upon inhibition is crucial to unravel how bacteria adapt to changes during such an essential process. Here, we developed an experimental approach that enabled us to characterize the effects of replication arrest and a subsequent non-growing state without the impact of disruptive environmental factors such as nutrient deprivation or antibiotic treatment. We switched our strategy of creating deletion mutants with CRISPR-Cas9 to a CRISPRi methodology that aims to circumvent the problems found in the previous setups: (i) cell heterogeneity, (ii) low frequency of the events, and (iii) elimination of DnaA, which is also an essential transcriptional regulator besides its role in replication[288].

5.2.1 From CRISPR-Cas9 to CRISPRi approach

In 2019, Richardson and collaborators created a minimal origin of replication in *B. subtilis,* identifying the most essential sequences within the origin. They found that different DnaA boxes fulfill a different role in replication initiation, and two of them (boxes 6 and 7) were required for DnaA-strand separation; therefore, those were essential for DNA unwinding and replication initiation[52].

We found that blocking both DnaA boxes 6 and 7 via CRISPRi prevents replication initiation, which could not be observed when targeting boxes 1 and 2, or 3 and 4 (Figure 17). Thus, our data confirm earlier work, which identified DnaA boxes 6 and 7 as the critical boxes necessary for a functional origin[54]. Moreover, this approach does not interfere with basal DnaA levels in the cell required for other cellular functions[288]. This result highlights the functionality of CRISPRi at specific boxes to block replication. Similar attempts to target *oriC* have previously been performed in *E. coli*[142,145,155]; however, these studies lack a more global proteome analysis of these cells. Other approaches have targeted *dnaA* and *dnaN* in *B. subtilis* and revealed multiple cell morphology phenotypes as a result[221]. For instance, the transcriptional interference of *dnaA* leads to morphological profiles of bending and growth halting, while blocking transcription of *dnaN* leads to various phenotypes such as bending, growth halting, lysis, and filamentation[221]. In our more targeted approach, most of the phenotypic profiles revealed cell elongation, which confirms that blocking replication by interfering with DnaA binding gives more homogenous phenotypes.

5.2.2 Insights into bacterial response to replication arrest by CRISPRi

Proteomic profiling

Proteins are the workhorses in all living cells and sustain all cellular functions, from copying DNA and catalyzing basic metabolism to cellular motion. Therefore, proteome analysis can provide crucial information for understanding cellular processes, in our case, the absence of DNA replication. Since the targeted boxes are located upstream of *dnaN*, we expected the observed decrease in DnaN protein levels. Although DnaA is encoded within the same operon, it is located upstream of the targeted sequence. Therefore we expected a less pronounced reduction of the DnaA protein[289], which is necessary due to the role of DnaA as a transcriptional regulator for other cellular processes[288]. These results confirm the functionality of our CRISPRi system (Figure 23).

We observed that in our CRISPRi approach, non-replicating cells decreased protein levels necessary for different metabolic pathways such as inositol catabolism, arginine, and branched chained amino acids (BCAA) synthesis (Figure 22 and S4). In addition, CRISPRi-induced non-replicating cells increased the oxaloacetate decarboxylase and malate dehydrogenase pathways after 5 hours of replication arrest. (TCA up?)

Replication arrested cells and their comparison with persister cells

A heatmap plot of the proteins of the CodY and the Stringent response regulons (Figure 27) revealed that CodY is active as a repressor and thus represses transcription of the target genes, reflected in less protein abundance. Moreover, SR is possibly not active during replication arrest because of the upregulation of ribosomal proteins, whose expression is inhibited by SR. CodY mediates the repression of the *ilvB* operon by GTP and BCAAs-binding. BCAAs increase the affinity of CodY for the *ilvB* promoter and for other CodY targets[300]. It is crucial to notice that in CRISPRi non-replicating cells, BCAA metabolism is downregulated and distances our system from a persister-like phenotype.

We evaluated the stringent response in the replication-arrested cells and the possibility of a persister-like phenotype. We observed that most CRISPRi replication arrested cells conserve their membrane integrity and are metabolically active (Figure 20 and 22). Several bacterial persisters studied under laboratory conditions are in a metabolically inactive state[298,299]. However, during infection conditions, *Salmonella*, *M. tuberculosis,* and *S. aureus* persisters have been shown to exist in

a non-growing but metabolically active state[152,285,299]. Interestingly, some non-growing phenotypes induced by e.g., carbon starvation or acid stress have also displayed an active metabolism[152,157]. Therefore, metabolic activity is not a determinant of a persister-like phenotype.

Furthermore, the (p)ppGpp synthetases RelA and YjbM are as abundant in CRISPRi^{box6-7} and WT cells, so we cannot infer that ppGpp levels are increased from our data or, by looking at protein abundance. However, to confirm that CRISPRi^{box6-7} cells are not persister-like cells or having an active SR, it will be worth measuring internal ppGpp levels or trying the experiments in a ppGpp^0 background. Likewise, it has been shown that depletion of GTP activates the P_{ilvB} promoter[301,302] and reduces the ribosomal P1 promoter activity[303]; therefore, a fusion of fluorescence proteins to these promoters could give us more information to address the creation of persistent-like cells in our case.

In wild-type conditions, when cells are reaching the stationary phase, they reduce translation[290]. For instance, (p)ppGpp synthesis arises during the entry into stationary phase and amino acid limitation[291]. Increased (p)ppGpp levels down-regulate metabolic processes such as transcription, replication, and GTP synthesis by direct interaction with DNA primase[292], RNA polymerase[293,294], the GTP biosynthetic enzymes[295] and translation.

Persisters are non-growing bacteria that can survive high concentrations of antibiotics without acquiring resistance to them[131,287,296]. They can either occur due to nutrient starvation and are enriched in the stationary phase of growth (Type I persisters) or spontaneously within a population by stochastic changes in GTP levels at the single-cell level (Type II persisters)[297]. In *B. subtilis*, persister cell formation has been described, and in both, Types I and II, (p)ppGpp levels play an essential role[116].

Recently, the proteome of persistent cells from *S. aureus* clinical isolates has been described[152]. These persistent cells, unlike most described, also upregulate translation and ribosomal proteins while downregulating other metabolic processes, division, and replication. The described phenotype was reversible when cells were shifted back to nutrient-rich conditions[152]. To verify if the CRISPRi phenotype is also reversible, one can think about using a carbon source switch from xylose to glucose, where dCas9 is repressed to see if cells resume growth. The reversibility of replication inhibition is an attractive feature that can be exploited for downstream biotechnological applications. Such as having a temporal control of up-regulated translation induces heterologous protein expression and the reverse effect to continue cell propagation.

SOS response in replication arrested cells

As mentioned in the introduction, a new category of non-growing cells has recently been explored, called SimCells[146,147]. These cells have no chromosome but retain all the original bacterial cell membrane, making them fall in the intersection between a living cell and a cell-free system. By introducing the glycolysis pathway in an artificial chromosome, they can regenerate ATP and NADH/NADPH, which results in extended cell longevity. Although they cannot reproduce, they maintain the functional machinery necessary to retain gene expression[304] and produce mCherry up to 10 days upon chromosomal removal[147]. The fate of bacteria that lose the chromosome has also been explored in *B. subtilis*, and they are termed DLC (DNA-less cells) and can retain many cellular activities like synthesizing proteins, elongating, and dividing up to 5 hours[305]. These results also support the idea that some cell machinery involved in transcription and translation preferentially remain in the cells to ensure cell survival. Additionally, one big advantage of these chromosome-free cells is the lack of stress responses. So far, data indicates that stringent response is not taking place in our system.

Profile plots of SOS-response-associated proteins indicate this stress response is not active (Figure S5). Additionally, the YneA promoter is generally used as a reporter for the SOS response in *B. subtilis,* and although YneA was not detected by proteome analysis, we used the translational fusion of this protein to GFP to detect the cellular SOS response. Fluorescence microscopy revealed a profile like the WT and indicated no DNA damage stress is present at the tested timepoints in the CRISPR strain (Figure 24). Having a non-replicating cell that is not subject to neither SOS response nor Stringent response could provide a good premise for exploring the cell factory potential of this cell.

Translation in replication-arrested cells

Proteomic analysis of non-replicating cells revealed that proteins involved in translation are more abundant compared to WT. Studies in several bacteria have suggested that protein synthesis continues during growth arrest and that maintaining functional translation machinery may be required for their viability[151,285,306,307]. Additionally, one study in *E. coli* demonstrated enhanced protein and biochemical production of GFP in replication arrested cells[142]. We further confirmed that non-replicating cells maintained a higher rate of protein synthesis than wild-type cells (Figure 26). Further analysis of protein synthesis should be performed by evaluating the production of reporter proteins, such as fluorescent or biotechnological-relevant proteins.

We also found that rRNA-binding, ribosomal proteins, tRNA-binding, and nucleoproteins are more abundant in non-replicating cells after 5 and 6 hours of induction (Figure 22). A study analyzing bacterial longevity in *Rhodopseudomonas palustris* indicated that the levels of tRNA charging and translation elongation proteins remained constant for growing and growth-arrested cells[157]. The explanation for these differences to our results could stem from how growth arrest is achieved. The study above induced growth arrest by nutrient starvation upon carbon source depletion, while the carbon levels provided in our experimental setup are sufficient to ensure continuous cellular protein synthesis, reflected in the dCas9 levels over time (Figure 21B and S3). Moreover, the experiments with *R. palustris* evaluate cells after 4 -14 days of growth, where the proteome is already gradually adjusted to the non-growing state, whereas we were interested in the immediate adaptation of the cells to replication arrest.

However, the comparisons between non-replicating to replicating cells (wt) at the proteomic level have limitations. Over time, replicating cells increase cell density, so nutrient availability is scarcer than for non-replicating cells. Hence, up- or downregulation of specific metabolic pathways in replicating cells could also be caused by nutrient limitation and entering stationary phase.

Although out of this project's scope, it would be interesting to circumvent the differences in cell density between growing and non-growing cells. This could be achieved by incorporating controlled cell growth state, density and amount of xylose in a chemostat. This controlled environment would enable more precise characterization of the proteome differences between replicating and non-replicating cells independent of growth rate and nutrient availability. In addition, it would also allow the characterization of a longer time frame and technically would permit the permanent creation of non-replicating cells. Hence, one could also characterize the reasons for cell death in non-replicating cells. (overkamp Kuipers).

5.3 Biotechnological perspectives of inhibition of replication initiation

The metabolism of non-growing bacteria has been recently reviewed due to its relevance in industrial and clinical contexts[286]. Non-growing bacteria are desirable for industrial processes because they can optimize microbial production of biobased compounds while avoiding excess biomass formation[142,145]. Instead, the carbon and energy spent for growth could be redirected to producing compounds of interest. Metabolically active states in non-growing bacteria have been previously reported, with some of them, displaying enhanced protein production[157,285,306,307].

To avoid a decrease in metabolic activity, several strategies have been adopted to artificially maintain a high energy demand, for instance, by expressing ATP-hydrolysing enzymes[308]. Induction of growth arrest has been explored for biotechnological applications to confer antibiotic tolerance to carbapenem-producing[309] and mevalonate-producing *E. coli* strains[310] to avoid cell lysis during biosynthesis of these products. This is achieved by expressing growth-arresting toxin proteins to induce the formation of persisters[311]. For instance, overexpression of the toxin HipA causes growth arrest and confers β-lactam tolerance by activating the synthesis of ppGpp[310], which inhibits the phospholipid synthesis enzyme PlsB[312]. Interestingly, HipA-arrested cultures survive β-lactam exposure and remain metabolically active while sustaining production of the isoprenoid precursors like mevalonate from a heterologous pathway for several days while resisting phage-induced lysis[310].

The inhibition of replication initiation by CRISPRi in *B. subtilis* and its effect of incremental translation compared to replicating cells could fully capitalize on this bacterium's strengths as a production host. Expression of dCas9 in this study was performed by induction of xylose; however, self-inducing promoters[313–315] could remove the dependence on chemical inducers, which are not economical at industrial scales. Moreover, replication inhibition could be reversible by attenuating the effect of dCas9[316] using temperature switches[317], degradation tags[155], light-activated and sensitive variants[317–319], split variants, or elimination of Cas9 by deletion upon editing as studied in Part1 of this project (Figure 6 and 12). Finally, this system could become a source for producing many toxins and antibiotics that target the DNA replication machinery.

5. Conclusion

In the first part of this thesis, we demonstrated the feasibility of producing deletion mutants of essential genes and sequences necessary for replication initiation using a CRISPR-Cas9 approach, utilizing artificial protospacers and homologous repair templates in the chromosome, and using a split GFP as an indicator of successful deletions. Our method to delete and study the absence of replication initiation, although inefficient, might become valuable in studying the role of other essential genes that lead to short-lived phenotypes studied by microfluidics and microscopy.

In the second part of this thesis, we adapted a CRISPRi system to target specific DnaA boxes to stop replication initiation without affecting the basal expression of DnaA, thereby enabling a global analysis of the cells. Proteomic analysis of a CRISPRi$^{box6\text{-}7}$ mutant revealed extensive proteome remodelling as an adaptation mechanism to replication arrest. We confirmed that DnaA boxes 6 and 7 are required to initiate DNA replication *in vivo*. We identified that translation is one of the up-regulated pathways during replication arrest, resulting in increased protein production compared to the WT, and that replication arrested cells had no sign of stress responses such as SR or SOS response induction. Moreover, temporal induction of replication inhibition could become a valuable tool in biotechnology to increase translation capacity on the cells and enhance heterologous protein expression.

Overall, our experiments allowed to describe the adaptation of *B. subtilis* to replication arrest by analysing the proteome changes. We could observe that CRISPRi-arrested *B. subtilis* cells are alive and metabolically active. These cells could be an interesting model to study cell longevity, long-term adaptation, or using this approach for biotechnological purposes.

6. Conclusion

In the first part of this thesis, we demonstrated the feasibility of producing deletion mutants of essential genes and sequences necessary for replication initiation using a CRISPR-Cas9 approach, utilizing artificial protospacers and homologous repair templates in the chromosome, and using a split GFP as an indicator of successful deletions. Our method to delete and study the absence of replication initiation, although inefficient, could become valuable in studying the role of other essential genes that lead to short-lived phenotypes or that do not propagate if coupled with microfluidics and microscopy.

In the second part of this thesis, we adapted a CRISPRi system to target specific DnaA boxes to stop replication initiation without affecting the basal expression of DnaA, thereby enabling a global analysis of the cells. Proteomic analysis of a CRISPRi$^{box6\text{-}7}$ mutant revealed extensive proteome remodeling as an adaptation mechanism to replication arrest. We confirmed that DnaA boxes 6 and 7 are required to initiate DNA replication *in vivo*. We identified that translation is one of the up-regulated pathways during replication arrest, resulting in increased protein production compared to the WT, and that replication arrested cells had no sign of SR or SOS response induction. Moreover, temporal induction of replication inhibition could become a valuable tool in biotechnology to increase translation capacity on the cells and enhance heterologous protein expression.

Overall, our data analyze the adaptation of *B. subtilis* to replication arrest and their proteome changes, observing that CRISPRi-arrested *B. subtilis* cells are alive and metabolically active. They could be further studied as a model for cell longevity, long-term adaptation, or using this approach for biotechnological purposes.

7. Bibliography

1. Ruiz-Mirazo, K., Peretó, J. & Moreno, A. A universal definition of life: autonomy and open-ended evolution. *Orig Life Evol Biosph* **34**, 323–346 (2004).
2. van Regenmortel, M. H. V. & Mahy, B. W. J. Emerging issues in virus taxonomy. *Emerging Infect. Dis.* **10**, 8–13 (2004).
3. Reyes-Lamothe, R. & Sherratt, D. J. The bacterial cell cycle, chromosome inheritance and cell growth. *Nat Rev Microbiol* **17**, 467–478 (2019).
4. Cooper, S. & Helmstetter, C. E. Chromosome replication and the division cycle of Escherichia coli B/r. *J. Mol. Biol.* **31**, 519–540 (1968).
5. Donachie, W. D. Relationship between cell size and time of initiation of DNA replication. *Nature* **219**, 1077–1079 (1968).
6. Donachie, W. D. The cell cycle of Escherichia coli. *Annu Rev Microbiol* **47**, 199–230 (1993).
7. J, H. & K, T. Linear plasmids and chromosomes in bacteria. *Molecular microbiology* **10**, (1993).
8. Es, E., Ma, F. & Mk, W. Divided genomes: negotiating the cell cycle in prokaryotes with multiple chromosomes. *Molecular microbiology* **56**, (2005).
9. Jm, K. DnaA: controlling the initiation of bacterial DNA replication and more. *Annual review of microbiology* **60**, (2006).
10. Mj, D., D, J., J, K. & M, O. Motors and switches: AAA+ machines within the replisome. *Nature reviews. Molecular cell biology* **3**, (2002).
11. Jameson, K. H. & Wilkinson, A. J. Control of Initiation of DNA Replication in Bacillus subtilis and Escherichia coli. *Genes (Basel)* **8**, (2017).
12. Mj, D. & M, O. Replicative helicase loaders: ring breakers and ring makers. *Current biology : CB* **13**, (2003).

13. Bruand, C., Ehrlich, S. D. & Jannière, L. Primosome assembly site in Bacillus subtilis. *EMBO J* **14**, 2642–2650 (1995).

14. Bruand, C., Farache, M., McGovern, S., Ehrlich, S. D. & Polard, P. DnaB, DnaD and DnaI proteins are components of the Bacillus subtilis replication restart primosome. *Mol Microbiol* **42**, 245–255 (2001).

15. Marsin, S., McGovern, S., Ehrlich, S. D., Bruand, C. & Polard, P. Early steps of Bacillus subtilis primosome assembly. *J Biol Chem* **276**, 45818–45825 (2001).

16. Velten, M. *et al.* A two-protein strategy for the functional loading of a cellular replicative DNA helicase. *Mol. Cell* **11**, 1009–1020 (2003).

17. Rokop, M. E., Auchtung, J. M. & Grossman, A. D. Control of DNA replication initiation by recruitment of an essential initiation protein to the membrane of Bacillus subtilis. *Mol Microbiol* **52**, 1757–1767 (2004).

18. Li, Y. *et al.* Identification of temperature-sensitive dnaD mutants of Staphylococcus aureus that are defective in chromosomal DNA replication. *Mol Genet Genomics* **271**, 447–457 (2004).

19. Li, Y. *et al.* DnaB and DnaI temperature-sensitive mutants of Staphylococcus aureus: evidence for involvement of DnaB and DnaI in synchrony regulation of chromosome replication. *Microbiology (Reading)* **153**, 3370–3379 (2007).

20. Smits, W. K., Goranov, A. I. & Grossman, A. D. Ordered association of helicase loader proteins with the Bacillus subtilis origin of replication in vivo. *Mol. Microbiol.* **75**, 452–461 (2010).

21. Reyes-Lamothe, R., Nicolas, E. & Sherratt, D. J. Chromosome replication and segregation in bacteria. *Annu Rev Genet* **46**, 121–143 (2012).

22. Mott, M. L. & Berger, J. M. DNA replication initiation: mechanisms and regulation in bacteria. *Nat. Rev. Microbiol.* **5**, 343–354 (2007).

23. Jameson, K. H. & Wilkinson, A. J. Control of initiation of DNA replication in Bacillus subtilis and Escherichia coli. *Genes* **8**, (2017).

24. Dervyn, E. *et al.* Two essential DNA polymerases at the bacterial replication fork. *Science* **294**, 1716–1719 (2001).

25. Sanders, G. M., Dallmann, H. G. & McHenry, C. S. Reconstitution of the B. subtilis replisome with 13 proteins including two distinct replicases. *Mol Cell* **37**, 273–281 (2010).

26. Robinson, A., Causer, R. J. & Dixon, N. E. Architecture and conservation of the bacterial DNA replication machinery, an underexploited drug target. *Curr Drug Targets* **13**, 352–372 (2012).

27. Beattie, T. R. & Reyes-Lamothe, R. A Replisome's journey through the bacterial chromosome. *Front Microbiol* **6**, 562 (2015).

28. Cox, M. M. *et al.* The importance of repairing stalled replication forks. *Nature* **404**, 37–41 (2000).

29. Lenhart, J. S., Schroeder, J. W., Walsh, B. W. & Simmons, L. A. DNA repair and genome maintenance in Bacillus subtilis. *Microbiol Mol Biol Rev* **76**, 530–564 (2012).

30. Dewar, J. M. & Walter, J. C. Mechanisms of DNA replication termination. *Nat Rev Mol Cell Biol* **18**, 507–516 (2017).

31. Fossum, S., Crooke, E. & Skarstad, K. Organization of sister origins and replisomes during multifork DNA replication in Escherichia coli. *EMBO J* **26**, 4514–4522 (2007).

32. Skarstad, K. & Katayama, T. Regulating DNA Replication in Bacteria. *Cold Spring Harb Perspect Biol* **5**, (2013).

33. Mackiewicz, P., Zakrzewska-Czerwinska, J., Zawilak, A., Dudek, M. R. & Cebrat, S. Where does bacterial replication start? Rules for predicting the oriC region. *Nucleic Acids Res* **32**, 3781–3791 (2004).

34. Luo, H. & Gao, F. DoriC 10.0: an updated database of replication origins in prokaryotic genomes including chromosomes and plasmids. *Nucleic Acids Res.* **47**, D74–D77 (2019).

35. Fuller, R. S. & Kornberg, A. Purified dnaA protein in initiation of replication at the Escherichia coli chromosomal origin of replication. *Proc Natl Acad Sci U S A* **80**, 5817–5821 (1983).

36. Fuller, R. S., Funnell, B. E. & Kornberg, A. The dnaA protein complex with the E. coli chromosomal replication origin (oriC) and other DNA sites. *Cell* **38**, 889–900 (1984).

37. Jakimowicz, D. *et al.* Structural elements of the Streptomyces oriC region and their interactions with the DnaA protein. *Microbiology (Reading)* **144 (Pt 5)**, 1281–1290 (1998).

38. Tsodikov, O. V. & Biswas, T. Structural and thermodynamic signatures of DNA recognition by Mycobacterium tuberculosis DnaA. *J Mol Biol* **410**, 461–476 (2011).

39. Leonard, A. C. & Grimwade, J. E. Regulating DnaA complex assembly: It is time to fill the gaps. *Current Opinion in Microbiology* (2010) doi:10.1016/j.mib.2010.10.001.

40. Messer, W. The bacterial replication initiator DnaA. DnaA and oriC, the bacterial mode to initiate DNA replication. *FEMS Microbiology Reviews* (2002) doi:10.1016/S0168-6445(02)00127-4.

41. Wolanski, M., Donczew, R., Zawilak-Pawlik, A. & Zakrzewska-Czerwinska, J. oriC-encoded instructions for the initiation of bacterial chromosome replication. *Frontiers in Microbiology* (2015) doi:10.3389/fmicb.2014.00735.

42. Schaper, S. & Messer, W. Interaction of the initiator protein DnaA of Escherichia coli with its DNA target. *J Biol Chem* **270**, 17622–17626 (1995).

43. Leonard, A. C. & Méchali, M. DNA replication origins. *Cold Spring Harb Perspect Biol* **5**, a010116 (2013).

44. Moriya, S., Atlung, T., Hansen, F. G., Yoshikawa, H. & Ogasawara, N. Cloning of an autonomously replicating sequence (ars) from the Bacillus subtilis chromosome. *Mol. Microbiol.* **6**, 309–315 (1992).

45. Donczew, R., Weigel, C., Lurz, R., Zakrzewska-Czerwinska, J. & Zawilak-Pawlik, A. Helicobacter pylori oriC--the first bipartite origin of chromosome replication in Gram-negative bacteria. *Nucleic Acids Res.* **40**, 9647–9660 (2012).

46. Krause, M., Rückert, B., Lurz, R. & Messer, W. Complexes at the replication origin of Bacillus subtilis with homologous and heterologous DnaA protein. *J. Mol. Biol.* **274**, 365–380 (1997).

47. Lewis, P. J., Ralston, G. B., Christopherson, R. I. & Wake, R. G. Identification of the replication terminator protein binding sites in the terminus region of the Bacillus subtilis chromosome and stoichiometry of the binding. *J. Mol. Biol.* **214**, 73–84 (1990).

48. Miller, D. T. *et al.* Bacterial origin recognition complexes direct assembly of higher-order DnaA oligomeric structures. *Proc. Natl. Acad. Sci. U.S.A.* **106**, 18479–18484 (2009).

49. Rozgaja, T. A. *et al.* Two oppositely oriented arrays of low-affinity recognition sites in oriC guide progressive binding of DnaA during Escherichia coli pre-RC assembly. *Mol. Microbiol.* **82**, 475–488 (2011).

50. McGarry, K. C., Ryan, V. T., Grimwade, J. E. & Leonard, A. C. Two discriminatory binding sites in the Escherichia coli replication origin are required for DNA strand opening by initiator DnaA-ATP. *Proc. Natl. Acad. Sci. U.S.A.* **101**, 2811–2816 (2004).

51. Kaur, G. *et al.* Building the bacterial orisome: high-affinity DnaA recognition plays a role in setting the conformation of oriC DNA. *Mol. Microbiol.* **91**, 1148–1163 (2014).

52. Richardson, T. T. *et al.* Identification of a basal system for unwinding a bacterial chromosome origin. *EMBO J* **38**, e101649 (2019).

53. Kowalski, D. & Eddy, M. J. The DNA unwinding element: a novel, cis-acting component that facilitates opening of the Escherichia coli replication origin. *EMBO J* **8**, 4335–4344 (1989).

54. Richardson, T. T., Harran, O. & Murray, H. The bacterial DnaA-trio replication origin element specifies single-stranded DNA initiator binding. *Nature* **534**, 412–416 (2016).

55. Bleichert, F., Botchan, M. R. & Berger, J. M. Mechanisms for initiating cellular DNA replication. *Science* **355**, (2017).

56. Richardson, T. T., Harran, O. & Murray, H. The bacterial DnaA-Trio replication origin element specifies single-stranded DNA initiator binding. *Nature* **534**, 412–416 (2016).

57. Briggs, G. S., Smits, W. K. & Soultanas, P. Chromosomal replication initiation machinery of low-G+C-content Firmicutes. *J. Bacteriol.* **194**, 5162–5170 (2012).

58. Ogasawara, N. & Yoshikawa, H. Genes and their organization in the replication origin region of the bacterial chromosome. *Mol. Microbiol.* **6**, 629–634 (1992).

59. Earl, A. M., Losick, R. & Kolter, R. Ecology and genomics of Bacillus subtilis. *Trends Microbiol* **16**, 269–275 (2008).

60. Westers, L., Westers, H. & Quax, W. J. Bacillus subtilis as cell factory for pharmaceutical proteins: a biotechnological approach to optimize the host organism. *Biochim Biophys Acta* **1694**, 299–310 (2004).

61. Zweers, J. C. *et al.* Towards the development of Bacillus subtilis as a cell factory for membrane proteins and protein complexes. *Microb Cell Fact* **7**, 10 (2008).

62. Ling Lin Fu, null *et al.* Protein secretion pathways in Bacillus subtilis: implication for optimization of heterologous protein secretion. *Biotechnol Adv* **25**, 1–12 (2007).

63. Kogoma, T. Stable DNA replication: interplay between DNA replication, homologous recombination, and transcription. *Microbiology and molecular biology reviews : MMBR* (1997).

64. Dimude, J. U. *et al.* The consequences of replicating in the wrong orientation: Bacterial chromosome duplication without an active replication origin. *mBio* (2015) doi:10.1128/mBio.01294-15.

65. Wallden, M., Fange, D., Lundius, E. G., Baltekin, Ö. & Elf, J. The Synchronization of Replication and Division Cycles in Individual E. coli Cells. *Cell* (2016) doi:10.1016/j.cell.2016.06.052.

66. Ogura, Y., Imai, Y., Ogasawara, N. & Moriya, S. Autoregulation of the dnaA-dnaN Operon and Effects of DnaA Protein Levels on Replication Initiation in Bacillus subtilis. *J Bacteriol* **183**, 3833–3841 (2001).

67. Messer, W. *et al.* Functional domains of DnaA proteins. *Biochimie* **81**, 819–825 (1999).

68. Sutton, M. D. & Kaguni, J. M. The Escherichia coli dnaA gene: four functional domains. *J Mol Biol* **274**, 546–561 (1997).

69. Hansen, F. G. & Atlung, T. The DnaA Tale. *Front Microbiol* **9**, 319 (2018).

70. Fukuoka, T., Moriya, S., Yoshikawa, H. & Ogasawara, N. Purification and characterization of an initiation protein for chromosomal replication, DnaA, in Bacillus subtilis. *J Biochem* **107**, 732–739 (1990).

71. Nishida, S. *et al.* A nucleotide switch in the Escherichia coli DnaA protein initiates chromosomal replication: evidnece from a mutant DnaA protein defective in regulatory ATP hydrolysis in vitro and in vivo. *J Biol Chem* **277**, 14986–14995 (2002).

72. Sekimizu, K., Bramhill, D. & Kornberg, A. ATP activates dnaA protein in initiating replication of plasmids bearing the origin of the E. coli chromosome. *Cell* **50**, 259–265 (1987).

73. Camara, J. E. *et al.* Hda inactivation of DnaA is the predominant mechanism preventing hyperinitiation of Escherichia coli DNA replication. *EMBO Rep* **6**, 736–741 (2005).

74. Katayama, T., Ozaki, S., Keyamura, K. & Fujimitsu, K. Regulation of the replication cycle: conserved and diverse regulatory systems for DnaA and oriC. *Nat. Rev. Microbiol.* **8**, 163–170 (2010).

75. Moriya, S., Fukuoka, T., Ogasawara, N. & Yoshikawa, H. Regulation of initiation of the chromosomal replication by DnaA-boxes in the origin region of the Bacillus subtilis chromosome. *EMBO J* **7**, 2911–2917 (1988).

76. Atlung, T., Clausen, E. S. & Hansen, F. G. Autoregulation of the dnaA gene of Escherichia coli K12. *Mol Gen Genet* **200**, 442–450 (1985).

77. Braun, R. E., O'Day, K. & Wright, A. Autoregulation of the DNA replication gene dnaA in E. coli K-12. *Cell* **40**, 159–169 (1985).

78. Kücherer, C., Lother, H., Kölling, R., Schauzu, M. A. & Messer, W. Regulation of transcription of the chromosomal dnaA gene of Escherichia coli. *Mol Gen Genet* **205**, 115–121 (1986).

79. Speck, C., Weigel, C. & Messer, W. ATP– and ADP–DnaA protein, a molecular switch in gene regulation. *The EMBO Journal* **18**, 6169–6176 (1999).

80. Noirot-Gros, M.-F. *et al.* An expanded view of bacterial DNA replication. *Proc. Natl. Acad. Sci. U.S.A.* **99**, 8342–8347 (2002).

81. Hayashi, M., Ogura, Y., Harry, E. J., Ogasawara, N. & Moriya, S. Bacillus subtilis YabA is involved in determining the timing and synchrony of replication initiation. *FEMS Microbiol. Lett.* **247**, 73–79 (2005).

82. Goranov, A. I., Breier, A. M., Merrikh, H. & Grossman, A. D. YabA of Bacillus subtilis controls DnaA-mediated replication initiation but not the transcriptional response to replication stress. *Mol. Microbiol.* **74**, 454–466 (2009).

83. Merrikh, H. & Grossman, A. D. Control of the replication initiator DnaA by an anti-cooperativity factor. *Mol. Microbiol.* **82**, 434–446 (2011).

84. Scholefield, G. & Murray, H. YabA and DnaD inhibit helix assembly of the DNA replication initiation protein DnaA. *Mol. Microbiol.* **90**, 147–159 (2013).

85. Noirot-Gros, M.-F. *et al.* Functional dissection of YabA, a negative regulator of DNA replication initiation in Bacillus subtilis. *Proc. Natl. Acad. Sci. U.S.A.* **103**, 2368–2373 (2006).

86. Bonilla, C. Y. & Grossman, A. D. The primosomal protein DnaD inhibits cooperative DNA binding by the replication initiator DnaA in Bacillus subtilis. *J. Bacteriol.* **194**, 5110–5117 (2012).

87. Martin, E. *et al.* DNA replication initiation in Bacillus subtilis: structural and functional characterization of the essential DnaA-DnaD interaction. *Nucleic Acids Res* **47**, 2101–2112 (2019).

88. Scholefield, G., Errington, J. & Murray, H. Soj/ParA stalls DNA replication by inhibiting helix formation of the initiator protein DnaA. *EMBO J.* **31**, 1542–1555 (2012).

89. Ireton, K., Gunther, N. W. & Grossman, A. D. spo0J is required for normal chromosome segregation as well as the initiation of sporulation in Bacillus subtilis. *J. Bacteriol.* **176**, 5320–5329 (1994).

90. Gerdes, K., Møller-Jensen, J. & Bugge Jensen, R. Plasmid and chromosome partitioning: surprises from phylogeny. *Mol. Microbiol.* **37**, 455–466 (2000).

91. Livny, J., Yamaichi, Y. & Waldor, M. K. Distribution of centromere-like parS sites in bacteria: insights from comparative genomics. *J. Bacteriol.* **189**, 8693–8703 (2007).

92. Lin, D. C. & Grossman, A. D. Identification and characterization of a bacterial chromosome partitioning site. *Cell* **92**, 675–685 (1998).

93. Breier, A. M. & Grossman, A. D. Whole-genome analysis of the chromosome partitioning and sporulation protein Spo0J (ParB) reveals spreading and origin-distal sites on the Bacillus subtilis chromosome. *Mol. Microbiol.* **64**, 703–718 (2007).

94. Murray, H., Ferreira, H. & Errington, J. The bacterial chromosome segregation protein Spo0J spreads along DNA from parS nucleation sites. *Mol. Microbiol.* **61**, 1352–1361 (2006).

95. Breier, A. M. & Grossman, A. D. Dynamic association of the replication initiator and transcription factor DnaA with the Bacillus subtilis chromosome during replication stress. *J. Bacteriol.* **191**, 486–493 (2009).

96. Leonard, T. A., Butler, P. J. & Löwe, J. Bacterial chromosome segregation: structure and DNA binding of the Soj dimer--a conserved biological switch. *EMBO J.* **24**, 270–282 (2005).

97. Lee, P. S. & Grossman, A. D. The chromosome partitioning proteins Soj (ParA) and Spo0J (ParB) contribute to accurate chromosome partitioning, separation of replicated sister origins, and regulation of replication initiation in Bacillus subtilis. *Mol. Microbiol.* **60**, 853–869 (2006).

98. Scholefield, G., Veening, J.-W. & Murray, H. DnaA and ORC: more than DNA replication initiators. *Trends Cell Biol.* **21**, 188–194 (2011).

99. Rahn-Lee, L., Merrikh, H., Grossman, A. D. & Losick, R. The sporulation protein SirA inhibits the binding of DnaA to the origin of replication by contacting a patch of clustered amino acids. *J Bacteriol* **193**, 1302–1307 (2011).

100. Burbulys, D., Trach, K. A. & Hoch, J. A. Initiation of sporulation in B. subtilis is controlled by a multicomponent phosphorelay. *Cell* **64**, 545–552 (1991).

101. Wu, L. J. & Errington, J. Bacillus subtilis SpoIIIE protein required for DNA segregation during asymmetric cell division. *Science* **264**, 572–575 (1994).

102. Piggot, P. J. & Hilbert, D. W. Sporulation of Bacillus subtilis. *Curr Opin Microbiol* **7**, 579–586 (2004).

103. Setlow, B. *et al.* Condensation of the forespore nucleoid early in sporulation of Bacillus species. *J. Bacteriol.* **173**, 6270–6278 (1991).

104. Fujita, M., González-Pastor, J. E. & Losick, R. High- and low-threshold genes in the Spo0A regulon of Bacillus subtilis. *J. Bacteriol.* **187**, 1357–1368 (2005).

105. Rahn-Lee, L., Gorbatyuk, B., Skovgaard, O. & Losick, R. The conserved sporulation protein YneE inhibits DNA replication in Bacillus subtilis. *J. Bacteriol.* **191**, 3736–3739 (2009).

106. Wagner, J. K., Marquis, K. A. & Rudner, D. Z. SirA enforces diploidy by inhibiting the replication initiator DnaA during spore formation in Bacillus subtilis. *Mol. Microbiol.* **73**, 963–974 (2009).

107. Jameson, K. H. *et al.* Structure and interactions of the Bacillus subtilis sporulation inhibitor of DNA replication, SirA, with domain I of DnaA. *Mol. Microbiol.* **93**, 975–991 (2014).

108. Bressuire-Isoard, C., Broussolle, V. & Carlin, F. Sporulation environment influences spore properties in Bacillus: evidence and insights on underlying molecular and physiological mechanisms. *FEMS Microbiology Reviews* **42**, 614–626 (2018).

109. Gray, D. A. *et al.* Extreme slow growth as alternative strategy to survive deep starvation in bacteria. *Nat Commun* **10**, 890 (2019).

110. Chubukov, V. *et al.* Engineering glucose metabolism of Escherichia coli under nitrogen starvation. *NPJ Syst Biol Appl* **3**, 16035 (2017).

111. Lempp, M. *et al.* Systematic identification of metabolites controlling gene expression in E. coli. *Nat Commun* **10**, 4463 (2019).

112. Chubukov, V. & Sauer, U. Environmental dependence of stationary-phase metabolism in Bacillus subtilis and Escherichia coli. *Appl Environ Microbiol* **80**, 2901–2909 (2014).

113. Bernhardt, J., Weibezahn, J., Scharf, C. & Hecker, M. Bacillus subtilis During Feast and Famine: Visualization of the Overall Regulation of Protein Synthesis During Glucose Starvation by Proteome Analysis. *Genome Res* **13**, 224–237 (2003).

114. Maaβ, S. *et al.* Highly Precise Quantification of Protein Molecules per Cell During Stress and Starvation Responses in Bacillus subtilis. *Mol Cell Proteomics* **13**, 2260–2276 (2014).

115. Otto, A. *et al.* Systems-wide temporal proteomic profiling in glucose-starved Bacillus subtilis. *Nat Commun* **1**, 137 (2010).

116. Fung, D. K., Barra, J. T., Schroeder, J. W., Ying, D. & Wang, J. D. A shared alarmone-GTP switch underlies triggered and spontaneous persistence. *bioRxiv* 2020.03.22.002139 (2020) doi:10.1101/2020.03.22.002139.

117. Masuda, A., Toya, Y. & Shimizu, H. Metabolic impact of nutrient starvation in mevalonate-producing Escherichia coli. *Bioresour Technol* **245**, 1634–1640 (2017).

118. Doucette, C. D., Schwab, D. J., Wingreen, N. S. & Rabinowitz, J. D. α-Ketoglutarate coordinates carbon and nitrogen utilization via enzyme I inhibition. *Nat Chem Biol* **7**, 894–901 (2011).

119. Antelmann, H., Scharf, C. & Hecker, M. Phosphate starvation-inducible proteins of Bacillus subtilis: proteomics and transcriptional analysis. *J Bacteriol* **182**, 4478–4490 (2000).

120. Rittershaus, E. S. C. *et al.* A Lysine Acetyltransferase Contributes to the Metabolic Adaptation to Hypoxia in Mycobacterium tuberculosis. *Cell Chem Biol* **25**, 1495-1505.e3 (2018).

121. Wilks, J. C. *et al.* Acid and base stress and transcriptomic responses in Bacillus subtilis. *Appl Environ Microbiol* **75**, 981–990 (2009).

122. Sun, Y., Fukamachi, T., Saito, H. & Kobayashi, H. Respiration and the F1Fo-ATPase enhance survival under acidic conditions in Escherichia coli. *PLoS One* **7**, e52577 (2012).

123. Hahne, H. *et al.* A comprehensive proteomics and transcriptomics analysis of Bacillus subtilis salt stress adaptation. *J Bacteriol* **192**, 870–882 (2010).

124. Höper, D., Bernhardt, J. & Hecker, M. Salt stress adaptation of Bacillus subtilis: a physiological proteomics approach. *Proteomics* **6**, 1550–1562 (2006).

125. Höper, D., Völker, U. & Hecker, M. Comprehensive characterization of the contribution of individual SigB-dependent general stress genes to stress resistance of Bacillus subtilis. *J Bacteriol* **187**, 2810–2826 (2005).

126. Hoffmann, T. *et al.* Synthesis, release, and recapture of compatible solute proline by osmotically stressed Bacillus subtilis cells. *Appl Environ Microbiol* **78**, 5753–5762 (2012).

127. Christodoulou, D. *et al.* Reserve Flux Capacity in the Pentose Phosphate Pathway Enables Escherichia coli's Rapid Response to Oxidative Stress. *Cell Syst* **6**, 569-578.e7 (2018).

128. Noster, J. *et al.* Impact of ROS-Induced Damage of TCA Cycle Enzymes on Metabolism and Virulence of Salmonella enterica serovar Typhimurium. *Front Microbiol* **10**, 762 (2019).

129. Tam, L. T. *et al.* Proteome signatures for stress and starvation in Bacillus subtilis as revealed by a 2-D gel image color coding approach. *Proteomics* **6**, 4565–4585 (2006).

130. Brauner, A., Fridman, O., Gefen, O. & Balaban, N. Q. Distinguishing between resistance, tolerance and persistence to antibiotic treatment. *Nature Reviews Microbiology* **14**, 320–330 (2016).

131. Lopatkin, A. J. *et al.* Bacterial metabolic state more accurately predicts antibiotic lethality than growth rate. *Nat Microbiol* **4**, 2109–2117 (2019).

132. Stokes, J. M., Lopatkin, A. J., Lobritz, M. A. & Collins, J. J. Bacterial Metabolism and Antibiotic Efficacy. *Cell Metab* **30**, 251–259 (2019).

133. Lobritz, M. A. *et al.* Antibiotic efficacy is linked to bacterial cellular respiration. *Proc Natl Acad Sci U S A* **112**, 8173–8180 (2015).

134. Díaz-Pascual, F. *et al.* Breakdown of Vibrio cholerae biofilm architecture induced by antibiotics disrupts community barrier function. *Nat Microbiol* **4**, 2136–2145 (2019).

135. Reyes-Lamothe, R., Possoz, C., Danilova, O. & Sherratt, D. J. Independent positioning and action of Escherichia coli replisomes in live cells. *Cell* **133**, 90–102 (2008).

136. Pennington, J. M. & Rosenberg, S. M. Spontaneous DNA breakage in single living Escherichia coli cells. *Nat. Genet.* **39**, 797–802 (2007).

137. Sauls, J. T. *et al.* Control of Bacillus subtilis Replication Initiation during Physiological Transitions and Perturbations. *mBio* **10**, (2019).

138. Si, F. *et al.* Mechanistic Origin of Cell-Size Control and Homeostasis in Bacteria. *Curr. Biol.* **29**, 1760-1770.e7 (2019).

139. Brophy, J. A. N. & Voigt, C. A. Principles of genetic circuit design. *Nat. Methods* **11**, 508–520 (2014).

140. Ganesan, B., Stuart, M. R. & Weimer, B. C. Carbohydrate starvation causes a metabolically active but nonculturable state in Lactococcus lactis. *Appl Environ Microbiol* **73**, 2498–2512 (2007).

141. Ercan, O., Wels, M., Smid, E. J. & Kleerebezem, M. Genome-wide transcriptional responses to carbon starvation in nongrowing Lactococcus lactis. *Appl Environ Microbiol* **81**, 2554–2561 (2015).

142. Li, S. *et al.* Enhanced protein and biochemical production using CRISPRi-based growth switches. *Metab Eng* **38**, 274–284 (2016).

143. Sonderegger, M., Schümperli, M. & Sauer, U. Selection of quiescent Escherichia coli with high metabolic activity. *Metab Eng* **7**, 4–9 (2005).

144. Bover-Cid, S., Izquierdo-Pulido, M. & Vidal-Carou, M. C. Effect of the interaction between a low tyramine-producing Lactobacillus and proteolytic staphylococci on biogenic amine production during ripening and storage of dry sausages. *Int J Food Microbiol* **65**, 113–123 (2001).

145. Li, S. *et al.* Genome-Wide CRISPRi-Based Identification of Targets for Decoupling Growth from Production. *ACS Synth Biol* **9**, 1030–1040 (2020).

146. Rampley, C. P. N. *et al.* Development of SimCells as a novel chassis for functional biosensors. *Sci Rep* **7**, 7261 (2017).

147. Fan, C. *et al.* Chromosome-free bacterial cells are safe and programmable platforms for synthetic biology. *Proc. Natl. Acad. Sci. U.S.A.* **117**, 6752–6761 (2020).

148. Chen, J. X. *et al.* Development of Aspirin-Inducible Biosensors in Escherichia coli and SimCells. *Appl Environ Microbiol* **85**, (2019).

149. Hassan, A. K. *et al.* Suppression of initiation defects of chromosome replication in Bacillus subtilis dnaA and oriC-deleted mutants by integration of a plasmid replicon into the chromosomes. *J Bacteriol* **179**, 2494–2502 (1997).

150. Arjes, H. A. *et al.* Failsafe mechanisms couple division and DNA replication in bacteria. *Current Biology* **24**, 2149–2155 (2014).

151. Stapels, D. A. C. *et al.* Salmonella persisters undermine host immune defenses during antibiotic treatment. *Science* **362**, 1156–1160 (2018).

152. Huemer, M. *et al.* Molecular reprogramming and phenotype switching in Staphylococcus aureus lead to high antibiotic persistence and affect therapy success. *Proc Natl Acad Sci U S A* **118**, (2021).

153. Nielsen, A. A. K. & Voigt, C. A. Multi-input CRISPR/Cas genetic circuits that interface host regulatory networks. *Mol Syst Biol* **10**, 763 (2014).

154. Wiktor, J., Lesterlin, C., Sherratt, D. J. & Dekker, C. CRISPR-mediated control of the bacterial initiation of replication. *Nucleic Acids Research* **44**, 3801–3810 (2016).

155. Wiktor, J., Lesterlin, C., Sherratt, D. J. & Dekker, C. CRISPR-mediated control of the bacterial initiation of replication. *Nucleic Acids Res.* **44**, 3801–3810 (2016).

156. Bergkessel, M., Basta, D. W. & Newman, D. K. The physiology of growth arrest: uniting molecular and environmental microbiology. *Nat Rev Microbiol* **14**, 549–562 (2016).

157. Yin, L. *et al.* Bacterial Longevity Requires Protein Synthesis and a Stringent Response. *mBio* **10**, (2019).

158. Sevastopoulos, C. G., Wehr, C. T. & Glaser, D. A. Large-scale automated isolation of Escherichia coli mutants with thermosensitive DNA replication. *Proc Natl Acad Sci U S A* **74**, 3485–3489 (1977).

159. Moriya, S., Kato, K., Yoshikawa, H. & Ogasawara, N. Isolation of a dnaA mutant of Bacillus subtilis defective in initiation of replication: amount of DnaA protein determines cells' initiation potential. *The EMBO journal* **9**, 2905–2910 (1990).

160. Hill, N. S., Kadoya, R., Chattoraj, D. K. & Levin, P. A. Cell size and the initiation of DNA replication in bacteria. *PLoS Genet* **8**, e1002549 (2012).

161. Winston, S. & Sueoka, N. DNA-membrane association is necessary for initiation of chromosomal and plasmid replication in Bacillus subtilis. *Proc Natl Acad Sci U S A* **77**, 2834–2838 (1980).

162. Gross, J. D., Karamata, D. & Hempstead, P. G. Temperature-sensitive mutants of B. subtilis defective in DNA synthesis. *Cold Spring Harb Symp Quant Biol* **33**, 307–312 (1968).

163. Karamata, D. & Gross, J. D. Isolation and genetic analysis of temperature-sensitive mutants of B. subtilis defective in DNA synthesis. *Mol Gen Genet* **108**, 277–287 (1970).

164. White, K. & Sueoka, N. Temperature-sensitive DNA synthesis mutants of Bacillus subtilis--appendix: theory of density transfer for symmetric chromosome replication. *Genetics* **73**, 185–214 (1973).

165. Bernheim, A. & Sorek, R. The pan-immune system of bacteria: antiviral defence as a community resource. *Nat Rev Microbiol* **18**, 113–119 (2020).

166. Labrie, S. J., Samson, J. E. & Moineau, S. Bacteriophage resistance mechanisms. *Nat Rev Microbiol* **8**, 317–327 (2010).

167. Stern, A. & Sorek, R. The phage-host arms race: shaping the evolution of microbes. *Bioessays* **33**, 43–51 (2011).

168. Samson, J. E., Magadán, A. H., Sabri, M. & Moineau, S. Revenge of the phages: defeating bacterial defences. *Nat Rev Microbiol* **11**, 675–687 (2013).

169. Westra, E. R. *et al.* The CRISPRs, they are a-changin': how prokaryotes generate adaptive immunity. *Annu Rev Genet* **46**, 311–339 (2012).

170. Bikard, D. & Marraffini, L. A. Innate and adaptive immunity in bacteria: mechanisms of programmed genetic variation to fight bacteriophages. *Curr Opin Immunol* **24**, 15–20 (2012).

171. Barrangou, R. *et al.* CRISPR provides acquired resistance against viruses in prokaryotes. *Science* **315**, 1709–1712 (2007).

172. Deltcheva, E. *et al.* CRISPR RNA maturation by trans-encoded small RNA and host factor RNase III. *Nature* **471**, 602–607 (2011).

173. Gasiunas, G., Barrangou, R., Horvath, P. & Siksnys, V. Cas9-crRNA ribonucleoprotein complex mediates specific DNA cleavage for adaptive immunity in bacteria. *Proc Natl Acad Sci U S A* **109**, E2579-2586 (2012).

174. Jinek, M. *et al.* A programmable dual-RNA-guided DNA endonuclease in adaptive bacterial immunity. *Science* **337**, 816–821 (2012).

175. Makarova, K. S. *et al.* Evolution and classification of the CRISPR-Cas systems. *Nat. Rev. Microbiol.* **9**, 467–477 (2011).

176. Sapranauskas, R. *et al.* The Streptococcus thermophilus CRISPR/Cas system provides immunity in Escherichia coli. *Nucleic Acids Res* **39**, 9275–9282 (2011).

177. Vigouroux, A. & Bikard, D. CRISPR Tools To Control Gene Expression in Bacteria. *Microbiol Mol Biol Rev* **84**, (2020).

178. Doench, J. G. *et al.* Optimized sgRNA design to maximize activity and minimize off-target effects of CRISPR-Cas9. *Nat Biotechnol* **34**, 184–191 (2016).

179. Jinek, M. *et al.* A programmable dual-RNA-guided DNA endonuclease in adaptive bacterial immunity. *Science* **337**, 816–821 (2012).

180. Mojica, F. J. M., Díez-Villaseñor, C., García-Martínez, J. & Almendros, C. Short motif sequences determine the targets of the prokaryotic CRISPR defence system. *Microbiology (Reading)* **155**, 733–740 (2009).

181. Leenay, R. T. & Beisel, C. L. Deciphering, Communicating, and Engineering the CRISPR PAM. *J Mol Biol* **429**, 177–191 (2017).

182. Deveau, H. *et al.* Phage response to CRISPR-encoded resistance in Streptococcus thermophilus. *J Bacteriol* **190**, 1390–1400 (2008).

183. Jiang, W., Bikard, D., Cox, D., Zhang, F. & Marraffini, L. A. RNA-guided editing of bacterial genomes using CRISPR-Cas systems. *Nat Biotechnol* **31**, 233–239 (2013).

184. Sternberg, S. H., Redding, S., Jinek, M., Greene, E. C. & Doudna, J. A. DNA interrogation by the CRISPR RNA-guided endonuclease Cas9. *Nature* **507**, 62–67 (2014).

185. Szczelkun, M. D. *et al.* Direct observation of R-loop formation by single RNA-guided Cas9 and Cascade effector complexes. *Proc Natl Acad Sci U S A* **111**, 9798–9803 (2014).

186. Anders, C., Niewoehner, O., Duerst, A. & Jinek, M. Structural basis of PAM-dependent target DNA recognition by the Cas9 endonuclease. *Nature* **513**, 569–573 (2014).

187. Mekler, V., Minakhin, L. & Severinov, K. Mechanism of duplex DNA destabilization by RNA-guided Cas9 nuclease during target interrogation. *Proc Natl Acad Sci U S A* **114**, 5443–5448 (2017).

188. Aniukwu, J., Glickman, M. S. & Shuman, S. The pathways and outcomes of mycobacterial NHEJ depend on the structure of the broken DNA ends. *Genes Dev* **22**, 512–527 (2008).

189. Bertrand, C., Thibessard, A., Bruand, C., Lecointe, F. & Leblond, P. Bacterial NHEJ: a never ending story. *Mol Microbiol* **111**, 1139–1151 (2019).

190. Chayot, R., Montagne, B., Mazel, D. & Ricchetti, M. An end-joining repair mechanism in Escherichia coli. *Proc Natl Acad Sci U S A* **107**, 2141–2146 (2010).

191. Cui, L. & Bikard, D. Consequences of Cas9 cleavage in the chromosome of Escherichia coli. *Nucleic Acids Res* **44**, 4243–4251 (2016).

192. Kowalczykowski, S. C., Dixon, D. A., Eggleston, A. K., Lauder, S. D. & Rehrauer, W. M. Biochemistry of homologous recombination in Escherichia coli. *Microbiol Rev* **58**, 401–465 (1994).

193. Yoshikawa, H., O'sullivan, A. & Sueoka, N. SEQUENTIAL REPLICATION OF THE BACILLUS SUBTILIS CHROMOSOME. 3. REGULATION OF INITIATION. *Proc Natl Acad Sci U S A* **52**, 973–980 (1964).

194. Migocki, M. D., Lewis, P. J., Wake, R. G. & Harry, E. J. The midcell replication factory in Bacillus subtilis is highly mobile: implications for coordinating chromosome replication with other cell cycle events. *Mol Microbiol* **54**, 452–463 (2004).

195. Mougiakos, I., Bosma, E. F., de Vos, W. M., van Kranenburg, R. & van der Oost, J. Next Generation Prokaryotic Engineering: The CRISPR-Cas Toolkit. *Trends Biotechnol* **34**, 575–587 (2016).

196. Mougiakos, I., Bosma, E. F., Ganguly, J., van der Oost, J. & van Kranenburg, R. Hijacking CRISPR-Cas for high-throughput bacterial metabolic engineering: advances and prospects. *Curr Opin Biotechnol* **50**, 146–157 (2018).

197. Amundsen, S. K. *et al.* Small-molecule inhibitors of bacterial AddAB and RecBCD helicase-nuclease DNA repair enzymes. *ACS Chem Biol* **7**, 879–891 (2012).

198. Wigley, D. B. Bacterial DNA repair: recent insights into the mechanism of RecBCD, AddAB and AdnAB. *Nat Rev Microbiol* **11**, 9–13 (2013).

199. de Vega, M. The minimal Bacillus subtilis nonhomologous end joining repair machinery. *PLoS One* **8**, e64232 (2013).

200. Shuman, S. & Glickman, M. S. Bacterial DNA repair by non-homologous end joining. *Nat Rev Microbiol* **5**, 852–861 (2007).

201. Della, M. *et al.* Mycobacterial Ku and ligase proteins constitute a two-component NHEJ repair machine. *Science* **306**, 683–685 (2004).

202. Gong, C. *et al.* Mechanism of nonhomologous end-joining in mycobacteria: a low-fidelity repair system driven by Ku, ligase D and ligase C. *Nat Struct Mol Biol* **12**, 304–312 (2005).

203. Bowater, R. & Doherty, A. J. Making ends meet: repairing breaks in bacterial DNA by non-homologous end-joining. *PLoS Genet* **2**, e8 (2006).

204. Pitcher, R. S. *et al.* NHEJ protects mycobacteria in stationary phase against the harmful effects of desiccation. *DNA Repair (Amst)* **6**, 1271–1276 (2007).

205. Moeller, R. *et al.* Role of DNA repair by nonhomologous-end joining in Bacillus subtilis spore resistance to extreme dryness, mono- and polychromatic UV, and ionizing radiation. *J Bacteriol* **189**, 3306–3311 (2007).

206. Paris, Ü. *et al.* NHEJ enzymes LigD and Ku participate in stationary-phase mutagenesis in Pseudomonas putida. *DNA Repair (Amst)* **31**, 11–18 (2015).

207. Leenay, R. T. *et al.* Identifying and Visualizing Functional PAM Diversity across CRISPR-Cas Systems. *Mol Cell* **62**, 137–147 (2016).

208. Bikard, D. *et al.* Programmable repression and activation of bacterial gene expression using an engineered CRISPR-Cas system. *Nucleic Acids Res* **41**, 7429–7437 (2013).

209. Qi, L. S. *et al.* Repurposing CRISPR as an RNA-guided platform for sequence-specific control of gene expression. *Cell* **152**, 1173–1183 (2013).

210. Wenyan Jiang, David Bikard, David Cox, Feng Zhang, and L. A. M. CRISPR-assisted editing of bacterial genomes. *Nature Biotechnology* (2013) doi:10.1038/nbt.2508.CRISPR-assisted.

211. Larson, M. H. *et al.* CRISPR interference (CRISPRi) for sequence-specific control of gene expression. *Nature Protocols* **8**, 2180–2196 (2013).

212. Peters, J. M. *et al.* A comprehensive, CRISPR-based functional analysis of essential genes in bacteria. *Cell* **165**, 1493–1506 (2016).

213. Liu, X. *et al.* High-throughput CRISPRi phenotyping in *Streptococcus pneumoniae* identifies new essential genes involved in cell wall synthesis and competence development. *Molecular Systems Biology* 1–18 (2017) doi:10.15252/msb.20167449.

214. Vigouroux, A., Oldewurtel, E., Cui, L., Bikard, D. & van Teeffelen, S. Tuning dCas9's ability to block transcription enables robust, noiseless knockdown of bacterial genes. *Molecular Systems Biology* **14**, e7899 (2018).

215. Cui, L. *et al.* A CRISPRi screen in E. coli reveals sequence-specific toxicity of dCas9. *Nat Commun* **9**, 1912 (2018).

216. Anton, B. P. & Raleigh, E. A. Complete Genome Sequence of NEB 5-alpha, a Derivative of Escherichia coli K-12 DH5α. *Genome Announc* **4**, (2016).

217. Youngman, P., Perkins, J. B. & Losick, R. Construction of a cloning site near one end of Tn917 into which foreign DNA may be inserted without affecting transposition in Bacillus subtilis or expression of the transposon-borne erm gene. *Plasmid* **12**, 1–9 (1984).

218. Aakre, C. D., Phung, T. N., Huang, D. & Laub, M. T. A bacterial toxin inhibits DNA replication elongation through a direct interaction with the β sliding clamp. *Mol. Cell* **52**, 617–628 (2013).

219. Gozzi, K. *et al.* Bacillus subtilis utilizes the DNA damage response to manage multicellular development. *NPJ Biofilms Microbiomes* **3**, 8 (2017).

220. Altenbuchner, J. Editing of the Bacillus subtilis Genome by the CRISPR-Cas9 System. *Appl. Environ. Microbiol.* **82**, 5421–5427 (2016).

221. Peters, J. M. *et al.* A Comprehensive, CRISPR-based Functional Analysis of Essential Genes in Bacteria. *Cell* **165**, 1493–1506 (2016).

222. Gibson, D. G. *et al.* Enzymatic assembly of DNA molecules up to several hundred kilobases. *Nat. Methods* **6**, 343–345 (2009).

223. Engler, C., Kandzia, R. & Marillonnet, S. A one pot, one step, precision cloning method with high throughput capability. *PLoS One* **3**, e3647 (2008).

224. Anagnostopoulos, C. & Spizizen, J. REQUIREMENTS FOR TRANSFORMATION IN BACILLUS SUBTILIS. *J Bacteriol* **81**, 741–746 (1961).

225. Hamoen, L. W., Smits, W. K., de Jong, A., Holsappel, S. & Kuipers, O. P. Improving the predictive value of the competence transcription factor (ComK) binding site in Bacillus subtilis using a genomic approach. *Nucleic Acids Res* **30**, 5517–5528 (2002).

226. Schneider, C. A., Rasband, W. S. & Eliceiri, K. W. NIH Image to ImageJ: 25 years of image analysis. *Nat Methods* **9**, 671–675 (2012).

227. Liu, J., Xu, Y., Stoleru, D. & Salic, A. Imaging protein synthesis in cells and tissues with an alkyne analog of puromycin. *Proc Natl Acad Sci U S A* **109**, 413–418 (2012).

228. Diez, S., Ryu, J., Caban, K., Gonzalez, R. L. & Dworkin, J. (p)ppGpp directly regulates translation initiation during entry into quiescence. *bioRxiv* 807917 (2019) doi:10.1101/807917.

229. Livak, K. J. & Schmittgen, T. D. Analysis of relative gene expression data using real-time quantitative PCR and the 2(-Delta Delta C(T)) Method. *Methods* **25**, 402–408 (2001).

230. Lorenz, R. *et al.* ViennaRNA Package 2.0. *Algorithms Mol Biol* **6**, 26 (2011).

231. Plubell, D. L. *et al.* Extended Multiplexing of Tandem Mass Tags (TMT) Labeling Reveals Age and High Fat Diet Specific Proteome Changes in Mouse Epididymal Adipose Tissue. *Mol Cell Proteomics* **16**, 873–890 (2017).

232. Tyanova, S. *et al.* The Perseus computational platform for comprehensive analysis of (prote)omics data. *Nat Methods* **13**, 731–740 (2016).

233. Narula, J. *et al.* Slowdown of growth controls cellular differentiation. *Mol Syst Biol* **12**, 871 (2016).

234. Chastanet, A. *et al.* Broadly heterogeneous activation of the master regulator for sporulation in Bacillus subtilis. *Proc Natl Acad Sci U S A* **107**, 8486–8491 (2010).

235. Molle, V. *et al.* The Spo0A regulon of Bacillus subtilis. *Mol Microbiol* **50**, 1683–1701 (2003).

236. Errington, J. Regulation of endospore formation in Bacillus subtilis. *Nat Rev Microbiol* **1**, 117–126 (2003).

237. Hilbert, D. W. & Piggot, P. J. Compartmentalization of gene expression during Bacillus subtilis spore formation. *Microbiol Mol Biol Rev* **68**, 234–262 (2004).

238. Stragier, P. & Losick, R. Molecular genetics of sporulation in Bacillus subtilis. *Annu Rev Genet* **30**, 297–241 (1996).

239. Sun, T. & Altenbuchner, J. Characterization of a mannose utilization system in Bacillus subtilis. *J Bacteriol* **192**, 2128–2139 (2010).

240. Martin-Verstraete, I., Débarbouillé, M., Klier, A. & Rapoport, G. Interactions of wild-type and truncated LevR of Bacillus subtilis with the upstream activating sequence of the levanase operon. *J Mol Biol* **241**, 178–192 (1994).

241. Yamanaka, K., Ogura, T., Niki, H. & Hiraga, S. Identification of two new genes, mukE and mukF, involved in chromosome partitioning in Escherichia coli. *Mol Gen Genet* **250**, 241–251 (1996).

242. Badrinarayanan, A., Le, T. B. K., Spille, J.-H., Cisse, I. I. & Laub, M. T. Global analysis of double-strand break processing reveals in vivo properties of the helicase-nuclease complex AddAB. *PLoS Genet* **13**, e1006783 (2017).

243. Cho, S. *et al.* High-Level dCas9 Expression Induces Abnormal Cell Morphology in Escherichia coli. *ACS Synth Biol* **7**, 1085–1094 (2018).

244. Rock, J. M. *et al.* Programmable transcriptional repression in mycobacteria using an orthogonal CRISPR interference platform. *Nat Microbiol* **2**, 16274 (2017).

245. Wendt, K. E., Ungerer, J., Cobb, R. E., Zhao, H. & Pakrasi, H. B. CRISPR/Cas9 mediated targeted mutagenesis of the fast growing cyanobacterium Synechococcus elongatus UTEX 2973. *Microb Cell Fact* **15**, 115 (2016).

246. Ungerer, J. & Pakrasi, H. B. Cpf1 Is A Versatile Tool for CRISPR Genome Editing Across Diverse Species of Cyanobacteria. *Sci Rep* **6**, 39681 (2016).

247. Farasat, I. & Salis, H. M. A Biophysical Model of CRISPR/Cas9 Activity for Rational Design of Genome Editing and Gene Regulation. *PLoS Comput Biol* **12**, e1004724 (2016).

248. Kim, L., Mogk, A. & Schumann, W. A xylose-inducible Bacillus subtilis integration vector and its application. *Gene* **181**, 71–76 (1996).

249. Soufo, C. D. *et al.* Cell-cycle-dependent spatial sequestration of the DnaA replication initiator protein in Bacillus subtilis. *Dev Cell* **15**, 935–941 (2008).

250. Berka, R. M. *et al.* Microarray analysis of the Bacillus subtilis K-state: genome-wide expression changes dependent on ComK. *Mol Microbiol* **43**, 1331–1345 (2002).

251. Lindner, C. *et al.* Differential expression of two paralogous genes of Bacillus subtilis encoding single-stranded DNA binding protein. *J Bacteriol* **186**, 1097–1105 (2004).

252. Mortier-Barrière, I. *et al.* A key presynaptic role in transformation for a widespread bacterial protein: DprA conveys incoming ssDNA to RecA. *Cell* **130**, 824–836 (2007).

253. Subramanian, A. *et al.* Gene set enrichment analysis: a knowledge-based approach for interpreting genome-wide expression profiles. *Proc Natl Acad Sci U S A* **102**, 15545–15550 (2005).

254. Mootha, V. K. *et al.* PGC-1alpha-responsive genes involved in oxidative phosphorylation are coordinately downregulated in human diabetes. *Nat Genet* **34**, 267–273 (2003).

255. Kanehisa, M. & Goto, S. KEGG: kyoto encyclopedia of genes and genomes. *Nucleic Acids Res* **28**, 27–30 (2000).

256. Kanehisa, M. Toward understanding the origin and evolution of cellular organisms. *Protein Sci* **28**, 1947–1951 (2019).

257. Kanehisa, M., Furumichi, M., Sato, Y., Ishiguro-Watanabe, M. & Tanabe, M. KEGG: integrating viruses and cellular organisms. *Nucleic Acids Res* **49**, D545–D551 (2021).

258. Ishikawa, S., Hara, Y., Ohnishi, R. & Sekiguchi, J. Regulation of a new cell wall hydrolase gene, cwlF, which affects cell separation in Bacillus subtilis. *J Bacteriol* **180**, 2549–2555 (1998).

259. Domínguez-Cuevas, P., Porcelli, I., Daniel, R. A. & Errington, J. Differentiated roles for MreB-actin isologues and autolytic enzymes in Bacillus subtilis morphogenesis. *Mol Microbiol* **89**, 1084–1098 (2013).

260. Carballido-López, R. *et al.* Actin homolog MreBH governs cell morphogenesis by localization of the cell wall hydrolase LytE. *Dev Cell* **11**, 399–409 (2006).

261. Gallant, J., Palmer, L. & Pao, C. C. Anomalous synthesis of ppGpp in growing cells. *Cell* **11**, 181–185 (1977).

262. Gentry, D. R. & Cashel, M. Mutational analysis of the Escherichia coli spoT gene identifies distinct but overlapping regions involved in ppGpp synthesis and degradation. *Mol Microbiol* **19**, 1373–1384 (1996).

263. Wells, D. H. & Gaynor, E. C. Helicobacter pylori initiates the stringent response upon nutrient and pH downshift. *J Bacteriol* **188**, 3726–3729 (2006).

264. Winther, K. S., Roghanian, M. & Gerdes, K. Activation of the Stringent Response by Loading of RelA-tRNA Complexes at the Ribosomal A-Site. *Mol Cell* **70**, 95-105.e4 (2018).

265. Sinha, K. M., Unciuleac, M.-C., Glickman, M. S. & Shuman, S. AdnAB: a new DSB-resecting motor-nuclease from mycobacteria. *Genes Dev* **23**, 1423–1437 (2009).

266. Schäfer, H. *et al.* The alarmones (p)ppGpp are part of the heat shock response of Bacillus subtilis. *PLoS Genet* **16**, e1008275 (2020).

267. Tagami, K. *et al.* Expression of a small (p)ppGpp synthetase, YwaC, in the (p)ppGpp(0) mutant of Bacillus subtilis triggers YvyD-dependent dimerization of ribosome. *Microbiologyopen* **1**, 115–134 (2012).

268. Westbrook, A. W., Moo-Young, M. & Chou, C. P. Development of a CRISPR-Cas9 Tool Kit for Comprehensive Engineering of Bacillus subtilis. *Appl. Environ. Microbiol.* **82**, 4876–4895 (2016).

269. Jakutyte-Giraitiene, L. & Gasiunas, G. Design of a CRISPR-Cas system to increase resistance of Bacillus subtilis to bacteriophage SPP1. *J Ind Microbiol Biotechnol* **43**, 1183–1188 (2016).

270. Zhang, K., Duan, X. & Wu, J. Multigene disruption in undomesticated Bacillus subtilis ATCC 6051a using the CRISPR/Cas9 system. *Sci Rep* **6**, 27943 (2016).

271. Burby, P. E. & Simmons, L. A. Regulation of Cell Division in Bacteria by Monitoring Genome Integrity and DNA Replication Status. *Journal of Bacteriology* **202**, (2020).

272. Price, M. A., Cruz, R., Baxter, S., Escalettes, F. & Rosser, S. J. CRISPR-Cas9 In Situ engineering of subtilisin E in Bacillus subtilis. *PLoS One* **14**, e0210121 (2019).

273. Zou, D. *et al.* Mining New Plipastatins and Increasing the Total Yield Using CRISPR/Cas9 in Genome-Modified Bacillus subtilis 1A751. *J Agric Food Chem* **68**, 11358–11367 (2020).

274. Watzlawick, H. & Altenbuchner, J. Multiple integration of the gene ganA into the Bacillus subtilis chromosome for enhanced β-galactosidase production using the CRISPR/Cas9 system. *AMB Express* **9**, 158 (2019).

275. Bikard, D., Hatoum-Aslan, A., Mucida, D. & Marraffini, L. A. CRISPR interference can prevent natural transformation and virulence acquisition during in vivo bacterial infection. *Cell Host Microbe* **12**, 177–186 (2012).

276. Tong, Y., Charusanti, P., Zhang, L., Weber, T. & Lee, S. Y. CRISPR-Cas9 Based Engineering of Actinomycetal Genomes. *ACS Synth Biol* **4**, 1020–1029 (2015).

277. Su, T. *et al.* A CRISPR-Cas9 Assisted Non-Homologous End-Joining Strategy for One-step Engineering of Bacterial Genome. *Sci Rep* **6**, 37895 (2016).

278. Zheng, X., Li, S.-Y., Zhao, G.-P. & Wang, J. An efficient system for deletion of large DNA fragments in Escherichia coli via introduction of both Cas9 and the non-homologous end joining system from Mycobacterium smegmatis. *Biochem Biophys Res Commun* **485**, 768–774 (2017).

279. Liu, D. *et al.* Development and characterization of a CRISPR/Cas9n-based multiplex genome editing system for Bacillus subtilis. *Biotechnol Biofuels* **12**, 197 (2019).

280. Jiang, Y. *et al.* Multigene editing in the Escherichia coli genome via the CRISPR-Cas9 system. *Appl Environ Microbiol* **81**, 2506–2514 (2015).

281. Pyne, M. E., Moo-Young, M., Chung, D. A. & Chou, C. P. Coupling the CRISPR/Cas9 System with Lambda Red Recombineering Enables Simplified Chromosomal Gene Replacement in Escherichia coli. *Appl Environ Microbiol* **81**, 5103–5114 (2015).

282. Reisch, C. R. & Prather, K. L. J. The no-SCAR (Scarless Cas9 Assisted Recombineering) system for genome editing in Escherichia coli. *Sci Rep* **5**, 15096 (2015).

283. Chung, M.-E. *et al.* Enhanced integration of large DNA into E. coli chromosome by CRISPR/Cas9. *Biotechnol Bioeng* **114**, 172–183 (2017).

284. Cobb, R. E., Wang, Y. & Zhao, H. High-efficiency multiplex genome editing of Streptomyces species using an engineered CRISPR/Cas system. *ACS Synth Biol* **4**, 723–728 (2015).

285. Choi, K. R. & Lee, S. Y. CRISPR technologies for bacterial systems: Current achievements and future directions. *Biotechnol Adv* **34**, 1180–1209 (2016).

286. Manina, G., Dhar, N. & McKinney, J. D. Stress and host immunity amplify Mycobacterium tuberculosis phenotypic heterogeneity and induce nongrowing metabolically active forms. *Cell Host Microbe* **17**, 32–46 (2015).

287. Lempp, M., Lubrano, P., Bange, G. & Link, H. Metabolism of non-growing bacteria. *Biol Chem* **401**, 1479–1485 (2020).

288. Lewis, K. Persister cells. *Annu Rev Microbiol* **64**, 357–372 (2010).

289. Washington, T. A., Smith, J. L. & Grossman, A. D. Genetic networks controlled by the bacterial replication initiator and transcription factor DnaA in Bacillus subtilis. *Mol Microbiol* **106**, 109–128 (2017).

290. Vigouroux, A., Oldewurtel, E., Cui, L., Bikard, D. & van Teeffelen, S. Tuning dCas9's ability to block transcription enables robust, noiseless knockdown of bacterial genes. *Mol. Syst. Biol.* **14**, e7899 (2018).

291. Kolter, R., Siegele, D. A. & Tormo, A. The stationary phase of the bacterial life cycle. *Annu Rev Microbiol* **47**, 855–874 (1993).

292. Steinchen, W. & Bange, G. The magic dance of the alarmones (p)ppGpp. *Mol Microbiol* **101**, 531–544 (2016).

293. Wang, J. D., Sanders, G. M. & Grossman, A. D. Nutritional control of elongation of DNA replication by (p)ppGpp. *Cell* **128**, 865–875 (2007).

294. Artsimovitch, I. *et al.* Structural basis for transcription regulation by alarmone ppGpp. *Cell* **117**, 299–310 (2004).

295. Ross, W. *et al.* ppGpp Binding to a Site at the RNAP-DksA Interface Accounts for Its Dramatic Effects on Transcription Initiation during the Stringent Response. *Mol Cell* **62**, 811–823 (2016).

296. Kriel, A. *et al.* Direct regulation of GTP homeostasis by (p)ppGpp: a critical component of viability and stress resistance. *Mol Cell* **48**, 231–241 (2012).

297. Balaban, N. Q. *et al.* Definitions and guidelines for research on antibiotic persistence. *Nat Rev Microbiol* **17**, 441–448 (2019).

298. Balaban, N. Q., Merrin, J., Chait, R., Kowalik, L. & Leibler, S. Bacterial persistence as a phenotypic switch. *Science* **305**, 1622–1625 (2004).

299. Shan, Y. *et al.* ATP-Dependent Persister Formation in Escherichia coli. *mBio* **8**, (2017).

300. Conlon, B. P. *et al.* Persister formation in Staphylococcus aureus is associated with ATP depletion. *Nat Microbiol* **1**, 16051 (2016).

301. Shivers, R. P. & Sonenshein, A. L. Activation of the Bacillus subtilis global regulator CodY by direct interaction with branched-chain amino acids. *Mol Microbiol* **53**, 599–611 (2004).

302. Handke, L. D., Shivers, R. P. & Sonenshein, A. L. Interaction of Bacillus subtilis CodY with GTP. *J Bacteriol* **190**, 798–806 (2008).

303. Kriel, A. *et al.* GTP dysregulation in Bacillus subtilis cells lacking (p)ppGpp results in phenotypic amino acid auxotrophy and failure to adapt to nutrient downshift and regulate biosynthesis genes. *J Bacteriol* **196**, 189–201 (2014).

304. Krásný, L. & Gourse, R. L. An alternative strategy for bacterial ribosome synthesis: Bacillus subtilis rRNA transcription regulation. *EMBO J* **23**, 4473–4483 (2004).

305. Meagher, R. B., Tait, R. C., Betlach, M. & Boyer, H. W. Protein expression in E. coli minicells by recombinant plasmids. *Cell* **10**, 521–536 (1977).

306. Elbaz, M. & Ben-Yehuda, S. Following the Fate of Bacterial Cells Experiencing Sudden Chromosome Loss. *mBio* **6**, (2015).

307. Gefen, O., Gabay, C., Mumcuoglu, M., Engel, G. & Balaban, N. Q. Single-cell protein induction dynamics reveals a period of vulnerability to antibiotics in persister bacteria. *Proc Natl Acad Sci U S A* **105**, 6145–6149 (2008).

308. Gefen, O., Fridman, O., Ronin, I. & Balaban, N. Q. Direct observation of single stationary-phase bacteria reveals a surprisingly long period of constant protein production activity. *PNAS* **111**, 556–561 (2014).

309. Boecker, S., Zahoor, A., Schramm, T., Link, H. & Klamt, S. Broadening the Scope of Enforced ATP Wasting as a Tool for Metabolic Engineering in Escherichia coli. *Biotechnol J* **14**, e1800438 (2019).

310. Shomar, H. *et al.* Metabolic engineering of a carbapenem antibiotic synthesis pathway in Escherichia coli. *Nat Chem Biol* **14**, 794–800 (2018).

311. Bokinsky, G. *et al.* HipA-triggered growth arrest and β-lactam tolerance in Escherichia coli are mediated by RelA-dependent ppGpp synthesis. *J Bacteriol* **195**, 3173–3182 (2013).

312. Korch, S. B. & Hill, T. M. Ectopic overexpression of wild-type and mutant hipA genes in Escherichia coli: effects on macromolecular synthesis and persister formation. *J Bacteriol* **188**, 3826–3836 (2006).

313. Heath, R. J., Jackowski, S. & Rock, C. O. Guanosine tetraphosphate inhibition of fatty acid and phospholipid synthesis in Escherichia coli is relieved by overexpression of glycerol-3-phosphate acyltransferase (plsB). *J Biol Chem* **269**, 26584–26590 (1994).

314. Wenzel, M., Müller, A., Siemann-Herzberg, M. & Altenbuchner, J. Self-inducible Bacillus subtilis expression system for reliable and inexpensive protein production by high-cell-density fermentation. *Appl Environ Microbiol* **77**, 6419–6425 (2011).

315. Guan, C. *et al.* Construction and development of an auto-regulatory gene expression system in Bacillus subtilis. *Microb Cell Fact* **14**, 150 (2015).

316. Tran, D. T. M. *et al.* Integrative expression vectors with Pgrac promoters for inducer-free overproduction of recombinant proteins in Bacillus subtilis. *Biotechnol Rep (Amst)* **28**, e00540 (2020).

317. Richter, F. *et al.* Switchable Cas9. *Curr Opin Biotechnol* **48**, 119–126 (2017).

318. Richter, F. *et al.* Engineering of temperature- and light-switchable Cas9 variants. *Nucleic Acids Res* **44**, 10003–10014 (2016).

319. Nihongaki, Y., Kawano, F., Nakajima, T. & Sato, M. Photoactivatable CRISPR-Cas9 for optogenetic genome editing. *Nat Biotechnol* **33**, 755–760 (2015).

320. Jain, P. K. *et al.* Development of Light-Activated CRISPR Using Guide RNAs with Photocleavable Protectors. *Angew Chem Int Ed Engl* **55**, 12440–12444 (2016).

8.Appendix

Supplementary data file 1. Proteomics of strains PY79 (WT) and CRISPRi$^{box6\text{-}7}$ under xylose induction.

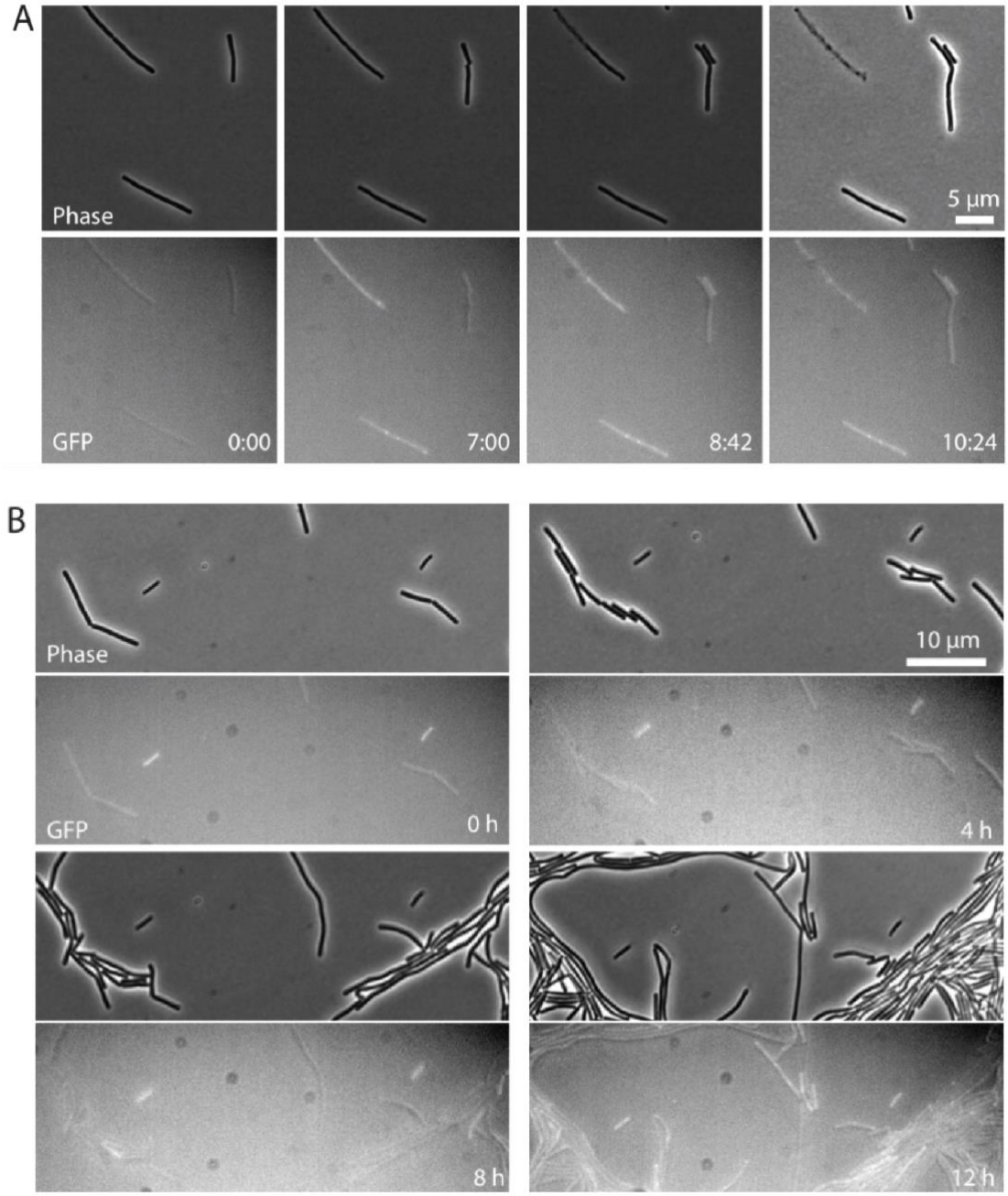

Figure S1. **Timelapse of a GFP+ cells for 10 hours**.

(A) Cell above appear fluorescent after 7 hours and looses fluorescence because of cell lysis at 8 hours and 42 min. Cell in the lower is fluorescent at 7 hours and continues to be fluorescent for the course of the experiment. (B)

Snapshots of cells in the microfluidic chamber for 12 hours. Snapshots show that fluorescent cells do not replicate while non-fluorescent ones undergo replication. Pictures depict most representative data.

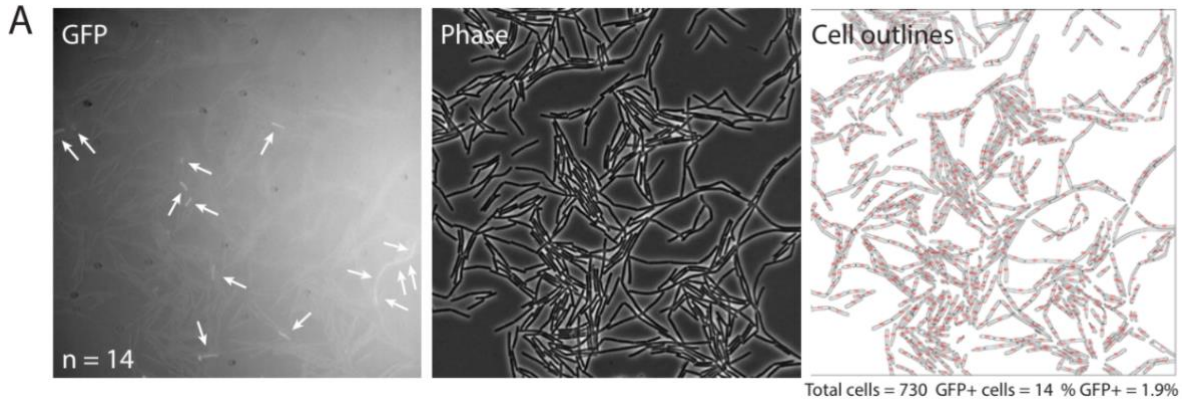

Figure S2. **Quantification of GFP+ cells.** Arrows show the GFP+ cells, phase contrast shows the general picture of the cells and the outlines represent the cells individually. A total of 730 cells were counted where 14 cells were GFP fluorescent, which represents the 1,9% of the cells. n=730.

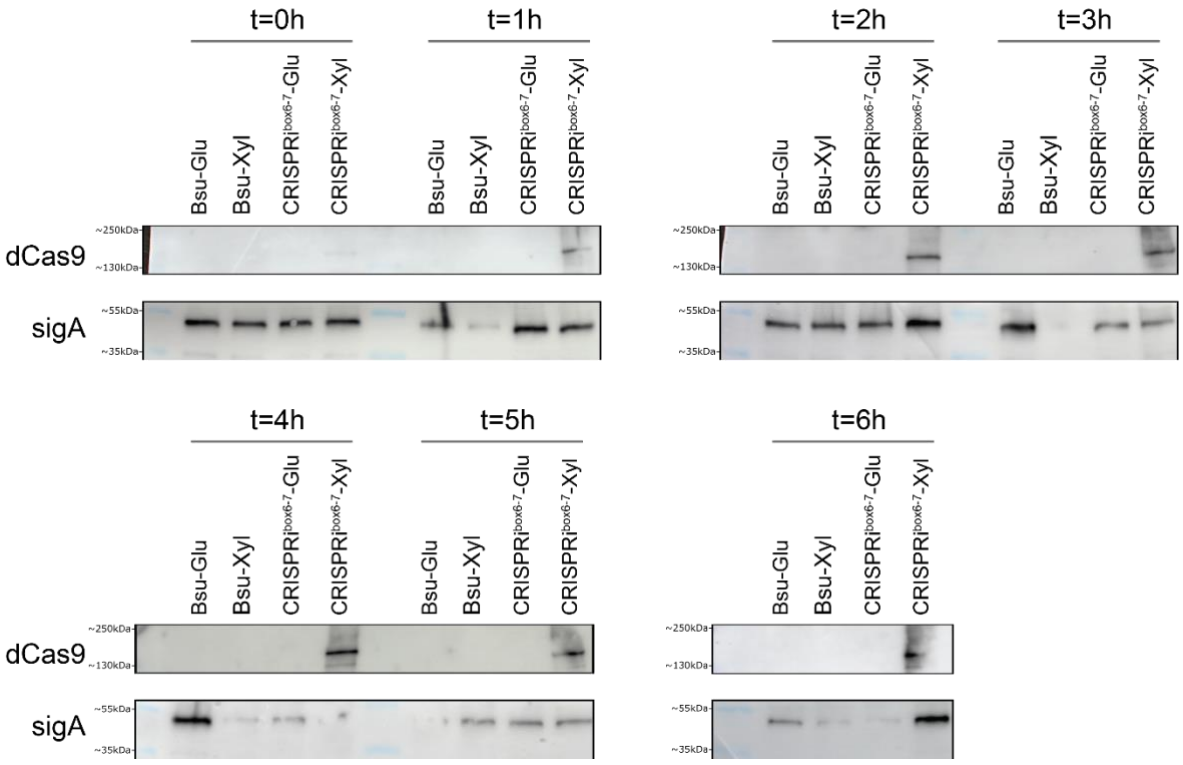

Figure S3. **dCas9 expression is observe after 1 hour of dCas9 induction.**

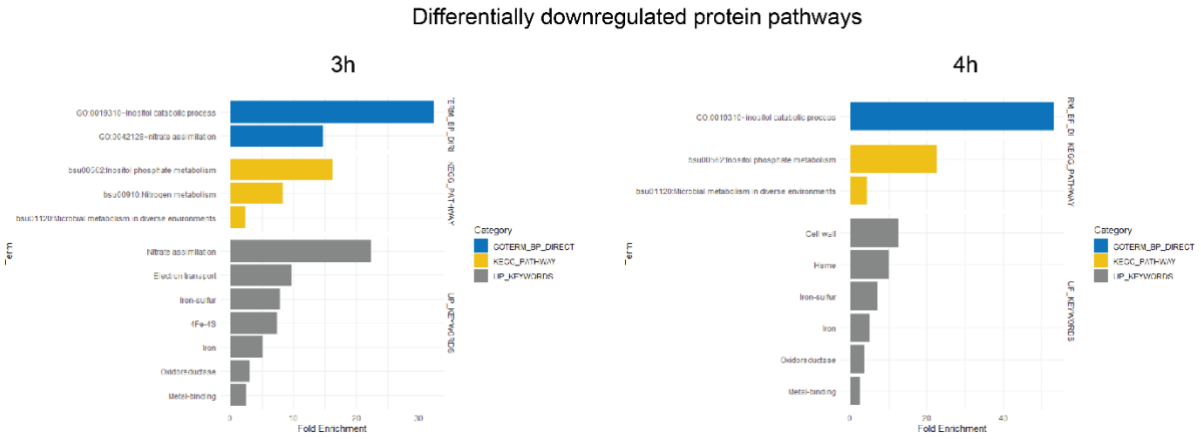

Figure S 4. **Pathways showing depletion of proteins in CRISPRi$^{box6\text{-}7}$.**
The fold enrichment value represents the fraction of quantified proteins belonging to a particular category compared to the total number of proteins assigned to that category in the genome.

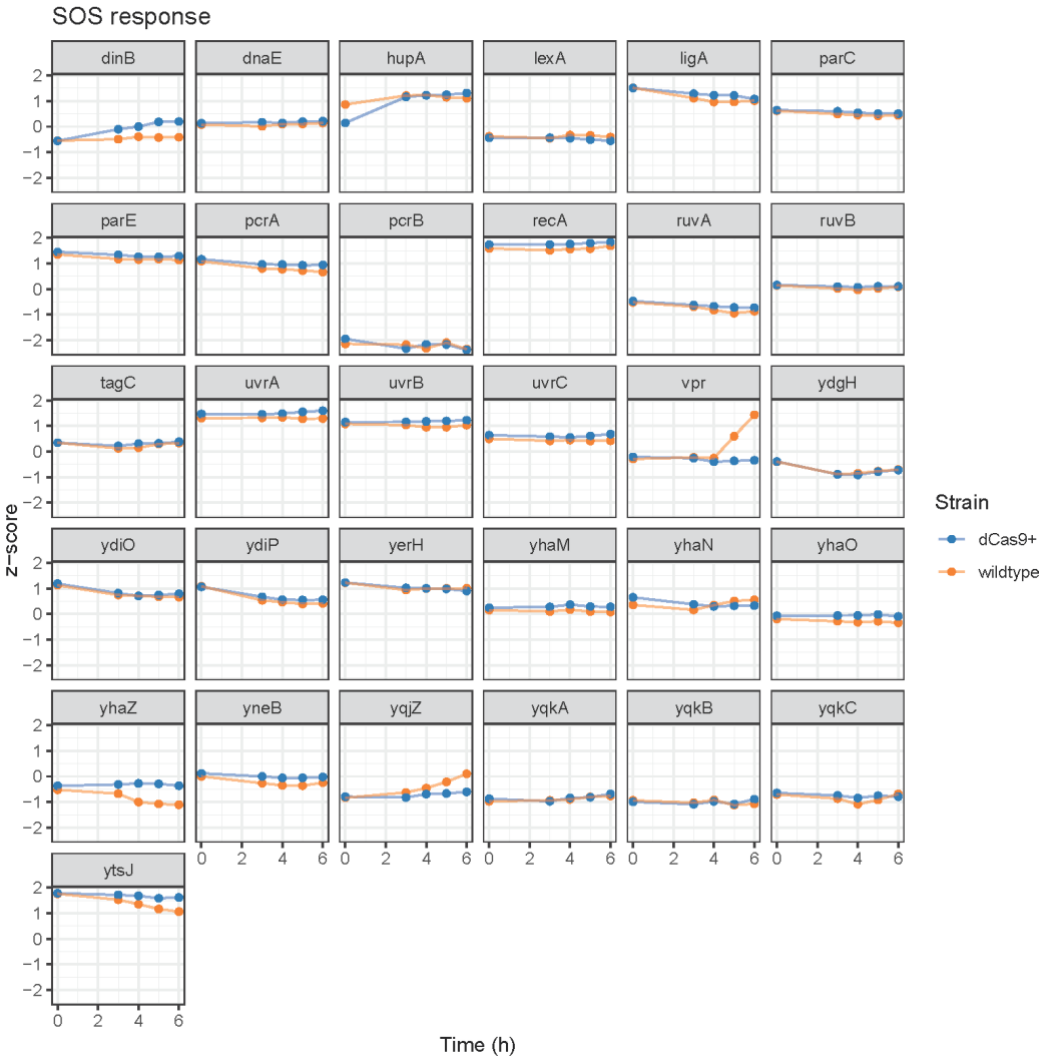

Figure S5. **Profile plots of SOS response associated proteins.**

Table S1. Evaluation of off-target (OT) events per guide present in the *oriC* of *B. subtilis*

Guide ID	Guide Seq	Number of Off-targets (OT)	Off-target sequence	Number of mismatches	OT Coordinate	Strand
guide_1	CAACTTATCCACAAATCCACAGG	16	AAAATTCACCGCAAATCCAACGG	6	3712599	F
guide_1	CAACTTATCCACAAATCCACAGG	16	AAACTGCTCCAACAATCCAAGGG	6	3530701	F
guide_1	CAACTTATCCACAAATCCACAGG	16	ATACATATCCATAAATACATTGG	6	1804434	R
guide_1	CAACTTATCCACAAATCCACAGG	16	CAACTTATCCACAAATCCACAGG	0	1847	F
guide_1	CAACTTATCCACAAATCCACAGG	16	CAACTTCTGAACAAAGCGACAGG	5	351056	F
guide_1	CAACTTATCCACAAATCCACAGG	16	CAAGTAAATCAGAAATCGACAGG	6	1660983	F
guide_1	CAACTTATCCACAAATCCACAGG	16	CAATGTAACCGCATATGCACAGG	6	75179	F
guide_1	CAACTTATCCACAAATCCACAGG	16	CAATTTAAGGACAAATCCAAAGG	5	1181795	R
guide_1	CAACTTATCCACAAATCCACAGG	16	CACCTGATGAACAAATCCGCAGG	5	2750390	R
guide_1	CAACTTATCCACAAATCCACAGG	16	CAGCTGAGACACAAATACATCGG	6	3063257	R
guide_1	CAACTTATCCACAAATCCACAGG	16	CAGCTTCGCCATAAATTCATCGG	6	3901323	F
guide_1	CAACTTATCCACAAATCCACAGG	16	CATCTGCTCCTTAAATCCAAAGG	6	3271050	R
guide_1	CAACTTATCCACAAATCCACAGG	16	CATTTTGTGCAAAACTCCACAGG	6	2603314	R
guide_1	CAACTTATCCACAAATCCACAGG	16	CCACTCATCCACCAAATGACTGG	6	216614	R
guide_1	CAACTTATCCACAAATCCACAGG	16	CTGCTTTTCCACACCTCAACAGG	6	60819	R
guide_1	CAACTTATCCACAAATCCACAGG	16	TATCTTCTCCACAAAAACGCGGG	6	129810	F
guide_2	ATACACAGTCTGTCCACATGTGG	9	AAACACAGCCTATCCACATGTGG	3	1811	R
guide_2	ATACACAGTCTGTCCACATGTGG	9	AAACACTTGCGGTCCACATTTGG	6	2396842	R
guide_2	ATACACAGTCTGTCCACATGTGG	9	ACACACAGCTTTTTCTCATGTGG	6	586642	F
guide_2	ATACACAGTCTGTCCACATGTGG	9	ACAGACACTCTTTCCAAACGAGG	6	1120342	F
guide_2	ATACACAGTCTGTCCACATGTGG	9	AGATAGAGTTTGTGGACATGTGG	6	3725471	R
guide_2	ATACACAGTCTGTCCACATGTGG	9	ATAATCAGTCCGTCAATAAGGGG	6	3559107	R
guide_2	ATACACAGTCTGTCCACATGTGG	9	ATACACAGTCTGTCCACATGTGG	0	1798	F
guide_2	ATACACAGTCTGTCCACATGTGG	9	ATACATAGGTTGTAAACATAAGG	6	1004807	R
guide_2	ATACACAGTCTGTCCACATGTGG	9	ATATACAGTCTGTCCGCATAAGG	3	2114624	F

guide_3	GGAAAGTGTGAATAACTTTTCGG	15	AGAAATTGTGAATACGCTGTCGG	6	2834017	F
guide_3	GGAAAGTGTGAATAACTTTTCGG	15	GAAAAATGCGAAGAGCTTCTGGG	6	3148115	F
guide_3	GGAAAGTGTGAATAACTTTTCGG	15	GAAAAGGAGGAACAACTTTAGGG	6	2681878	F
guide_3	GGAAAGTGTGAATAACTTTTCGG	15	GCAGATTTTGAAGAGCTTTTCGG	6	1111642	F
guide_3	GGAAAGTGTGAATAACTTTTCGG	15	GGAAACTGTGAATGAATGCTTGG	5	295660	F
guide_3	GGAAAGTGTGAATAACTTTTCGG	15	GGAAAGAGTGATTATCGGATAGG	6	1380432	F
guide_3	GGAAAGTGTGAATAACTTTTCGG	15	GGAAAGTGTGAATAACTTTTCGG	0	1770	F
guide_3	GGAAAGTGTGAATAACTTTTCGG	15	GGAAATTGTAAAGGATTTTACGG	6	44237	F
guide_3	GGAAAGTGTGAATAACTTTTCGG	15	GGAATATGCGAAGGACATTTGGG	6	2981609	R
guide_3	GGAAAGTGTGAATAACTTTTCGG	15	GGAGAGCGGGAAGAACGCTTCGG	6	2121324	R
guide_3	GGAAAGTGTGAATAACTTTTCGG	15	GGAGAGCGTGAAAGATTTTCCGG	6	657817	F
guide_3	GGAAAGTGTGAATAACTTTTCGG	15	GGGAAGTGTGCAGAGCTTTGCGG	5	1524145	F
guide_3	GGAAAGTGTGAATAACTTTTCGG	15	GGGAATTGCGAATATCATTGCGG	6	3259366	R
guide_3	GGAAAGTGTGAATAACTTTTCGG	15	GGTAAGCGTGACGAGCTTCTCGG	6	129014	F
guide_3	GGAAAGTGTGAATAACTTTTCGG	15	GGTCGATGTGAATCTCTTTTAGG	6	441140	F
guide_4	GGATAAGTTGTGAAAAAGACAGG	49	AGAAAAGAGCGGAAAAAGACTGG	6	1290499	F
guide_4	GGATAAGTTGTGAAAAAGACAGG	49	AGAAAAGATGTGAAAAAAATGGG	5	423600	F
guide_4	GGATAAGTTGTGAAAAAGACAGG	49	AGAAAAGGCTTGAAAAAGAAGGG	6	2474858	R
guide_4	GGATAAGTTGTGAAAAAGACAGG	49	AGAAAAGGTGTGTAAAATACTGG	5	3985910	R
guide_4	GGATAAGTTGTGAAAAAGACAGG	49	AGACAAATTATGAAATATACAGG	6	3467747	R
guide_4	GGATAAGTTGTGAAAAAGACAGG	49	AGAGAAGAATTGAAAAAGCCGGG	6	3198510	F
guide_4	GGATAAGTTGTGAAAAAGACAGG	49	AGATAAATCTTGAAAAAGCGAGG	6	840296	R
guide_4	GGATAAGTTGTGAAAAAGACAGG	49	AGATTCTTCGTGAAAAATACGGG	6	3580370	R
guide_4	GGATAAGTTGTGAAAAAGACAGG	49	AGTGAAATTGTGAAAAAAGCTGG	6	566134	F
guide_4	GGATAAGTTGTGAAAAAGACAGG	49	GAACAAGCTTTGAAAAAGCGTGG	6	3408155	F
guide_4	GGATAAGTTGTGAAAAAGACAGG	49	GAAGAAATTGTGAAAAAGCTGGG	5	2626168	R
guide_4	GGATAAGTTGTGAAAAAGACAGG	49	GAATAAGTTTTGAAAAATATTGG	4	2847064	R
guide_4	GGATAAGTTGTGAAAAAGACAGG	49	GAATGAATTGTTAACAAAACCGG	6	3199957	R
guide_4	GGATAAGTTGTGAAAAAGACAGG	49	GCAATAGATGAAAAAAAGACTGG	6	3547293	F
guide_4	GGATAAGTTGTGAAAAAGACAGG	49	GCATATGTTGTGCAGAAGCCTGG	5	379671	F

guide_4	GGATAAGTTGTGAAAAAGACAGG	49	GGAAAAGATGGGGAAAACAGCGG	6	2330167	R
guide_4	GGATAAGTTGTGAAAAAGACAGG	49	GGAAAAGTTGCGATCATTACTGG	6	985396	F
guide_4	GGATAAGTTGTGAAAAAGACAGG	49	GGAAATGTTTTGAACAAAATCGG	6	2656586	R
guide_4	GGATAAGTTGTGAAAAAGACAGG	49	GGACAAGTATTGAAGCTGACAGG	6	975438	R
guide_4	GGATAAGTTGTGAAAAAGACAGG	49	GGACAAGTCCTGAAACTGAAAGG	6	982400	F
guide_4	GGATAAGTTGTGAAAAAGACAGG	49	GGACAGGTTGTGAAGAATGTGGG	6	1910686	F
guide_4	GGATAAGTTGTGAAAAAGACAGG	49	GGACATGTGGCGCGAAAGACTGG	6	1541520	F
guide_4	GGATAAGTTGTGAAAAAGACAGG	49	GGAGAAGTTGTGACGATTATCGG	6	2822878	R
guide_4	GGATAAGTTGTGAAAAAGACAGG	49	GGAGAATTTGTTACAAAAAAAGG	6	292178	F
guide_4	GGATAAGTTGTGAAAAAGACAGG	49	GGAGAGCTGGGGAAAAAAACCGG	6	334267	F
guide_4	GGATAAGTTGTGAAAAAGACAGG	49	GGATAAATGGAGCGGAAGACGGG	6	166016	R
guide_4	GGATAAGTTGTGAAAAAGACAGG	49	GGATAAGATCTTTTAGAGACGGG	6	2175648	F
guide_4	GGATAAGTTGTGAAAAAGACAGG	49	GGATAAGGGTTAGAAAATACAGG	6	2156044	F
guide_4	GGATAAGTTGTGAAAAAGACAGG	49	GGATAAGTTGTGAAAAAGACAGG	0	1834	R
guide_4	GGATAAGTTGTGAAAAAGACAGG	49	GGATACATCGTCAGTAAGACAGG	6	2545278	F
guide_4	GGATAAGTTGTGAAAAAGACAGG	49	GGATCGGTTGTAAACACGCCTGG	6	2728052	F
guide_4	GGATAAGTTGTGAAAAAGACAGG	49	GGATGAGCTGAGAAGAAATCTGG	6	157090	F
guide_4	GGATAAGTTGTGAAAAAGACAGG	49	GGATGAGCTTTCGAAAACACTGG	6	2261670	R
guide_4	GGATAAGTTGTGAAAAAGACAGG	49	GGCAATGTTGTAAAAGAGATCGG	6	2864271	R
guide_4	GGATAAGTTGTGAAAAAGACAGG	49	GGCGAACTTGAGAAAACGTCAGG	6	739305	F
guide_4	GGATAAGTTGTGAAAAAGACAGG	49	GGGAAAGTTCTGAAATATAATGG	6	3479144	R
guide_4	GGATAAGTTGTGAAAAAGACAGG	49	GGGTAAAACGCAAAAAAGACCGG	6	3005921	R
guide_4	GGATAAGTTGTGAAAAAGACAGG	49	GGTTAAGTTCAAAAATAGAACGG	6	2954075	R
guide_4	GGATAAGTTGTGAAAAAGACAGG	49	GGTTGATTTGTAAAAAAGTCTGG	5	2040435	F
guide_4	GGATAAGTTGTGAAAAAGACAGG	49	GTATAATGTGTAAAAAAGGGGGG	6	1129746	F
guide_4	GGATAAGTTGTGAAAAAGACAGG	49	GTTTAAGCAGTGAAAAGGACTGG	5	2839435	R
guide_4	GGATAAGTTGTGAAAAAGACAGG	49	TACTAAGTTATGAAAAATAAGGG	6	2150897	F
guide_4	GGATAAGTTGTGAAAAAGACAGG	49	TATTATATTGTGAAAAAGTCAGG	6	406311	F
guide_4	GGATAAGTTGTGAAAAAGACAGG	49	TGACAAGTTTAGAAAAAAAGAGG	6	1014869	F
guide_4	GGATAAGTTGTGAAAAAGACAGG	49	TGATCAGGAGTTAAAAAGAAGGG	6	16208	R

guide_4	GGATAAGTTGTGAAAAAGACAGG	49	TGATGCGGTGTGAAAAAATCAGG	6	1435942	F
guide_4	GGATAAGTTGTGAAAAAGACAGG	49	TGATTAGATTTGAAAAATGCTGG	6	1900215	R
guide_4	GGATAAGTTGTGAAAAAGACAGG	49	TGGGAAATTGTGAAAAAGTGCGG	6	1322426	F
guide_4	GGATAAGTTGTGAAAAAGACAGG	49	TGGTTAGTTGCGAAAAAAAACGG	6	1228498	R
guide_5	TAGTAGGGCCTGTGGATTTGTGG	8	AAAAAGAGCTTGAGGATTTGCGG	6	1539584	F
guide_5	TAGTAGGGCCTGTGGATTTGTGG	8	TAATAAGGCTTGTGAATCAGCGG	6	2947403	R
guide_5	TAGTAGGGCCTGTGGATTTGTGG	8	TAGCAAAGCCGGTTGATTTAGGG	6	3105164	R
guide_5	TAGTAGGGCCTGTGGATTTGTGG	8	TAGGCTGGTCTGTGGACTTCAGG	6	3564668	F
guide_5	TAGTAGGGCCTGTGGATTTGTGG	8	TAGTAGGGCCTGTGGATTTGTGG	0	1855	R
guide_5	TAGTAGGGCCTGTGGATTTGTGG	8	TGGCATGGACTTTGGTTTTGTGG	6	2506641	R
guide_5	TAGTAGGGCCTGTGGATTTGTGG	8	TGGTATGGTCGGCGGATTTATGG	6	1473432	F
guide_5	TAGTAGGGCCTGTGGATTTGTGG	8	TTCTAGGCCCTTTAGATATGGGG	6	2011578	R
guide_6	AAACACAGCCTATCCACATGTGG	17	AAAAACAGCATATGAAAAAGCGG	6	1810525	F
guide_6	AAACACAGCCTATCCACATGTGG	17	AAAAAGAGCCCATCCCAATAAGG	6	3764962	R
guide_6	AAACACAGCCTATCCACATGTGG	17	AAAATAACCTTATCAACATGGGG	6	416085	R
guide_6	AAACACAGCCTATCCACATGTGG	17	AAACACAGCCTATCCACATGTGG	0	1811	R
guide_6	AAACACAGCCTATCCACATGTGG	17	AAACACGGCTTAGTCACTTGGGG	5	3021190	R
guide_6	AAACACAGCCTATCCACATGTGG	17	AAACACTTGCGGTCCACATTTGG	6	2396842	R
guide_6	AAACACAGCCTATCCACATGTGG	17	AAAGGCAGCTTTTTTACATGTGG	6	3424578	R
guide_6	AAACACAGCCTATCCACATGTGG	17	AAATACAGCCATTGAACATACGG	6	2429437	R
guide_6	AAACACAGCCTATCCACATGTGG	17	AAGCACATTCTATCCTGAAGCGG	6	3040568	F
guide_6	AAACACAGCCTATCCACATGTGG	17	AATCATAGCCTAATAAAATGTGG	6	473985	R
guide_6	AAACACAGCCTATCCACATGTGG	17	ACACACAGCTTTTTCTCATGTGG	5	586642	F
guide_6	AAACACAGCCTATCCACATGTGG	17	ACAGACAGCATATGCCCATGTGG	5	2439274	F
guide_6	AAACACAGCCTATCCACATGTGG	17	AGCCAAGCCCTATCCGCATGTGG	6	3239295	F
guide_6	AAACACAGCCTATCCACATGTGG	17	ATACACAGTCTGTCCACATGTGG	3	1798	F
guide_6	AAACACAGCCTATCCACATGTGG	17	ATATACAGTCTGTCCGCATAAGG	6	2114624	F
guide_6	AAACACAGCCTATCCACATGTGG	17	GAAAACAGCCGTTCCACTTGCGG	5	1607480	R
guide_6	AAACACAGCCTATCCACATGTGG	17	TAACCCAGCATACCAATATGCGG	6	3039174	R

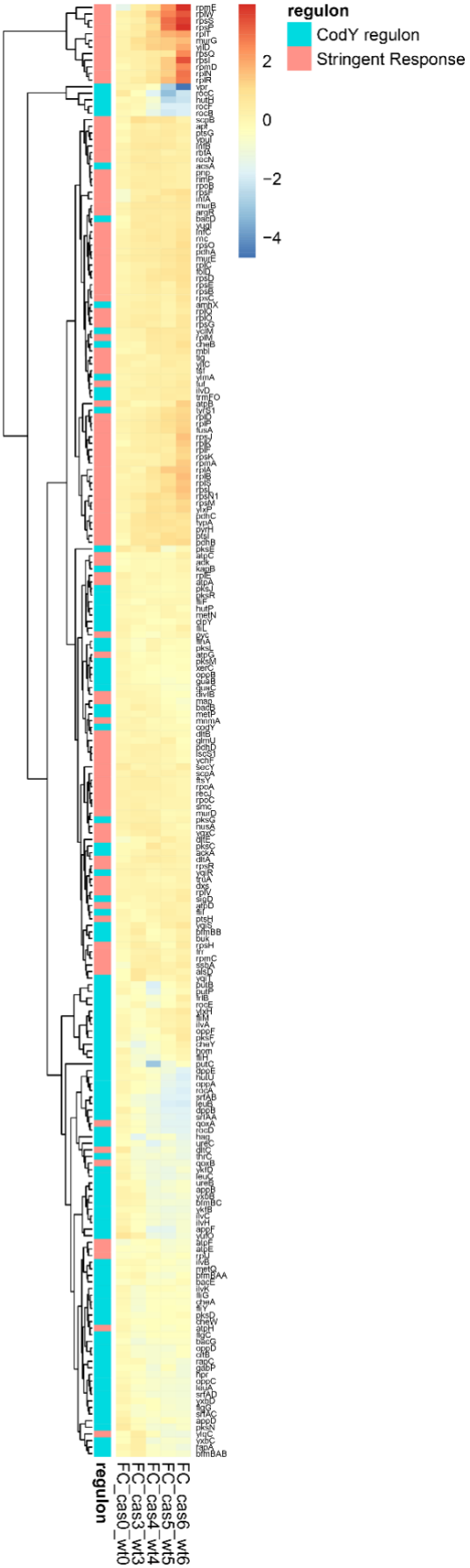

Figure S6. **CodY regulon associated proteins are downregulated and ribosomal proteins related to stringent regulon are upregulated**.
Heatmap showing expression pattern of differentially expressed proteins in three biological samples each.

Acknowledgments

I'm finally coming to the end of writing this thesis. This is the section I left for last but the one I wanted to write the most. This is proof that this PhD journey is coming to an end, and it is bittersweet. On one hand, I feel nostalgic for the culmination of this journey, but on the other hand, I feel happy that I made it. Most of all, I feel incredibly grateful for all the lessons learned during the last 4 years. At every step of this journey, I found myself surrounded by smart and kind people who inspired me and helped me in so many ways. It is good to finally have a chance to thank you properly.

First, I want to thank Prof. Emmanuelle Charpentier for the excellent opportunity to come as a PhD student to the lab. These last 4 years have been an enriching experience of professional and personal growth. Thank you for your supervision, encouragement and for allowing me to explore my scientific curiosity. I also want to thank you for the lab retreats, Christmas dinners, lab outings, and social activities that now look like a far past but are still very present in my memory.

My deep gratitude goes to my co-supervisor, Dr. Alexander Elsholz. Thank you for trusting me in what started as the craziest project I heard about. Even though I took it to a different road, I hope you were happy to change the ride. Thank you for your trust and for always finding the time to discuss and correct the multiple versions of this thesis. I'm also very thankful to my Doktorvater, Prof. Kürşad Turgay. Thank you for being an endless source of knowledge and literature. Your love for science is contagious, and your memory is something I will always envy. I know you don't like PY79, but I hope this thesis makes you at least accept that it is a fantastic strain, do not *discard* its potential. I would also like to thank the members of my thesis committee Prof. Heath Murray, Prof. Jan-Willem Veening, Prof. Marc Erhard, and Dr. David Bikard, for the advice, the trips to Berlin, the seminars, the support during my TAC meetings, and their interest in my work.

My immense gratitude also to all other RIIB/MPUSP members. The space is limited to mention you all individually, but I want to thank you all for the support, helpful discussions, and the great international and open-minded work environment. Very quickly after starting my PhD, the RIIB family welcomed me. Lina, I have missed you so much in the past years! You were always

like a PhD sister to me. Thank you for always being in the best mood, for great science discussions, for all your help showing me how things worked in the lab, and for making me feel welcome. Laura, it was incredible to share all these PhD years together. Thank you for your friendship. Many good memories remain, especially our trip to Colombia, our weekends buying face masks and creams, riding bikes around berlin as professionals, and trying to be life-achievers. I will always admire the great discipline you put into everything you do. Andrés, a man of many talents: a great sportsman (juggling and running marathons), intelligent scientist, and good friend. Thank you for always listening to my science concerns and pretend that you cared about my project. It was always a pleasure to show you new restaurants around Berlin, especially when they were conveniently within walking distance from my house. Victoria, I am glad we arrived together at the lab and that many years after, you decided to join again for your PhD. I feel this life cycle begins and ends with you and your positivity, and I could not be happier about that. Eric JC, thank you for making the best arepas of Berlin and probably of Germany. I also want to thank you for being a great host, cook, and life advisor.

Frank, thank you for your genuine interest in my project, for not losing patience when coffee breaks became troubleshooting sessions, and always coming with life hacks to overcome my anxiety like meditation and breathwork exercises; those habits have stayed with me. Matteo, thank you for bringing humor, laughter, sarcasm, and memes to my life. I will never forget your amazing presentations, the trip to Colombia, and your gifted memory. Marlene, thank you for your book recommendations, the long talks, and your efforts in making the c*nt office a space of pure joy filled with soap bubbles and advent calendars. Tim, thank you very much for your motivation, for having an eye for details, for being extremely efficient, and for the off-target analysis of sgRNA. Daniel B., thank you for teaching me how to teach; it was fun having you in the lab and letting me transfer you my (still limited) knowledge in cloning. I'm happy my lessons are still valuable for your PhD life. Nina, thank you for being a great bench neighbour and office mate. Thomas and Sandra, thanks for all the amazing cakes and for organizing the lab's social events. Thomas, let's keep the spirit of the cold room sessions alive! I'm pleased we supported each other during our struggles writing the thesis. I would also like to thank Andrea for her diligence and help during my visa paperwork. I literally would not be physically here if it wasn't for you.

Christian and Florian, thank you for all the help with the MS experimental design and data processing. Kathir and Christian, thank you for checking my thesis and making it (hopefully) nicer to read. I also want to thank Knut Finstermeier for the help with the artificial protospacer design. To our collaborators Dr. Johannes Kabisch and Silke Hackenschmidt for the support. Silke, thank

you for the strains, the meetings, and the discussions. To Dr. Matthew Cabeen, many thanks for the microfluidics and timelapse analysis. Gisela, thank you for the careful examination of the methods of this thesis, and for all your helpful input. To the Bacillus crew, Regina, Heinrich, Kristina, Victoria, and Fabian, it has been great to have people at the bench who care about *B. subtilis;* thank you all for your generosity.

Katja, where do I start? Many thanks for embarking on the CRISPRi adventure during the last part of my PhD. Thank you for the technical support and motivation. Working with you was always productive, and I really enjoyed seeing your genuine excitement with every new result we were getting. Fabian, this thesis would not exist if it were not for all the time you invested in helping me out with the proteomics data analysis. Thank you for your endless support checking the thesis too. You are a brilliant scientist and easy-going person; your character is also reflected in how you offer your help to everyone in the lab. I am sure you will have a bright future in science, and you will become a great PI.

I could not stop thanking Daniel Schindler, Nico Claasens, Pablo Nikel for great scientific discussions. Daniel, you were also a great support in the most stressful moments, and I will never thank you enough for that. Nico and Pablo, thank you for taking time out of your tight schedule to have scientific chats. Talking to you was always encouraging and motivating!

Thank you to all my friends in Berlin who made me feel at home: Jan, Alicia, Ana Maria, Jennifer, Arianna. To my favourite neuroscientists: Susana, Tiziano, and Meng, thank you for all the fantastic dinners together, the co-working days, and the emotional support. Thank you to the friends who withstood the distance and showed support and love by visiting me, keeping in contact, and checking on me when I get on hermit mode. Evelio, thank you for visiting me every time you were in Europe and for your endless empathy. Santi J, thank you for always calling and having words of support. Diana, thank you for listening to my endless stories and for all the life lessons I get by being your friend.

Finalmente, quiero darle gracias a mi familia. Papi y mami, gracias por el apoyo incondicional durante todos estos años. Por estar conmigo en mis mayores alegrías cuando las cosas iban bien y especialmente por entenderme y tenerme paciencia cuando estaba en estrés o frustración. Gracias por visitarme en Berlín, por darme tanto gusto en mis visitas a Colombia, y por hacerme sentir que los tengo cerca a pesar de la distancia. Juanjo, gracias por ser un buen hermano y una persona tan alegre, positiva y llena de humor. Gracias a ustedes tres por siempre apoyar mis decisiones de vida.

Curriculum vitae

Vivian Vanessa Muñoz Gutiérrez
Born on 13.04.1990 in Florencia, Colombia

Education

2020-2021 **Promotion in Biologie (PhD), Institut für Mikrobiologie**
Leibniz Universität Hannover
Thesis tittle: Life without replication in *Bacillus subtilis*
Hannover, Germany

2013-2015 **MSc. in Biotechnology**
Wageningen University
Specialization: Cellular and Molecular Biotechnology Wageningen, The Netherlands

2007-2012 **BSc. in Microbiology**
Universidad de los Andes
Specialization: molecular microbiology
Bogotá, Colombia

Experience

2017-present **PhD student** (Funded by the VollksWagen Stiftung grant: LIFE, awarded to Dr. Alexander Elsholz)
Max Planck Unit for the Science of Pathogens
Berlin, Germany

2016-2017 **Research assistant**
SYNMIKRO
Project: Genome organization and localization in Sinorhizobium meliloti
Marburg, Germany

2015 **MSc. intern**
Pasteur Institute
Laboratory of Microbiology, Synthetic biology group
Paris, France

2012-2013 **Consultant and sales representative**
ASEI S.A.S.
Medellin, Colombia

List of publications

In preparation:

Muñoz Gutiérrez V., Cornejo F.A., Schmidt K., Frese C., Turgay K., Elsholz A. and Charpentier E. A CRISPRi-based replicative block in targeted DnaA boxes unravels proteome-wide effects in *Bacillus subtilis*.